The Role of Oxidative Stress in Prion Provoked Neurotoxicity

by

Margot Maureen Plews

A Thesis submitted to the Faculty of Graduate Studies of

The University of Manitoba

in partial fulfilment of the requirements of the degree of

MASTER OF SCIENCE

Department of Medical Microbiology

University of Manitoba

Winnipeg

THE UNIVERSITY OF MANITOBA

FACULTY OF GRADUATE STUDIES

*****

COPYRIGHT PERMISSION

The Role of Oxidative Stress in Prion Provoked Neurotoxicity

BY

Margot Maureen Plews

A Thesis/Practicum submitted to the Faculty of Graduate Studies of The University of Manitoba in partial fulfillment of the requirement of the degree

MASTER OF SCIENCE

Table of Contents

Abstract

Oxidative stress has been implicated in the pathology of many neurodegenerative diseases. In prion disease the accumulation of PrP^{d} correlates with disease progression and coincides with the appearance of markers of oxidative stress in the brains of infected mice. This suggests that disease-associated neurodegeneration may in part be due to oxidative damage. To investigate the role of oxidative stress in prion provoked neurotoxicity both an *in vitro* and *in vivo* model system were used. In the *in vitro* model system a neuronally enriched culture of P19 cells suitable for studying the molecular and cellular processes involved in $PrP^{106-126}$ cytotoxicity was generated and the exacting culture conditions required delineated. Culture composition was determined qualitatively by staining with cell-type specific antibodies and quantitatively by measuring the level of cell-type specific transcripts. Flow cytometry experiments intended to measure the temporal relationship of oxidative stress and cell death demonstrated that P19 neurons are extremely sensitive to mechanical manipulation. This suggested that they would be more amenable to determining the changes in gene expression as a result of $PrP^{106-126}$ cytotoxicity. In the *in vivo* model system the influence of a dietary supplement on oxidative stress and disease progression was determined. Brains and urine were collected at various time points throughout the course of disease. Markers of antioxidant capacity, lipid peroxidation, DNA damage, and changes in gene expression were measured. Scrapie-infected mice displayed reduced total glutathione levels, increased 4-HNE levels and increased 8-OHdG levels as compared to control mice. Microarray analysis revealed that a major source of ROS was activated glial cells and that prion infection impairs the ability of cells to recognize and repair oxidative DNA damage. The data demonstrates

that oxidative stress is associated with prion disease well before clinical signs are apparent suggesting that oxidative stress is more a cause than a consequence of disease progression. The modest amelioration of the adverse effects resulting from disease associated oxidative stress achieved by the antioxidant diet was not sufficient to delay the onset of terminal stage disease. Due to the inability of the antioxidant diet to reduce the disease associated oxidative stress to control levels, the extent of the contribution of oxidative stress to prion disease pathogenesis remains unresolved.

Acknowledgements

It is with great pleasure that I would like to thank my supervisor David Knox for his patience, understanding and guidance during the course of my research and thesis preparation.

I would also like to thank my committee members Dr. Ed Rector and Dr. Joanne Embree for their comments and expertise.

Thank you to Angela Nelson for helping me to navigate the path that it is obtaining a Master's degree in the department of Medical Microbiology at the University of Manitoba.

Thank you to Dr. Michael Coulthart for providing me with the opportunity to obtain my Master's degree in the department of the Prion Disease Program. With a special thanks for the opportunity to travel to NeuroPrion 2006.

Thank you to all members in the department of the Prion Disease Program for making my experience a positive one. With a special thank you to all the students in the department for your help, input, experience, and wisdom.

A huge thank you to Sharon Simon and Michael Stobart for your endless help, support, advice, and kindness.

Thank you to the Natural Sciences and Engineering Research Council of Canada, for funding my degree.

A final thank you to my family, for you unwavering support and love. You truly are the best parents in the world. Without you, none of this would have been possible!

List of Tables

List of Figures

List of Abbreviations

4-HNE	4-hydroxy-2,3-*trans*-nonenal
8-OHdG	8-Hydroxyguanosine
AD	Alzheimer's disease
AMPA/kainate	α-amino-3-hydroxy-5-methyl-4-isoxazolepropionic acid
aRNA	amplified RNA
ATP	Adenosine triphosphate
BSE	Bovine Spongiform Encephalopathy
Ca^{2+}	calcium
cDNA	complementary DNA
CJD	Creutzfeldt-Jakob disease
CNS	Central Nervous System
Cytox	Cytochrome C oxidase
dpi	Days Post Infection
FFI	fatal familial insomnia
FSC	forward angle light scatter
gDNA	genomic DNA
Galacto	Galactocerebrosidase
Gfap	Glial fibrillary acidic protein
GPI	glycosyl phosphatidyl inositol
GSH	glutathione
GSS	Gerstmann-Straussler-Scheinker syndrome
GSSG	oxidized GSH
H_2O_2	hydrogen peroxide
i.c.	intracerebral
Mn-SOD	mitochondrial SOD
Mtap2	Microtubule-associated protein 2
Na^{2+}	Sodium
NGF	nerve growth factor
NMDA	N-Methyl-D-aspartate
NO	nitric oxide
O_2^-	super oxide
OH^*	hydroxyl radical
$ONOO^-$	peroxynitrite
PI	propidium iodide
PrP^c	cellular prion protein
PrP^d	disease prion protein
PrP^{res}	protease resistant prion protein

PrP^{Sc}	Scrapie prion protein
PBGD	Porphobilinogen deaminase
PBS	phosphate buffered saline
PS	phosphatidyl serine
qPCR	quantitative real-time PCR
RA	retinoic acid
RNS	reactive nitrogen species
ROS	reactive oxygen species
RT	reverse transcription
sCJD	sporadic CJD
SOD	superoxide dismutase
SSC	side light scatter
TSE	Transmissible Spongiform Encephalopathy
vCJD	variant CJD

1-Introduction

1.1 Transmissible Spongiform Encephalopathies

Transmissible Spongiform Encephalopathies (TSEs) or prion diseases are rare, invariably fatal neurodegenerative disorders of the central nervous system characterized by a loss of motor control, dementia, paralysis, wasting, and eventual death [1,2]. TSEs have been reported in humans as well as in a variety of animals (see Table 1) [3].

The earliest evidence of TSEs dates back to the 18th century in Iceland when shepherds recognized scrapie, a prion disease of sheep [3]. The name scrapie arose from the observation that affected animals rubbed against the fences of their pens to stay upright, most likely reflecting the manifestation of ataxia [4]. Transmissibility was demonstrated in 1943, when a population of Scottish sheep was inoculated using a formalin extract of lymphoid tissue, unknowingly derived from a sheep with scrapie [4].

The first human TSE disease, Kuru, was described in a remote area of New Guinea in the 1950's by Carleton Gajdusek who later won the Nobel Prize for correctly concluding that the disease was transmitted via the ritualistic eating of the brains of deceased relatives [5]. The transmissibility of Kuru was later demonstrated by the development of the disease in chimpanzees following intracerebral inoculation of homogenate from Kuru infected brains [6,7]. Kuru results in progressive cerebellar ataxia causing victims to become helpless within a few months. Victims display emotional changes, including inappropriate euphoria and compulsive laughter, but rarely display progressive dementia, until advanced stages of disease [7]. No remission or survival has ever been recorded.

Table 1: Transmissible spongiform encephalopathies in humans and animals [3].

Disease	**Host**
Scrapie	Sheep, Goat
Transmissible mink encephalopathy	Mink
Chronic Wasting Disease	Deer, Elk
Bovine Spongiform encephalopathy	Cow
Transmissible Spongiform encephalopathy of captive wild ruminants	Nyala, Gemsbok, Arabian Oryx, Eland Kudu, Scimitar-horned Oryx, Ankole, Bison
Feline Spongifrom encephalopathy	Domestic Cat, Puma, Cheetah, Ocelot, Tiger
Kuru	Human
Sporadic CJD	Human
Familial CJD	Human
Iatrogenic CJD	Human
Variant CJD	Human
Gerstmann-Straussler-Scheinker syndrome	Human
Familial Fatal Insomnia	Human

Based upon the similarities in clinical, pathological and epidemiological data, kuru and scrapie established a new class of diseases, collectively called TSEs [3,7]. Human TSEs are further divided into sporadic, infectious and inherited disorders.

Sporadic Creutzfeldt-Jakob disease (sCJD), the most common type of human TSE, occurs at an incidence of approximately 1 x 10^6 persons per year [8]. The etiology of sCJD is currently unknown. It is hypothesized that the disease could be caused by the horizontal transmission of prions from humans or animals, a somatic mutation of the PrP gene, or by spontaneous conversion of PrP^c into PrP^{sc} [9]. Interestingly, increased susceptibility to the disease has been associated with methionine or valine homozygosity at codon 129 of the *prnp* gene [2,10].

Inherited forms of the disease, familial CJD, Gerstmann-Straussler-Scheinker syndrome (GSS) and fatal familial insomnia (FFI) are transmitted as autosomal dominant traits, which consistently co-segregate with mutations of the *prnp* gene [2,9]. Over 95% of familial CJD cases can be accounted for by four point mutations (codons 102, 178, 200 and 210) in the *prnp* gene and insertions of 5 or 6 octapeptide repeats [3,9]. Most kindred's diagnosed with GSS have a point mutation at codon 102 in the *prnp* gene, although several other mutations have been described [3]. FFI has been associated with the combination of a mutation at codon 178 and methionine homozygosity at codon 129 [3].

The threat of contracting an infectious form of CJD through dietary exposure or iatrogenic transmission has raised the most public concern. Possible routes of iatrogenic

exposure include transplantation of infected tissues, administration of pituitary hormones or blood transfusions from unrecognized TSE positive individuals, as well as the use of contaminated instruments in neurosurgical interventions [11]. The most publicized form of human TSE is vCJD caused by the ingestion of meat products derived from infected cattle. The bovine spongiform encephalopathy (BSE) epidemic first became evident in England in 1985 [4]. It is hypothesized that either BSE was transmitted to cows through feedstuff supplemented with by-products from scrapie-infected sheep or a sporadic case of BSE in a cow initiated the epidemic [2,3]. The conclusion that BSE could be transmitted to humans via the ingestion of contaminated food products, has struck fear into meat eaters world-wide [12]. In addition, it has been suggested that humans, like cows, may be exposed to prions via products of the rendering industry. The white nearly tasteless solid rendered fat (tallow) of cattle and sheep is used in cosmetics, soap and gelatin. Also bone meal, a component of gardening products, may pose a risk to humans upon exposure [3]. To date, all clinical vCJD cases have tested positive for methionine homozygosity at codon 129 [3,4].

1.2 The Protein-Only Hypothesis

In 1997, Stanley B. Prusiner received the second Nobel peace prize in prion research (physiology/medicine) for his discovery of strange proteinaceous infectious particles or "prions" which are resistant to inactivation by most procedures that modify nucleic acids [13]. The proposed absence of nucleic acids, ruling out the involvement of a bacteria or slow virus, resulted in the protein-only hypothesis [13].

The hypothesis states that the pathological protein, PrP^{sc} is a misfolded conformer composed of a normal cellular protein, the prion protein or PrP^{c}. PrP^{sc} is thought to reproduce by preferentially binding to homologous PrP^{c} and converting it into nascent PrP^{sc} [9]. Evidence in support of this hypothesis is provided by transgenic studies in which PrP^{c} knockout mice have proven to be resistant to scrapie infection. The mice lack symptoms and pathology of the disease and do not allow PrP^{sc} replication to occur [9,14]. Furthermore, even heterozygous $prnp^{0/+}$ mice are partially protected, with incubation times and disease progression being inversely related to the level of PrP^{c} [14].

Presently, it remains unclear whether PrP^{sc} alone accounts for the infectious agent. Although PrP^{sc} is always present in infected animal brain, and is never present in a normal animal, no one has ever been able to generate infectious PrP^{sc} by inducing misfolding of the prion protein *in vitro* [15,16]. This has caused some researchers to support an alternative viral hypothesis. They suggest that TSEs are caused by a 25-30nm virus-like particle with a protected nucleic acid genome, which is less than 4kb. Some key features which support this hypothesis are; the infectious particles of 25-30nm can be separated from all forms of PrP, the route of TSE transmission is the same as some viruses, and TSE agents of differing virulence have virus-like interfering capacities [16,17,18,19].

1.3 Biochemistry of Prion Proteins

The pathogenic mechanism underlying TSEs is the conformational conversion of the normally occurring cellular prion protein (PrP^{c}) expressed by a broad range of cells, and

in particular by neuronal cells into an infectious agent termed protease resistant PrP (PrP^{res}) or Scrapie PrP (PrP^{sc}). This altered isoform is able to induce further transitioning of normal PrP into the infectious PrP^{d}, which accumulates in the brain. The accretion of PrP^{sc} in the brain is associated with neuronal death, gliosis, and extensive (sponge-like) tissue vacuolization [20].

The gene coding for PrP^{c}, *prnp*, is on the short arm of chromosome 20 in humans [2]. PrP^{c} is encoded in a single exon, which consists of 254 amino acids (see Figure 1) [2,21]. It is a membrane bound protein with a molecular weight of approximately 27-35 kDa [9]. Structural studies of PrP^{c} have revealed that its' N-terminal half is a flexible, random coil lacking any secondary structures, while its' C-terminal half is structured, consisting of three α-helices (with a disulfide bond connecting helix 2 and helix 3) and a short β pleated sheet [2,22,23]. Two main signal sequences are encoded in the primary structure of this protein, one at the N-terminus and the other at the C-terminus [23]. The N terminus is cleaved at residue 23, generating a signal peptide for prion trafficking into the endoplasmic reticulum [2,23]. The C terminus is cleaved at residue 231, mediating the attachment of the glycosyl phosphatidyl inositol (GPI) anchor [2,23]. PrP^{c} also contains an octapeptide-repeat in the N-terminus, consisting of four sequential repeats of the sequence Pro-His-Gly-Gly-Gly-Trp-Gly-Gln, which serves as the major copper (II) binding site [24,25].

PrP^{c} is synthesized in the rough endoplasmic reticulum and is imported co-translationally into the smooth endoplasmic reticulum [2,23]. During synthesis, the N-terminal signal

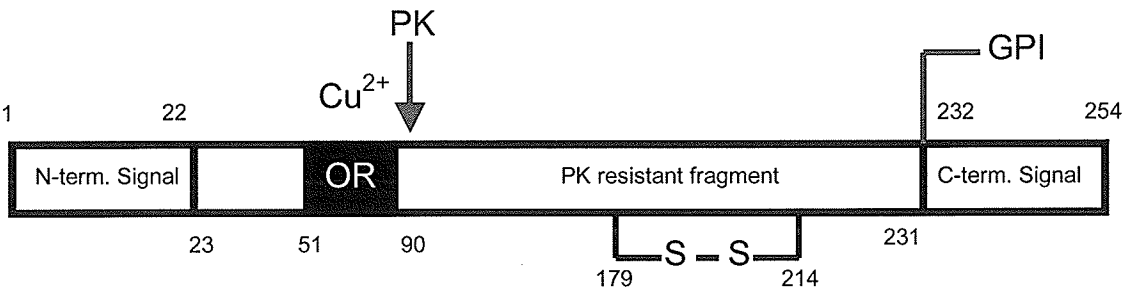

Figure 1: The primary structure and posttranslational modifications of the prion protein. OR is the octapeptide repeat sequence involved in copper binding [21].

peptide must be cleaved, oligosaccharide chains are added (generating unglycosylated, monoglycosylated and diglycosylated PrP^c isoforms), a single disulfide bond is formed, and the C-terminal is cleaved and modified for the attachment of the GPI anchor [2,23]. PrP^c is then translocated through the Golgi complex and anchored to the cell surface via its GPI anchor [2]. Currently the function of PrP^c is unknown. Researchers have hypothesized many functions including: neuroprotection, playing a role in long-term memory, acting as an antioxidant, being a major copper-binding protein or as a copper delivery protein, and playing a role in signal transduction [2,26].

Although the function of PrP^c remains elusive, it has been firmly established that the conversion of PrP^c to PrP^{res}, via an unknown autocatalytic process, is found in all prion diseases [4]. PrP^{res} has an identical amino acid sequence (primary structure) as PrP^c, but significantly differs in respect to its biochemistry and/or secondary/tertiary/quaternary structure [21,27]. PrP^c is soluble in detergents and sensitive to proteinase K digestion, whereas PrP^{res} is highly insoluble in common detergents tending to aggregate and digestion of PrP^{res} with proteinase K leads to the generation of protease resistant fragments with molecular weights of 27-30kDa (see Figure 2) [9]. These fragments are truncated at their N-terminus, yet still retain full infectivity [2,4,22,27]. As well, boiling PrP^{res}, or treating it with alcohol does not reduce its level of infectivity [12]. Structurally, PrP^{res} differs from PrP^c as it has a higher content of β-sheets and fewer α-helices; 54% as compared to 43%, and 21% as compared to 30% respectively [22]. Thus the β-pleated domains arise at the expense of the unstructured N-terminal region [22]. It should be noted that protease resistance might not be necessary for neurotoxicity [2].

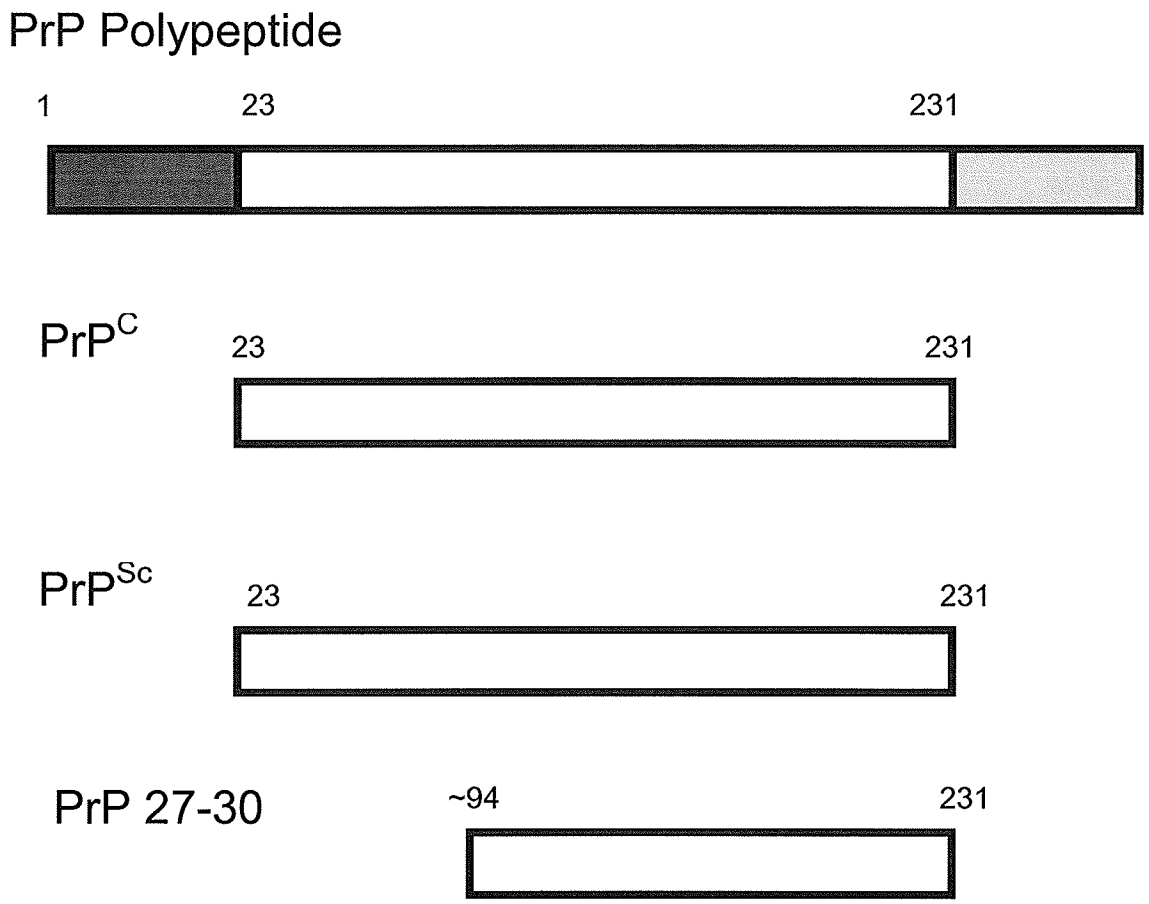

Figure 2: Primary structures of the various prion protein isoforms [9].

1.4 Prion Strains and the Species Barrier

Classically, scientists have described a strain as a specific biologic version of a microorganism (i.e. bacterium or virus). The identity of a strain is defined by its genetic makeup, or nucleic acid sequence. However, according to the protein-only hypothesis, which describes the pathogenic and infectious prion, PrP^{sc}, as consisting solely of protein and demonstrating a complete lack of nucleic acid, the meaning of the term "strain" is difficult to comprehend. Typically prion strains are distinguished based upon characteristics exhibited by the host in response to the disease. These include; length of incubation time, clinical manifestations and phenotypic traits such as type and distribution of the lesions and topography of PrP^{sc} deposition [28,29]. They can also be distinguished based upon sensitivity to proteinase K digestion, electrophoretic banding patterns following proteinase K digestion, and the heterology between the PrP^{sc} amino acid sequence and the host PrP genotype [30].

Transmission of prion diseases between different species (such as from sheep to mice) is inefficient due to a species barrier. The species barrier is determined based upon the prolonged incubation period during the first passage of prions. Only a small fraction of inoculated animals from a different species are affected after prolonged exposure. However, subsequent propagation in the new host results in efficient transmission and a shortening and stabilizing the incubation time [9,28]. The extent of the species barrier depends upon many things: the homology of amino acid sequences, the conformation of the exogenous prion strain and the ability of the host to replicate the conformation of the inoculum [4,9,28,29].

1.5 Oxidative Stress and Prion Disease

There is a wealth of evidence implicating oxidative stress in the pathology of many neurodegenerative diseases. Oxidative stress is used to describe that imbalance, which results from a mismatch between the production of free radicals and the ability of the cell to defend against them. Oxidative stress occurs as a result of one of three factors: 1) an increase in reactive oxygen species (ROS), 2) a decrease in antioxidant protection, or 3) the failure to repair oxidative damage.

Prn-$p^{0/0}$ mice, as well as scrapie-infected mice and derived cell lines show increased oxidation of lipids and proteins and decreased superoxide dismutase (SOD) activity. Scrapie infected mice and derived cell lines also show decreased glutathione peroxidase activity as well as increased levels of nitrite, nitrate and by-products of nitric-oxide degeneration [15,20,31,32,33,34,35,36].

Human models show different oxidation profiles depending upon the type of prion disease. In cases of sCJD redox metal deposition is not associated with PrP^d deposition and lipid peroxidation, and heme oxygenase 1 induction are not detected [32]. However, in cases of GSS and vCJD, metal deposition is always associated with PrP^d deposits and weak lipid peroxidation and heme oxygenease 1 induction is detected [32]. Interestingly the DNA adduct 8-hydroxyguanosine (8-OHdG) is found to be increased in both sCJD and GSS [32].

1.6 Prion Pathogenesis

The unusual properties that prion diseases possess have made studying the pathogenesis of the disease extremely difficult. The incubation period can range from a few months to several years and there is no classic inflammation or disease-specific immune response associated with infection [2,3,9]. Prions exert their destructive effects exclusively within the CNS. They cause vacuolation and death of nerve cells, activation of astrocytes and microglial cells and the invariable lethal impairment of electrical functions of the brain [22]. The precise cause of neurodegeneration remains poorly understood.

One hypothesis is that neurodegeneration is the result of disease-associated oxidative stress. Prion infection may alter redox homeostasis within the CNS by converting PrP^c into PrP^d as well as by stimulating the innate immune system or by altering a wide variety of cellular events.

The loss of PrP^c as it is converted into PrP^d may result in a loss of antioxidant protection. There is some evidence that PrP^c when bound to copper possesses SOD-like activity, thus it is capable of scavenging the ROS superoxide (O_2^-) [38]. However, the physiological function of PrP^c as an antioxidant is a widely debated issue. Some studies have shown that PrP^c has SOD-like activity, while other studies refute the possibility [37,38,39,40]. PrP^c may also indirectly provide antioxidant protection. PrP^c binds copper via its octapeptide repeat regions and hydrophobic domain in the N-terminus [9,41]. Trace amounts of copper are essential as a cofactor of many enzymes in cells; however its redox reactivity may cause irreversible damage to cells and tissues. Reaction of the reduced form of copper

with oxygen produces toxic ROS such as O_2^-, H_2O_2, and the hydroxyl radical (OH*) [42,43]. Thus any functional disturbance of PrP^c may result in oxidative damage as a result of excess free copper.

Although no disease-specific immune response is associated with prion disease, there is increasing evidence that inflammation plays a key role in neurodegeneration. Disease-associated inflammation is partially due to the activation of glial cells in response to neuronal cell damage [44,45,46]. Activated astrocytes and microglial cells release of a large number of pro-inflammatory cytokines and chemokines, as well as large amounts of nitric oxide and ROS [44]. For example, in Alzheimer's disease (AD) it has been suggested that activated astrocytes swamp their associated neurons with nitric oxide (NO) and the highly lethal ROS peroxynitrite ($ONOO^-$) [44]. In AD it has also been shown that activated microglial cells undergo an oxidative burst releasing ROS, such as O_2^- and H_2O_2 [47].

Oxidative stress has the potential to alter a wide variety of cellular events. Prion infection is associated with mitochondrial dysfunction, proteasome dysfunction, and changes in Ca^{2+} metabolism.

Brains of scrapie-infected mice show structural and functional damage of mitochondria [48]. Choi *et al.* found that in the hippocampus and cerebral cortex, most mitochondria had lost their cristae or were structurally abnormal, and some had also lost their matrix. An interesting possibility is that the breakdown of membrane phospholipids as a result of oxidative stress induces mitochondrial dysfunction in the brains of scrapie-infected mice

[48,49]. Functional damage to mitochondria manifests in decreased levels of respiratory enzymes, depletion of ATP, and depletion of Mn-SOD [48,49,50]. Significant decreases in the amount of Cytochrome C Oxidase (Cytox) in the cerebral cortex, brain stem and cerebellum of scrapie-infected mice have been described [48]. This loss may lead to an increase in ROS, as Cytox normally prevents the release of partially reduced oxygen species during oxidative phosphorylation [50]. Functional damage to mitochondria resulting in an ATP deficiency in turn limits the production of reduced GSH. The reduced concentration of antioxidant protection triggers an increase in oxidative stress, which in turn leads to mitochondrial dysfunction and a further loss of antioxidant protection [48].

In mammalian cells, the majority of intracellular proteins are degraded by the proteasome [51,52]. Disturbances or obstruction of the ubiquitin-proteasome system may cause oxidative stress, impair cellular function and increase sensitivity to neurotoxins such as 4-HNE, H_2O_2, and neurotoxic metal ions [51]. Levels of proteasome activity are decreased in prion disease [52]. Confirming these findings, Kang *et al.* demonstrated that increased ubiquitination of brain proteins and the appearance of detectable levels of PrP^{res} were found to correspond with initial clinical symptoms in scrapie-infected mice [53]. This may be particularly detrimental, as Ma *et al.* demonstrated that upon proteasome inhibition an increasing amount of cytosolic PrP^{c} was converted to a PrP^{sc}-like conformation [54]. It has been suggested that impaired proteasome function may be the result of PrP^{sc} overloading the system; i.e. it is difficult to degrade and is therefore clogging up the system. Currently the role between impaired proteasome function and oxidative stress remains

unknown. Impaired proteasome function may allow abnormal proteins, such as PrP^{sc} to accumulate/aggregate causing oxidative damage [51]. Alternatively, oxidative ROS may directly damage the proteasome altering the structure and inhibiting degradative functioning, thereby causing the proteasome to become overloaded with proteins [51].

The presence of PrP^{d}, which tends to form aggregates, may modify the intracellular redox status and free Ca^{2+} levels [55,56]. Modifications in the intracellular redox status are associated with a dramatic increase in ROS. Increases in ROS may be the consequence of Ca^{2+} entry into the cells. A Ca^{2+} influx could stimulate oxidative metabolism aimed at providing ATP needed to support the activity of membrane ion pumps involved in clearing excess Ca^{2+} [55]. Stimulation of oxidative metabolism would also indirectly increase the number of ROS, compounding the problem.

There are two main theories of prion pathogenesis [46]. The first is the "gain of function hypothesis" which suggests a neurotoxic effect of the abnormally folded, no longer degradable protein, PrP^{d} that is deposited in considerable amounts in the brains of infected individuals. The second is the "loss of function hypothesis" which suggests that the continuous conversion of PrP^{c} to PrP^{d} might lead to decreased availability or functional impairment of normal PrP^{c} activities, potentially losing/altering its neuroprotective effect.

Neurodegeneration as a result of disease-associated oxidative stress supports both the "loss of function hypothesis" and the "gain of function hypothesis".

The loss of PrP^c is thought to result in a loss of antioxidant protection. The decreased SOD activity, combined with increased levels of lipid and protein oxidation observed in Prnp $^{0/0}$ mice provides support for this hypothesis [20]. As well, the loss of PrP^c may circuitously result in oxidative stress as it is no longer available to bind copper.

The presence/gain of PrP^d is thought to directly and/or indirectly result in oxidative damage. Scrapie-infected mice display increased levels of oxidized lipids, proteins and DNA as well as increased levels of nitrite, nitrate and by-products of nitric-oxide degeneration. It has been suggested that PrP^d may interact with cell membranes and essentially destabilize them [55,56]. Intracellular ROS elevation following exposure to PrP^d aggregates could lead to the failure in regulating appropriate membrane proteins such as receptors or ion pumps, and/or to impairment of mitochondrial function, ultimately leading to neuronal cell death [57]. Additionally PrP^d may be clogging up the ubiquitin-proteasome system, causing oxidative stress and increasing sensitivity to neurotoxins. A dramatic increase in inflammation has been associated with the presence of PrP^d. In the CNS, activation of glial cells in response to neuronal insult results in the production of ROS and reactive nitrogen species (RNS).

The oxidative state in cells depends upon the delicate balance between the production of free radicals and the ability of the cell to defend against them. In the case of prion disease, cells are being subjected to compounding insults. PrP^d is increasing the production of free radicals and at the same time decreasing the amount of PrP^c, thereby

decreasing the ability of the cell to defend against them. Therefore, it is most likely a combination of both hypotheses, which results in neurotoxicity.

1.7 Project Goals

My hypothesis was that oxidative stress was partially responsible for prion-provoked neurotoxicity. The objective of my project was to demonstrate that oxidative stress is a cause rather than a consequence of prion disease development and progression. To test my hypothesis I used both *in vitro* and i*n vivo* model systems. The *in vitro* system was a neuronally enriched culture of P19 cells used to investigate the role of oxidative stress in $PrP^{106-126}$ neurotoxicity. The *in vivo* system was ME7 infected C57BL/6 mice used to measure the level of oxidative stress throughout disease and to determine the effect of an antioxidant diet on disease progression.

The Search for an *in vitro* Model

2-Introduction

Cell culture models represent versatile and advantageous experimental models of TSEs. These models impart the ability to: 1) analyze the biological properties of PrP^{c} and PrP^{sc} at the molecular and cellular levels, 2) determine the nature of the infectious agent and factors governing its propagation, 3) search for biological markers of infection of either diagnostic or physiological interest, and 4) screen potentially therapeutic drugs [58,59,60]. Additionally, *in vitro* models are relatively inexpensive.

The search for prion susceptible cell lines began as early as 1970 when Clarke and Haig established the SMB cell line from the brain of a mouse, which was inoculated with the Chandler strain of mouse adapted scrapie [61]. The most traditional approach used to propagate prions *in vitro* is to directly apply scrapie infected brain homogenate or scrapie-associated fibrils to neuronal cells in culture. Neuronal cells are an attractive tissue culture model for the study of TSEs as they express high levels of PrP^{c} and their loss is one of the main manifestations of prion disease. Presently, N2a cells, GT1 cells and PC12 cells are the three main neuronal cell lines used to study prion diseases. This is because although most cell lines and primary cells express PrP^{c}, only a limited few are susceptible to prion-infection.

The mouse neuroblastoma N2a cell line, which is chronically infected with mouse-adapted scrapie, is the most intensively described and commonly used cell line [60,62,63,64]. N2a cells are a simple, undemanding *in vitro* model of TSE infection. They are easy to manipulate, grow quickly and can be infected with a number of different TSE strains.

They support stable and persistent replication of PrP^{sc} allowing reproducible results to be generated. However, only small populations of N2a cells appear to be susceptible to prion infection, thus they must be subcloned or PrP^{c} must be overexpressed to improve PrP^{sc} yield [62,63]. Another disadvantage of N2a cells is that no phenotypic alterations are visible upon exposure to prions [58]. Finally, N2a cells growth and viability remains unaffected by prion infection [62]. This is contradictory to what is observed *in vivo* where neurons are not actively dividing.

Another widely used cell line is the hypothalamic or GT1 cells, which is an immortalized well-differentiated neuronal cell line. They originate from the central nervous system and were established from gonadotropin-releasing hormone neurons in transgenic mice [65,66]. Overall they resemble neuronal cells with neurite extensions. They have fast Na^{+} channels found in neurons and express neuronal cell markers. Originally they were designed for the study of hypothalamic neurosecretory neurons that regulate reproduction [66]. When infected with prions, GT1 cells show reduced viability, morphological signs of neurodegeneration, vacuolation and characteristics of apoptosis [65]. However although well-differentiated, GT1 cells retained their ability to undergo mitosis, unlike the *in vivo* situation where neurons are postmitoic. As well, they must be stably transfected with the nerve growth factor (NGF) receptor to be able to withstand persistent prion infection [65].

PC12 rat pheochromocytoma cells, in the presence of low concentrations of NGF cease cell division and undergo morphological, physiological and biochemical differentiation. In the presence of NGF they develop neurite extensions, exhibit excitability and synthesize neurotransmitters. They allow specialized neuronal functions to be analyzed

and are thought to be similar to peripheral nerve cells [67,68]. PC12 cells infected with mouse scrapie were the first documented account that the species barrier could be overcome in cell culture [67]. Some drawbacks associated with PC12 cells include a lack of morphological change between infected and control cells and that NGF is required for replication to be maintained [58,68]. Removal of NGF from infected cells reverses the differentiation process with the resumption of cell division resulting in failure of scrapie replication [68]. As well, NGF increases the expression of the PrP gene, which most likely does not mimic an *in vivo* situation.

N2a mouse neuroblastoma cells, PC12 rat pheochromocytoma cells and GT1 hypothalamic neurons, have all provided valuable insights into the study of TSE infection. However, new cell lines are needed to study prion disease as the above cell lines have distinct disadvantages outlined above.

P19 mouse embryonal carcinoma stem cells treated with retinoic acid (RA) are able to differentiate into an enriched neuronal culture with some glia- and fibroblast like cells, making them an excellent *in vitro* model [69]. *In vivo,* neurodegeneration as the result of oxidative stress is most likely due to the complex interactions between different cell types. P19's divide rapidly, maintain their ability to differentiate after many passages, produce stably transfected clonal sub-lines at a high frequency that are still able to differentiate [69]. Many observations have been made suggesting that P19 neurons closely resemble neurons present in the mammalian nervous system. P19 neurons morphology is similar to that of cultured brain cells, are stable post-mitotically, possess functional synapses and have functional ionotropic glutamate receptors of both N-Methyl-D-

Aspartate (NMDA) and α-amino-3-hydroxy-5-methyl-4-isoxazolepropionic acid (AMPA/Kainate) types which are all hallmarks of neurons located in the CNS [69]. As well they express a variety of neurotransmitter, associated gene transcripts and enzymes, a number of cell surface carbohydrate antigens characteristic of neurons and a variety of neuron specific genes and proteins not directly involved in neurotransmission [69].

P19 cells were chosen, as they possess two distinct advantages. First, they are stable post-mitotically. Oxidative insult to neurons within the CNS results in their death, and eventual death of the organism. This is because neurons within the CNS are terminally differentiated, lacking the ability to regenerate. It is very difficult to study prion induced cell death in cells that are able to continually grow. Second, under the influence of RA a mixed population of neuronal and glial cells is generated. The culture generated may be a better representation of events that occur *in vivo*. This is because *in vivo* the CNS is dynamic with neurons, glial cells and non-neuronal cells all physically interacting. Thus neuronal cells may respond differently to oxidative stress when isolated from other cell populations

Isolating PrP^{sc} from brain homogenate has proven to be cumbersome and taxing with the resultant product being of questionable purity. This difficulty has lead many researchers to primarily use synthetic peptides. In 1993, Forloni *et al.* identified a 21 amino acid peptide ($PrP^{106-126}$) that appeared to emulate the neurotoxic core of PrP^{sc} [70]. Currently $PrP^{106-126}$ is the predominant model used in *in vitro* studies. This synthetic peptide is rich in β-sheet structure, forms aggregates that are detergent insoluble and proteinase-K resistant, is cytotoxic most likely via the programmed cell death pathway, is more soluble

than PrP^{sc}, can be used in a level 2 laboratory and is easy to manipulate in cell culture studies [71].

A neuronally enriched culture of P19 cells will be used to investigate the role of oxidative stress in PrP^{sc} neurotoxicity. Specifically, it will be determined if oxidative stress is occurring prior to neuronal cell death as a result of prion infection. Cell death will be measured using flow cytometry and the oxidative state of the cells will be assessed. It is expected that levels of oxidative stress will increase prior to cell death indicating that changes in redox status play a fundamental role in the pathogenesis of TSEs.

2.1 Project Goals

The goals of this project were:

1. To design an *in vitro* model suitable for the study of prion pathogenesis.
2. To investigate the role of oxidative stress in $PrP^{106-126}$ neurotoxicity.

3-Materials and Methods

3.1 Cell Culture

3.1.1 Maintenance of parental cells in the undifferentiated state

P19 embryonic carcinoma stem cells were maintained in P19+ media (DMEM high glucose, no L-glutamine or amino acids, supplemented with 10% FBS, 1% antibiotic/antimycotic and 0.2% normocin) at 37°C, 5% CO_2 in a Forma Scientific CO_2 water-jacketed incubator.

3.1.2 Neuronal Differentiation of P19 mouse EC stem cells

An expontentially growing culture of P19 cells were lifted using trypsin, the cells were counted using a Bright-Line hemocytometer (Hausser Scientific, cat. #3120), and plated at a concentration of 2.5 x 10^4 cells/mL in 6 well collagen coated plates (BD biosciences BIOCOAT cat. #CACB355400). The cells were grown at 37C / 5% CO_2 for 24 hours. To initiate the differentiation process, old media was removed and replaced with $P19^+$ media containing 10^{-6}M retinoic acid (dissolved in 95% ethanol). On the first day, all of the media was removed and replaced with 5+ day old Almazan media (see Appendix 1). On the second, third, fifth, seventh and ninth day, half of the old media was removed and replaced with 5+ day old Almazan media. During the removal and replacement of media, the culture plates were tilted at about 45° in an extremely gentle manner, care being taken not to add media directly on the cells. New media was added drop by drop.

3.2 Composition of the Cultures

3.2.1 Quantitaive real-time PCR

3.2.1.1 Cell-type specific transcript plasmid construction:

Calibrator plasmids for each cell-type specific transcript were constructed. Briefly, primers were designed using the computer program Primer Select from DNASTAR. A PCR reaction was performed, the product was cleaned up using the ChargeSwitch PCR clean-up kit (Invitrogen, cat. #CS12000) and ligated into either pCR2.1 vector or pCR4-Topo vector. The ligation mixture was transformed into TOP 10 E.coli cells. Cells were grown on LB + 100μg/mL carbenicillin plates at 37°C overnight. White colonies were picked from the plates and grown in 2mL LB + 100μg/mL carbenicillin at 37°C overnight with shaking (225rpm). Plasmid was isolated using QIAprep Spin Miniprep kit (Qiagen, cat. #27106) and submitted for sequencing in the DNA Core Facility at the Canadian Science Centre for Human and Animal Health (Winnipeg, Canada).

See Appendix 2 and 3 for complete procedural details.

3.2.1.2 Real-time PCR using Roche 1.0 Lightcycler

Standard curves for PBGD, Mtap2, Gfap, and Galacto were generated. Briefly, the plasmids (generated above) were diluted in Nuclease-free water to an initial concentration between 200pg/μL - 200fg/μL. 20 ng μL^{-1} pGEM-NZ empty vector was added to stabilize the target plasmid concentration over time. The mixture was serially diluted in tenfold increments and amplified on the Roche LightCycler® Real-Time PCR machine. Using the Roche LightCycler® 1.0 and the Relative Quantification Software

version 1.0 (Roche Diagnostics), coefficient files were created from exported standard curves of target genes Mtap2, Gfap and Galacto and the reference gene, PBGD.

See Appendix 4 for complete procedural details.

3.2.1.3 cDNA Synthesis for RT PCR

On days 3-9 of the differentiation process, total RNA was extracted using the RNeasy Mini Kit (Qiagen cat.# 74104). The RNA was treated with TURBO DNA-free (Ambion cat.# 1907) to remove any genomic DNA contamination. 1-2 ug of total RNA was reverse transcribed into cDNA using Superscript III (Invitrogen, cat. #18080-093) according to manufactures protocol. All incubation steps were performed using a PTC-200 MJ Thermocyler. The cDNA obtained was concentrated using YM-30 Microcon centrifugal filter units (Millipore cat.#42422). Sample concentrations were determined using a NanoDrop® ND-1000 and then adjusted to 25ng/ul.

3.2.1.4 Cell-type Quantification using q-PCR :

Relative quantification of all cDNAs was performed using the SYBR® Green Taq ReadyMix for Quantitative PCR, Capillary Formulation (cat. #S1816), on a LightCycler® 1.0 Real-time PCR instrument. Amplification conditions utilized for qPCR of target cDNA can be found in Appendix 3. Following amplification, the purity of the product was confirmed by melt curve analysis and visualized on a 1% agarose gel for fragment size. Relative expression levels were calculated using the Relative Quantification software from Roche Diagnostics, with cell-type specific gene expression levels normalized relative to PBGD expression levels.

3.2.2 Immunocytochemistry

3.2.2.1 Cell-type Quantification using Immunocytochemistry:

Briefly, the differentiation process was carried out as described above, except cells were grown on collagen coated coverslips in 6 well plates. On the appropriate day of the differentiation process, the coverslips were removed from the bottom on the 6 well plate and rinsed with PBS. 4% paraformaldehyde was added for 5 minutes to fix the cells and 0.1% Triton X was added for 5 minutes to permeabilize the cells.

The cells were washed with PBS and incubated with the appropriate primary antibody for 30 minutes. The cells were washed with PBS and incubated with appropriate secondary antibody for 30 minutes (see Appendix 5). The cells were washed with PBS, incubated with the appropriate chromagin for 20 minutes and washed with PBS. When a second antigen was targeted, this process was repeated.

Coverslips were placed into a silver dipping rack, and dipped into hematoxylin stain for 3 minutes. Purple colour was washed off of the coverslips by placing the rack into a running water bath. The rack was dipped into Scott's tap water substitute for 30 seconds and then placed back under the running water bath for 30 seconds. The cells were dehydrated by dipping the rack into 70%, 80%, 90%, 100% ethanol and xylene for 10 seconds and mounted onto a slide.

3.3 Flow Cytometry

3.3.1 Preparation of Differentiated P19 cells for Flow Cytometry

The Annexin V-FITC Apoptosis Detection Kit (Sigma-Aldrich, cat. #APOAF) was used to distinguish between alive, apoptotic, and dead P19 neuronal cells.

Initially, positive control experiments were conducted using Staurosporine. Briefly, on Day 8 of the differentiation process 3 wells were treated with 1μL of staurosporine (Sigma-Aldrich, cat. #S 5921) (1μg/mL) and incubated at 37°C for 1 hour, 2 hours and 4 hours respectively. The cells were then prepared for flow cytometry as described below.

For all other experiments, on Day 8 of the differentiation process 3 wells were chosen as controls; 1 well was the negative control (healthy looking cells), 1 well was the PI positive control (greatest percentage of dead cells) and 1 well was the FITC positive control (healthy looking cells). The FITC positive control was then treated with 1μL of staurosporine (1μg/mL) and incubated at 37°C for 1 hour.

Media, containing floating cells and debris, from control and sample wells was transferred into 15mL conical tubes. The tubes were spun at 162 x g for 5 minutes and the supernatant discarded. The cells were gently resuspended in 1mL of Accumax (Chemicon, cat. # SCR006), a cell detachment solution of proteolytic, collagenolytic and DNAse enzymes and incubated at 37°C for 30 minutes, to create a single cell suspension. 1mL of Accumax was also added to the original control and sample wells to detach the

cells from the collagen matrix, incubated at 37°C for 30 minutes, and then the cells were gently dislodged. The cells from both wells and tubes were combined, centrifuged at 162 x g for 5 minutes and the supernatant discarded. The cells were washed twice with PBS. Cells were filtered using a 35 micron filter unit (Becton Dickinson, cat. #352235). The cells were centrifuged at 162 x g for 5 minutes and the supernatant was discarded. The cells were resuspended in 100μL of Annexin-Binding buffer. Add 5μL of annexin V-FITC to the FITC positive control, 10μL of propidium iodide to the PI positive control and no dye to the negative control tube. 5μL of annexin V-FITC and 10μL of propidium iodide was added to all samples. The samples were then incubated at room temperature for exactly 10 minutes in the dark.

3.3.2 Analysis of Immunofluorescence by flow cytometry

Flow cytometry was carried out on a Becton Dickinson FacsCalibur flow cytometer. For all experiments data was acquired for 10 000 cells. Forward angle light scatter (FSC) vs. 90° side scatter (SSC) dot plots were used to identify P19 neuronal cells. FITC and Propidium iodide fluorescent signals were measured on a logarithmic scale. The parameters used to identify the neuronal cells (G5 subpopulation) can be found in Table 2.

Table 2: Flow Cytometry parameters used to identify the neuronal cells (G5 subpopulation).

Instrument Settings			
	Voltage	**Amp Gain**	**Mode**
FSC	E-1	7.04	Linear
SSC	372	1.0	Linear
FITC	474	1.0	Logarithmic
PI	412	1.0	Logarithmic
Threshold			
	Primary Parameter:	FSC	
	Value:	52	
Compensation			
	FITC – 1.4% PI		
	PI – 28.8% FITC		

4-Results

4.1 The Design of an in vitro model of prion infection

The pathogenic mechanism underlying TSEs is the conformational coversion of PrP^c into PrP^{sc}. The accretion of PrP^{sc} in the brain is associated with vacuolation and death of nerve cells, activation of astrocytes and microglial cells and the lethal impairment of electrical functions of the brain [25]. Nerve cells are an attractive *in vitro* model as they express high levels of PrP^c making them a primary target of PrP^d. In prion disease the loss of nerve cells is consistently linked to neurodegeneration and eventual death. As a result, a neuronal-enriched culture of P19 cells was used to investigate the role of oxidative stress in PrP^{sc} neurotoxicity.

4.2 Growth and maintenance of a neuronal-enriched culture of P19 cells

4.2.1 Maintenance of parental cells in the undifferentiated state

Dr. Micheline Paulin-Levasseur from the University of Ottawa graciously donated the original culture of P19 mouse embryonal carcinoma stem cells. To maintain a population of undifferentiated P19 cells, cells were initially plated at ~1.5 x 10^4 cells/mL and grown at 37°C, 5% CO_2 in a Forma Scientific $C0_2$ water-jacketed incubator. The parental cells were split 1/10 once they had reached ~30-50% confluence (see Figure 3). It was determined that the cells must be passaged at least four times before beginning the differentiation process to ensure maximal efficiency of differentiation.

4.2.2 Neuronal Differentiation of P19 mouse EC stem cell

The differentiation process is very sensitive and as such stringent conditions were necessary. Cells could only be grown on a collagen-coated surface and the serum-free

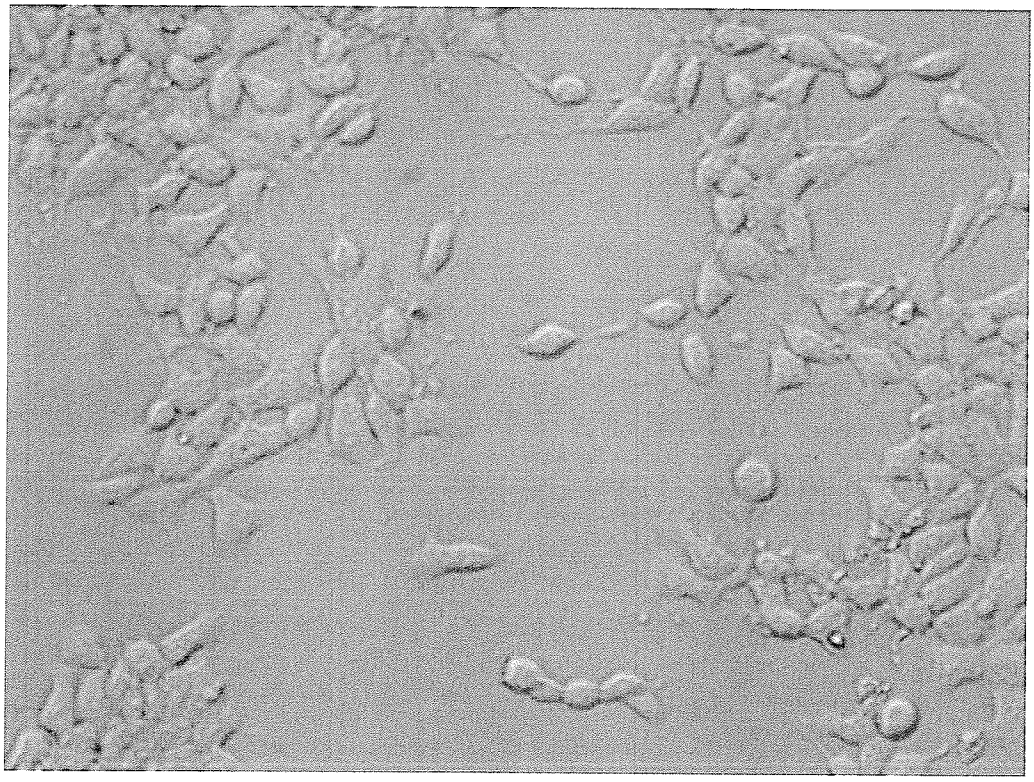

Figure 3: Undifferentiated P19 cells at approximately 50% confluency.

media used for promoting neuronal growth had to be made 5 days before use. As well, the media needed to be changed every day for Days 1-3 of the differentiation process and then every second day (Days 5 and 7).

Parental P19 cells at a confluency of 50-70% were treated with 10^{-6}M retinoic acid initiating differentiation into an enriched neuronal culture with some glia- and fibroblast like cells. A minor die-off is noticed in the cultures after the treatment with retinoic acid (Day 1). By the third change of serum-free medium (Day 3), a substantial portion of the total cell population is dead. Beginning on Day 4, you notice the formation of embryoid bodies (aggregations of differentiating cells) along with neurite extension from above and below the bodies. Cell death of neuronal cells should be minimal until day 8 and a modest proliferation of non-neuronal cells is apparent. Figure 4 shows the differentiation process described above.

4.3 Determining Culture Composition

4.3.1 Determining Culture Composition using Immunocytochemistry

Immunocytochemical staining with cell-type specific antibodies was used to qualitatively determine the composition of the culture throughout the differentiation process. Early in the differentiation process (Day 4 and 5) you are able visualize the initial stages of neuronal cell proliferation (see Figure 5). The culture appears to be composed of entirely P19 parental cells and neurons, astrocytes and oligodendrocytes do not appear to be present. By Day 8 in the differentiation process you see a large number of elaborate neural networks, with a few astrocytes and little/no oligodendrocytes (see Figure 6).

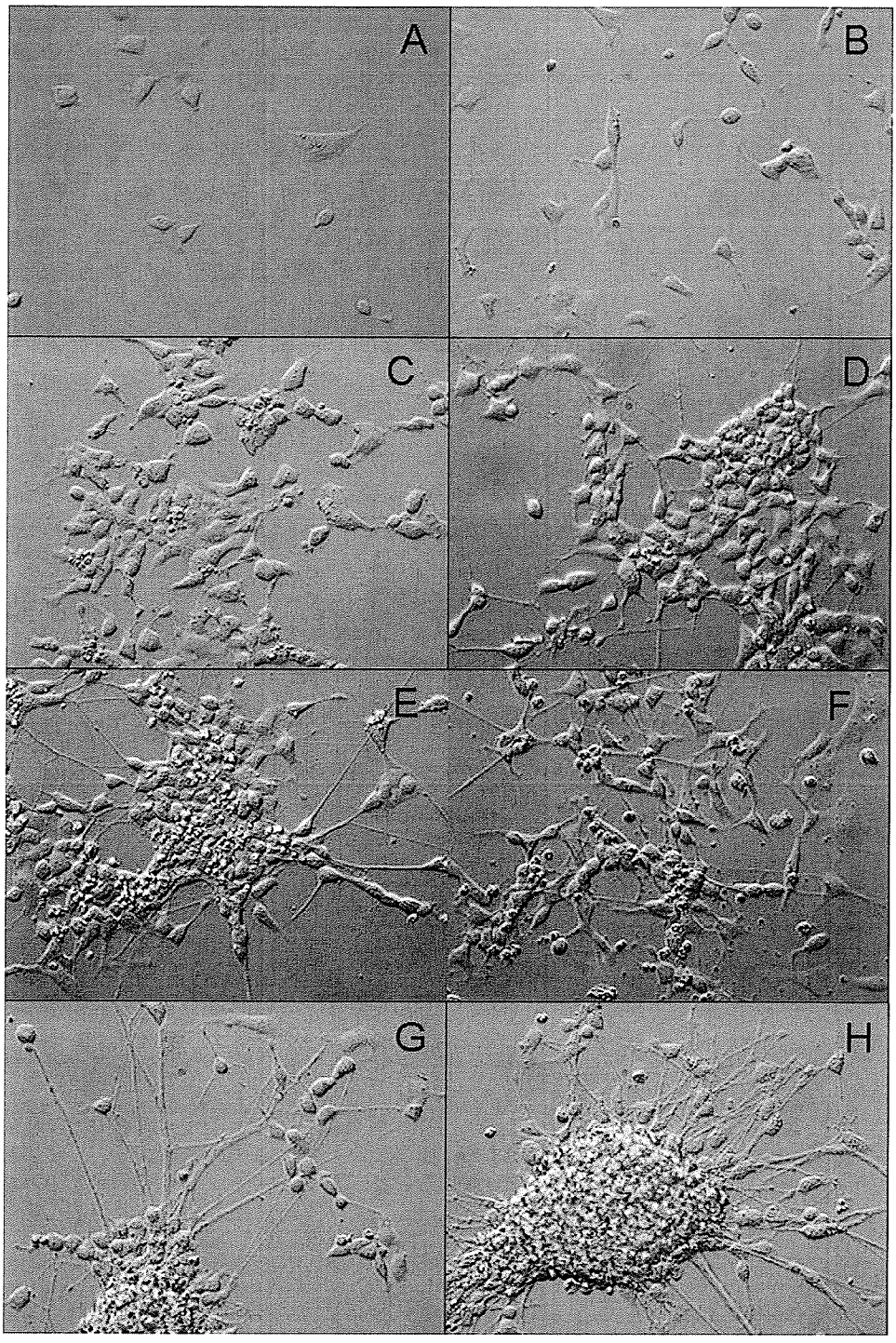

Figure 4: Neuronal differentiation of P19 mouse EC stem cells. Day 1-8 of the differentiation process correspond to A-H. 10^{-6}M retinoic acid was added to parental P19 cells. On Day 1, a minor die-off is noticed in the cultures (A). On days 2 and 3, cells recover from the retinoic acid treatment and begin to proliferate (B-C). Beginning on Day 4, you notice the formation of embryoid bodies and neurite extensions (D-F). By Day 7/8, you can visualize elaborate neural networks (G-H).

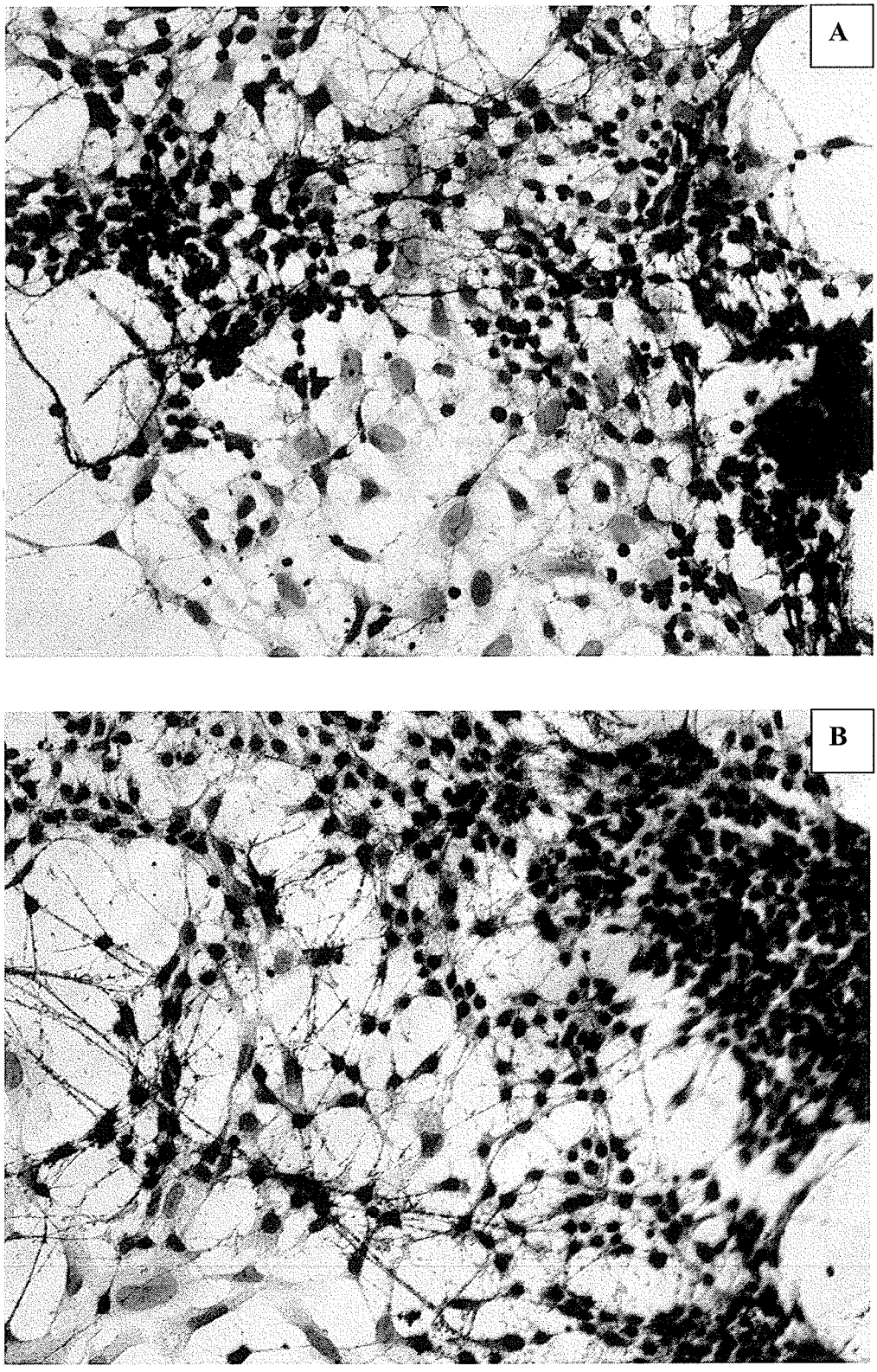

Figure 5: Initial stages of neuronal cell proliferation on Day 4 and 5 of the differentiation process (A and B respectively). Neuronal cells were stained with Class III ß-Tubulin (red). Hematoxylin (purple) was used to stain the nucleus.

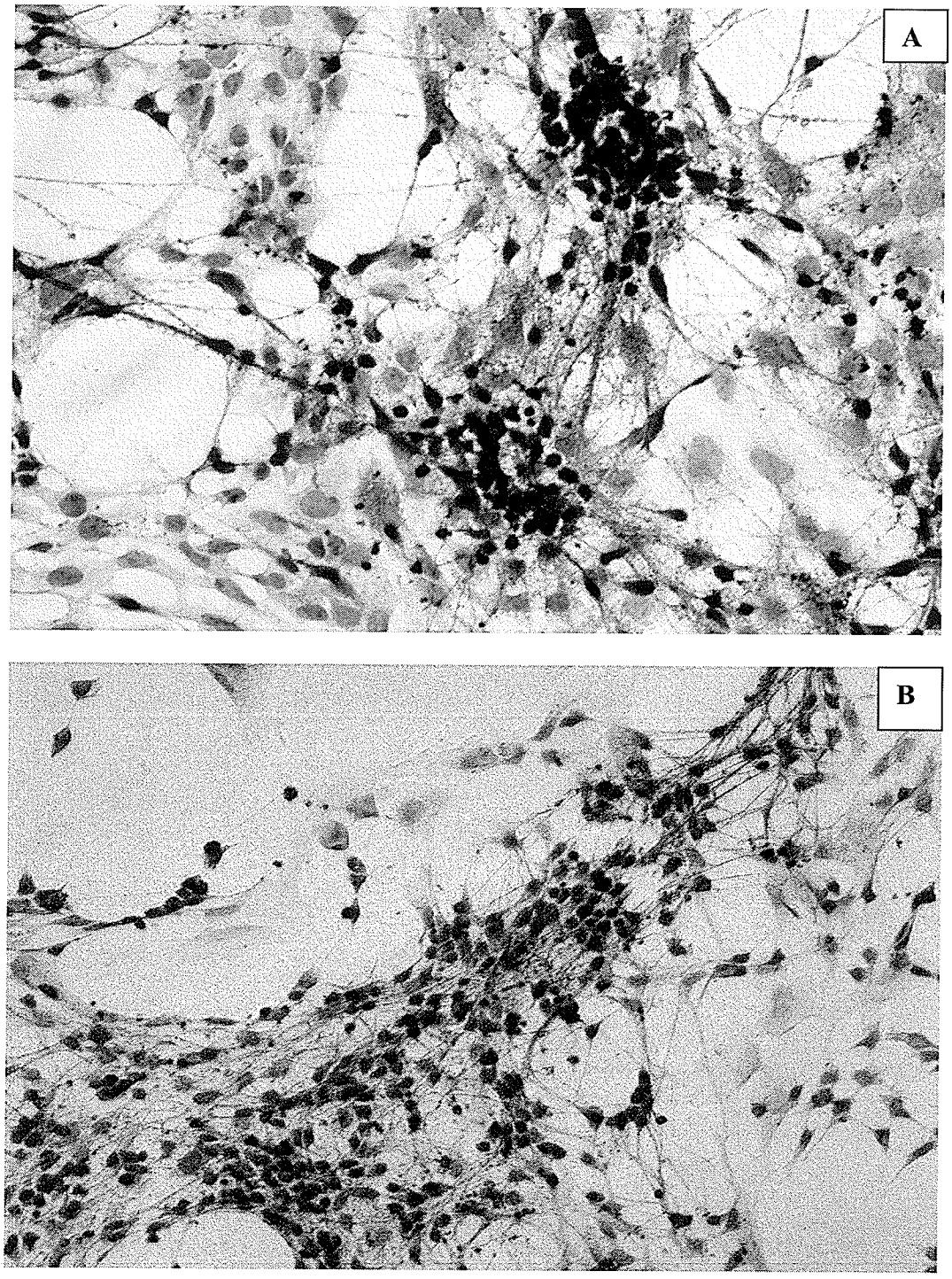

Figure 6: Day 8 of the differentiation process. In both A and B, neuronal cells were stained with Class III ß-Tubulin (red) and hematoxylin (purple) was used to stain the nucleus. In A, astrocytes were stained with Gfap (brown) and in B, oligodendrocytes were stained with myelin basic protein (brown). A large number of elaborate neural networks with a few astrocytes and little/no oligodendrocytes can be seen.

4.3.2 Determining Culture Composition using q-PCR

Quantitative real-time PCR was used to confirm the composition of the culture throughout the differentiation process. Relative expression levels of cell-type specific transcripts were measured; microtubule-associated protein 2 (neurons), glial fibrillary acidic protein (astrocytes) and galactocerebrosidase (oligodendrocytes). All gene expression levels were normalized relative to porphobilinogen deaminase (housekeeping gene) expression levels. Over the course of differentiation there is a very slight proliferation of astrocytes and oligodendrocytes, concomitant with a huge increase in neurons. From Figure 7 it is apparent that by Day 8, we were able to create a neuronally enriched population.

4.3.3 Measuring Cell Death using Flow Cytometry

Flow Cytometry was used to measure neuronal cell death on Day 8 of the differentiation process. The plasma membrane of cells is an asymmetric mosaic of phospholipid species. When cells undergo apoptosis they lose the ability to translocate the phosphatidyl serine (PS) molecules, thus the molecules become stuck in the outer leaflet of the membrane. Annexin V has been shown to specifically bind phospholipid membranes containing PS. The plasma membrane remains intact for a significant time during apoptotic events, however eventually it becomes permeable to dyes like propidium iodide (PI). Upon entrance PI is able to intercalate with DNA, causing the nucleus to fluoresce red. Taking advantage of the differences in membrane permeability, live, dead, and apoptotic cell populations were identified by double staining cells with Annexin V-FITC and PI.

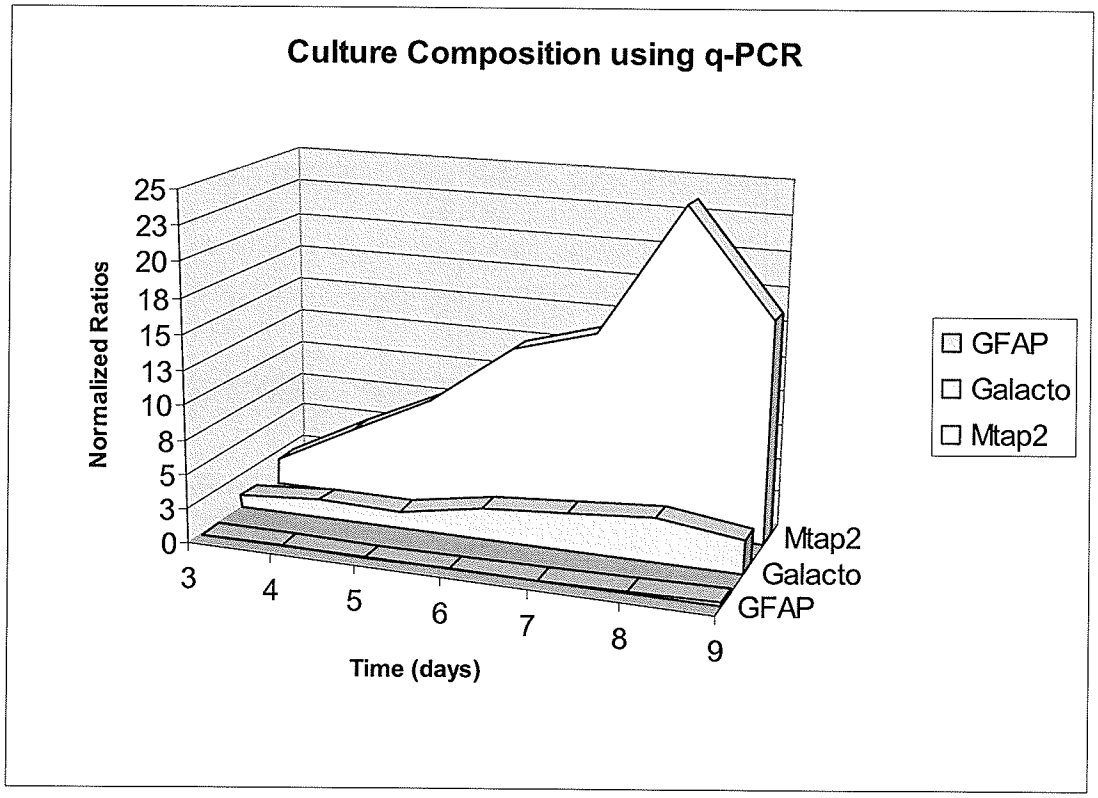

Figure 7: Quantitative real-time PCR was used to confirm the composition of the culture through-out the differentiation process. Over the differentiation process there is a very slight proliferation of astrocytes (GFAP) and oligodendrocytes (Galacto), concomitant with a huge increase in neurons (Mtap2). On Day 8 of the differentiation process we had created a neuronal-enriched population.

Figure 8, is a light scatter dot plot, which represents neuronal cells, non-neuronal cells and cell debris on Day 8 of the differentiation process. This figure demonstrates that two distinct sub populations are present in the population: non-neuronal cells and cell debris (left side of the plot) and neuronal cells (G5 region). As cells under go early stages of apoptosis they condense resulting in a decrease in forward scatter. For this reason it was extremely difficult to define the G5 subpopulation of neuronal cells. As the neuronal cells die they shift left into the other subpopulation (non-neuronal cells and cell debris). The G5 region represents a compromise between measuring only neuronal cells and including neuronal cells, which are dying. Figure 9 includes representative dot plots, which depict the relative light scatter positions of intact, early apoptotic and dead cells based upon "colour backgating" of Figure 12. Based upon this "colour backgating" the G5 region was defined to include intact, apoptotic and dead neuronal cells.

Positive control experiments were performed using staurosporine to determine the apoptotic pattern of P19 cells on Day 8 of the differentiation process (see Figure 10). As the cells progress through early to late stage apoptosis they shift fluorescence from only FITC positive to FITC and PI positive.

Using Annexin V conjugated to FITC neuronal cells that were undergoing early stages of apoptosis were detected, as seen in the lower right hand quadrant of Figure 11. Regions 1-4 represent: alive, early apoptotic, dead and apoptotic and dead cells respectively (Figures 11 and 12). Region 1 contains cells, which have a fluorescent signal of $\leq 10^1$ in both the FITC and PI channel. Region 2 contains cells, which have a fluorescent signal

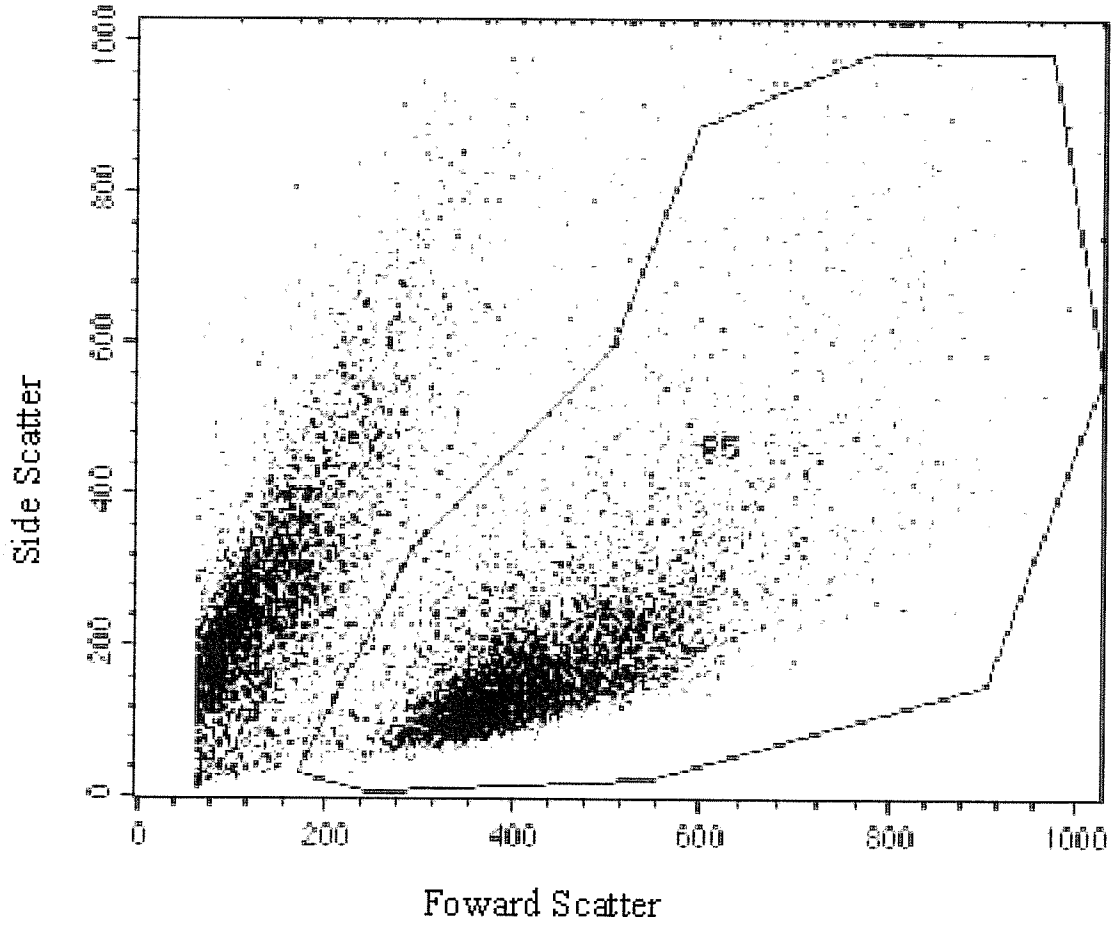

Figure 8: Representative lights scatter dot plot of neuronal, non-neuronal, and cell debris on Day 8 of the differentiation process. Data is shown for 10 000 cells. Region 5 (R5) represents untreated P19 neuronal cells on Day 8 of the differentiation process.

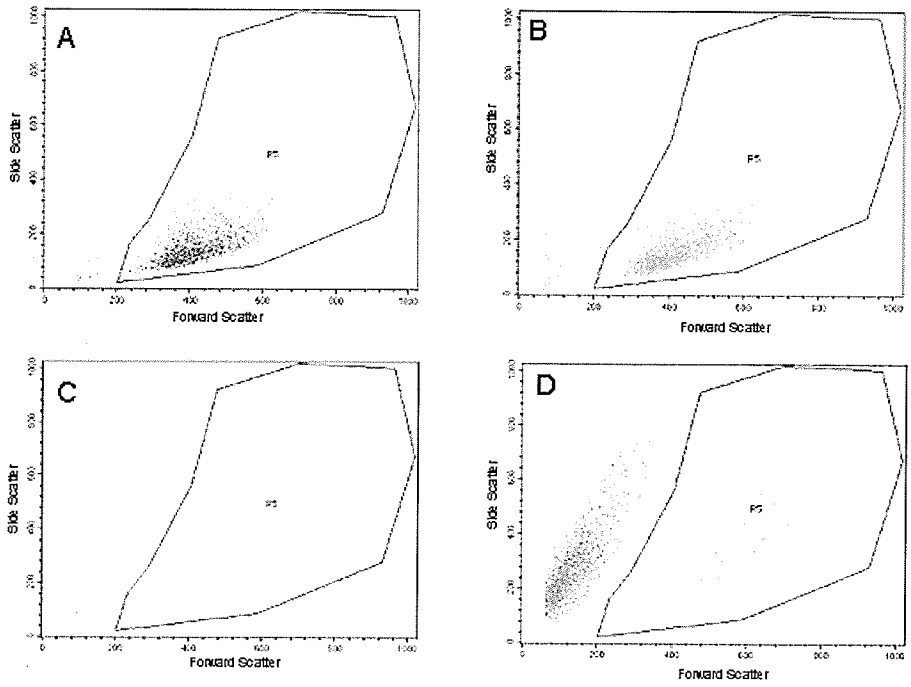

Figure 9: Representative dot plots of Day 8 untreated P19 neuronal cells, which are "back-gated" based upon the regions identified in Figure13, stained with Annexin V-FITC and PI. The dot plots depict the relative light scatter positions of intact, early apoptotic, and dead cells. In A, the live cells identified in R1 of Figure 13 are shown (FITC and PI negative). In B, the cells undergoing early stages of apoptosis identified in R2 of Figure 13 are identified (FITC positive). In C and D, the dead cells identified in R3 and R4 respectively of Figure 13 are shown (PI positive and FITC and PI positive respectively).

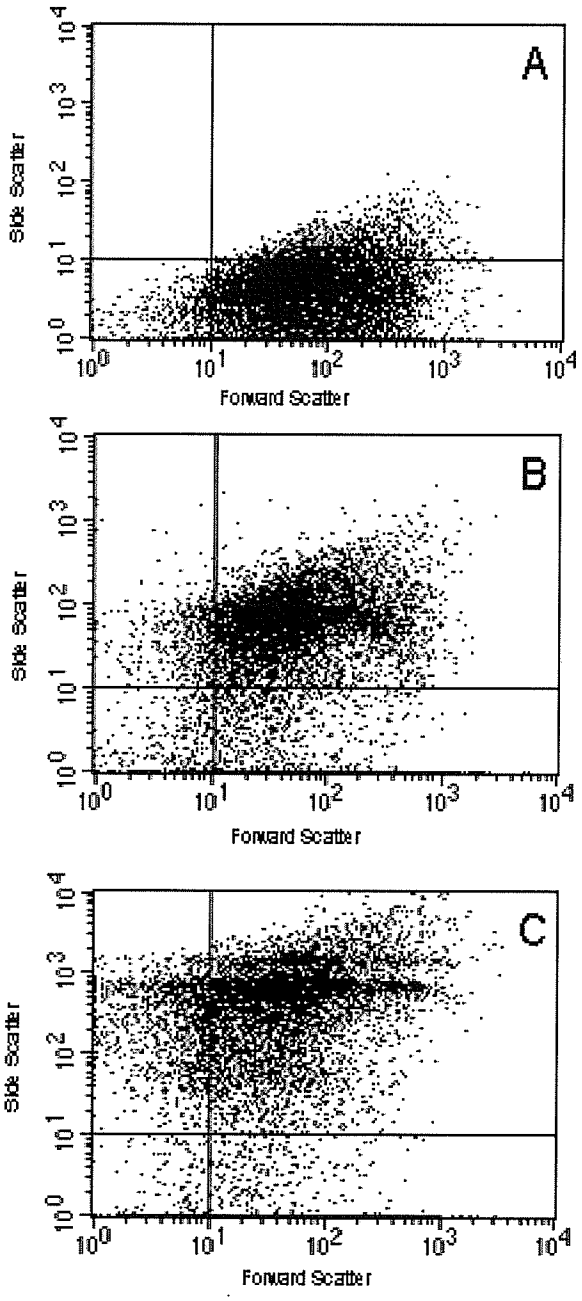

Figure 10: Staurosporine time-course. Representative dot plots of Day 8 untreated P19 neuronal cells treated with staurosporine and then stained with Annexin V-FITC and PI. Cells treated with 1 μL staurosporine (1 μg/mL) for 1 hour (A) are undergoing early stages of apoptosis. Cells treated with 1μL of staurosporine (1μg/mL) for 2 hours (B) are undergoing late stages of apoptosis. Cells treated 1μL of staurosporine (1μg/mL) for 4 hours (C) are mostly dead.

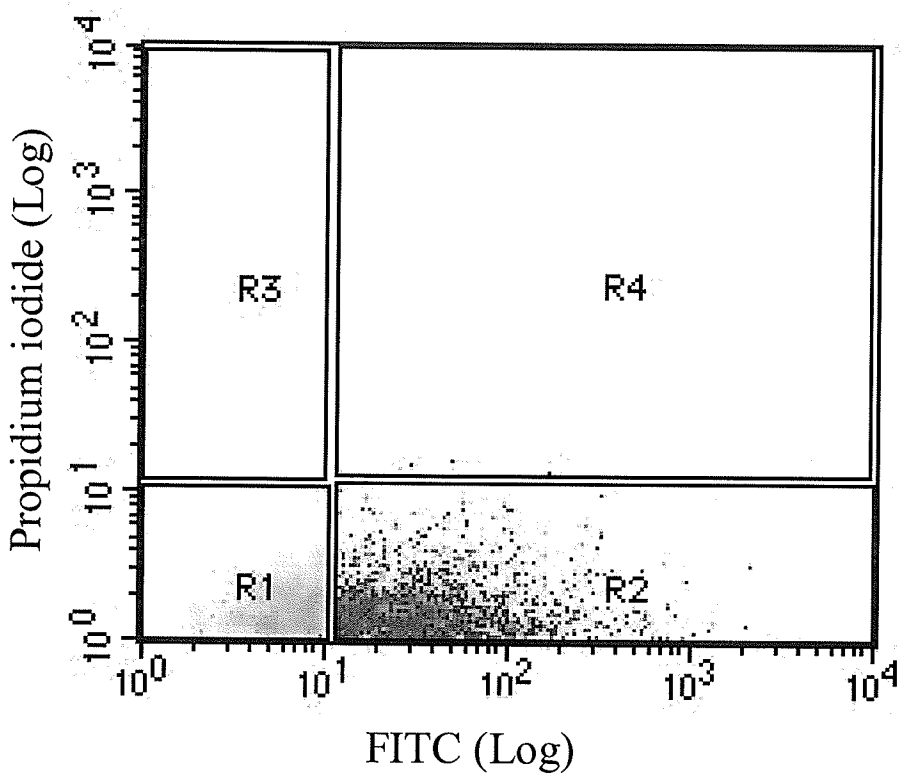

Figure 11: Representative dot plot of Day 8 untreated P19 neuronal cells, which are the G5 subpopulation identified in Figure 9, stained with Annexin V conjugated to FITC. Data is shown for 10 000 cells. Cells in the lower right quadrant are undergoing early stages of apoptosis (R2) while cells in lower left quadrant (R1) are still alive.

of $\geq 10^1$ in the FITC channel. Region 3 contains cells, which have a fluorescent signal of $\geq 10^1$ in the PI channel. Region 4 contains cells, which have a fluorescent signal of $\geq 10^1$ in both the FITC and PI channel. Figure 12 shows untreated Day 8 P19 neurons; 42.34% of the population is alive (yellow), 9.48% is dead (blue) and 45.64% are apoptotic (green).

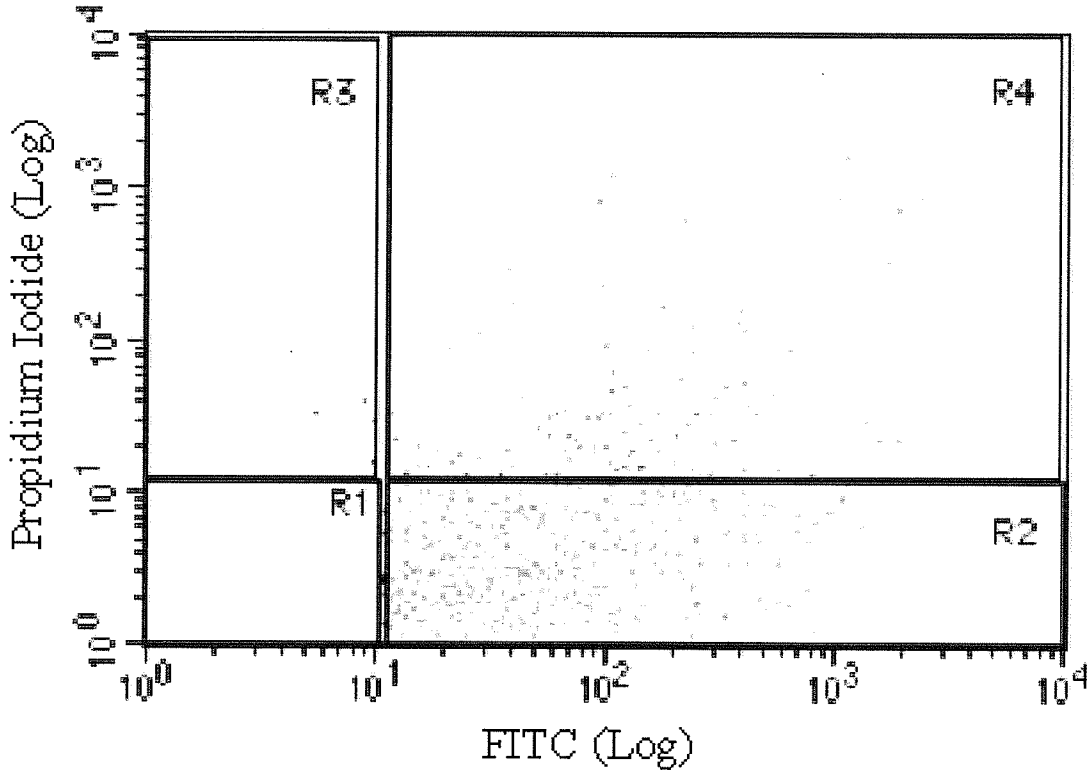

Figure 12: Representative dot plot of Day 8 untreated P19 neuronal cells, which are the G5 subpopulation identified in Figure 9, stained with Annexin V-FITC and PI. Data is shown for 10 000 cells. Approximately 42% of the population is alive (R1), 10% is apoptotic and dead (R4), and 46% of the population is apoptotic (R2).

5-Discussion

Since 1970, *in vitro* models have been used to further our understanding of prion pathogenesis [61]. The search for the ideal *in vitro* model has lead researchers to study prion infection in a wide variety of cell types. *In vivo*, the death of neuronal cells is responsible for the fatal outcome of persons or animals infected with TSEs [72]. It is therefore not surprising that neuronal cells have become the most commonly used model. The majority of *in vitro* studies have been performed on 3 main neuronal cell lines: mouse neuroblastoma N2a cells, mouse hypothalamic GT1 cells and PC12 rat pheochromocytoma cells [58]. The knowledge gained from the above cell lines has appreciably furthered our understanding of prion diseases, however new models are needed as the above cell lines have limited application.

Using P19 embryonal carcinoma stem cells under the influence of retinoic acid a new *in vitro* model, which will help to better understand TSEs on a molecular and cellular level was generated. P19 neurons have been extensively described, and have been shown to share many characteristics with neurons present in the mammalian nervous system [69]. Morphologically they are similar to cultured brain cells. They are stable post-mitotically, possess functional synapses and have functional ionotropic glutamate receptors. As well the differentiation process is relatively synchronous thus the differentiated cells form with a reproducible kinetics and characteristics [69].

P19 neurons have several advantages over the commonly used neuronal cell lines described previously. P19 cells require only addition of RA to differentiate and it has been suggested that this process resembles the developmental events, which occur *in*

vivo. P19 neurons are terminally differentiated, mimicking CNS neurons, such that any insult has the possibility of resulting in irreplaceable cell death. The differentiation process of P19 cells results in a mixed population, thus the interactions between neuronal and glial cells can be studied.

When treated with 10^{-6}M retinoic acid P19 cells differentiated into a neuronally enriched culture with some glia- and fibroblast like cells. Differentiated P19 neurons are extremely fragile. To achieve the desired culture, cells needed to be maintainted in aged serum-free Almazan media, which was changed according to a strict protocol (described previously). All media changes were done particularly gently and slowly to prevent the cells from lifting off the collagen coated surface.

The composition of the culture was determined both qualitatively and quantitatively. Immunocytochemistry using cell-type specific antibodies and quantitative PCR using cell-type specific transcripts proved that proliferation of neurons was occurring as early as Day 4 of the differentiation process. By Day 8 an extensive neural network is visible, with a few astrocytes and little/no oligodendrocytes. Beyond Day 8 of the differentiation process, extensive neuronal cell death occurred.

To prove that oxidative stress is occurring prior to neuronal cell death as a result of prion infection, preliminary studies on the flow cytometer were performed measuring cell death of untreated P19 neurons. Cell death was quantitatively determined using FITC conjugated Annexin V in combination with PI. Annexin V's ability to bind to PS, in the presence of Ca^{2+}, makes it a powerful discriminator between viable and apoptotic cells [73].

Under viable conditions the PS molecule is translocated via PS translocase and scramblase, from the outer to the inner leaflet of the plasma membrane. This creates a situation of asymmetry because the outer leaflet of the plasma membrane is almost completely devoid of PS under normal, healthy growth conditions. However, when cells undergo apoptosis PS translocase and scramblase activity is inhibited which causes PS to remain in the outer leaflet of the plasma membrane [73]. PI's ability to differentiate between cells, which are alive and dead, also depend upon the architecture of the plasma membrane. The plasma membrane of dead cells becomes permeable to PI which intercalates with nuclear DNA producing a red fluorescent signal [73]. Therefore, after being stained with both Annexin V-FITC and PI cells that do not fluoresce are alive, those that fluoresce green are apoptotic and those that fluoresce red are dead.

On Day 8 of the differentiation process untreated P19 neurons were stained with Annexin V and PI to determine culture viability. It was determined that 42.34% of neuronal cells were alive, 45.64% of neuronal cells were apoptotic and 9.48% of neuronal cells were dead. Thus, over half of the neuronal cells in culture were either undergoing apoptosis or already dead due to the physical manipulation necessary to prepare the cells for flow cytometer analysis. This phenomenon is not uncommon in adherent cell lines [73,74]. Previous studies have shown that for adherent cell survival cellular integrins must be continuously connected to the extra cellular matrix. Detachment of adherent cells from the extra cellular matrix, even by gentle trypsinization, induces apoptosis immediately resulting in PS exposure in the outer plasma membrane [73,74]. As a result, flow analysis

would have been unable to discriminate between cell death due to the presence of the cytotoxic peptide $PrP^{106-126}$ and cell death due to preparatory methods.

These experiments demonstrated that under the influence of RA, P19 EC stem cells are able to differentiate into an enriched neuronal culture that includes some glial cells. The P19 neurons generated were stable post mitotically, making them an excellent representation of neurons in the CNS. Therefore the goal of generating post mitotic neuronal cells suitable for studying the molecular and cellular processes involved in $PrP^{106-126}$ toxicity was achieved and the exacting culture conditions required delineated. Unfortunately the terminally differentiated neurons generated were exceptionally sensitive to physical insults making them incompatible with the planned experiments. Nonetheless, in the future the advantageous characteristics of this model system can be exploited provided experimental approaches requiring minimal manipulation of the cells prior to sample collection are used. An example would be determining the changes in gene expression as a result of $PrP^{106-126}$ toxicity.

An *in vivo* model investigating the role of oxidative stress in prion provoked neurotoxicity

6-Introduction

Studying the pathogenesis of prion disease most commonly involves directly measuring PrP^{sc} infectivity in organs during incubation [75]. However, the extremely long incubation periods and the existence of a species barrier have made *in vivo* studies challenging [75,76]. In 1962, evidence that mice could be inoculated with scrapie-infected brain homogenate revolutionized the field of prion research [77]. Mice exposed to the scrapie agent (from brain or spleen) via intracerebral or intragastric inoculation developed brain lesions both in the neurons and in the extraneuronal substance [77]. These changes were distinctly similar to those seen in the brain of scrapie sheep. Remarkably it was also observed that subinoculations of brain material from scrapie-infected mice into healthy mice (both by intracerebral and intraperitoneal routes) resulted in a shortening of the incubation period [78].

Although certain strains of scrapie could be transmitted to mice the species barrier remained for bovine and human forms of the disease. Creation of transgenic mice either via conventional transgenesis (pronuclear injection) or gene targeting has had an enormous impact on the field of prion research, as researchers for the first time were able to overcome the species barrier [76]. Mice were created that expressed PrP from a wide range of species including human, bovine and ovine (see Table 3) [76]. These homologous models strongly reduced the species barrier following inoculation, allowing transmission that often failed in wild-type mice. Subsequent incubation periods became often less than one year. Researchers also discovered that the disease incubation period could be modified if PrP was overexpressed in these mouse models [76]. Transgenic mice may also

Table 3: Mouse models and the field of application in prion disease transmission [76].

Mouse Models	Field of Application
Wild-Type Mice	Transmission and species barrier Resistance to prion diseases Genetic Control of Prion Diseases Biological and Molecular Typing Putative role of associated factors in strain formation
$PrP^{0/0}$ mice	Transmission and species barrier Doppel protein studies
Hamster Transgenic Mice	Transmission and species barrier
Mouse Transgenic Mice	Transmission and species barrier Models of human genetic disease
Human Transgenic Mice	Transmission studies of CJD Putative role of associated factors in transmissibility Biological typing of vCJD Molecular origin of strains
Ovine Transgenic Mice	Transmission of scrapie Biological typing of BSE and scrapie
Bovine Transgenic Mice	Transmission of BSE Biological typing of vCJD, BSE, and scrapie

prove useful in predicting transmission of TSE across different species, specifically animal to human transmission.

Unfortunately there is no known therapy for TSEs, as all still remain lethal. Due to the overwhelming evidence that oxidative stress plays a role in the pathology of prion disease, it has been suggested that an anti-oxidant therapeutic strategy has the potential to be an effective treatment [79]. Oxidative stress is a complicated process to modulate. Cellular homeostasis maintains the delicate balance of good ROS which function as signaling molecules, to bad ROS, which lead to cell death. Dietary supplements intended to ameliorate oxidative stress have produced inconsistent and undesirable results. Most studies have only tested one, possibly a few supplements at a time. Lemon *et al.* have demonstrated that a cocktail approach was able to abolish age-related cognitive decline and shortened life span otherwise observed in transgenic C57BL/6 mice over expressing growth hormone [80,81]. The cocktail dietary supplement was designed based on the known efficacy of ingredients to reduce ROS and inflammation, promote membrane and mitochondrial integrity, and increase insulin sensitivity [80,81].

The brains of the scrapie-infected mice and the transgenic growth hormone mice have similar oxidative profiles. Both have elevated and progressively increasing levels of lipid peroxidation and superoxide radicals [80,81,82]. To study the role of oxidative stress in prion provoked neurotoxicity, scrapie-infected C57BL/6 mice were fed the anti-oxidant diet. It was hypothesized that the antioxidant diet would be able to ameliorate the adverse effects resulting from disease-associated oxidative stress and thus prolong the lifespan of

scrapie-infected mice. In addition, the influence of the diet on the levels of oxidative stress in infected mice was measured throughout disease progression.

Oxidative Stress has many different manifestations. To reflect this, a variety of methods were chosen for the study reported in this thesis, to measure the level of oxidative stress throughout the incubation period of the disease.

6.1 Measuring Antioxidant Capacity

Glutathione (GSH) is found in all forms of life and plays an essential role in maintaining cellular health. It is involved in catalysis, metabolism, signal transduction, gene expression and apoptosis [83,84,85]. It is a tripeptide composed of glutamate, cysteine and glycine [85]. In the brain, it is the most abundant non-protein thiol and has powerful anti-oxidant capabilities [84]. Glutathione functions as a redox buffer donating it's thiol groups to keep other proteins in a reduced condition. The resulting oxidized form of GSH consists of two molecules disulfide bonded together (GSSG) and can be recycled by glutathione reductase with the help of NADPH back into two molecules of GSH [85].

6.2 Measuring End products of Oxidative Stress

Measuring lipid peroxidation products is the most widely used method to assess oxidative stress. Lipid peroxidation is the result of free radical attack, usually on polyunsaturated fatty acids, which initiates a chain reaction resulting in a loss of membrane function and integrity [86,87,88]. The first products created in this chain are conjugated dienic hydroperoxides, which are broken down into various aldehydes or if the original fatty acid is arachidonic acid into isoprostanes [87]. All of the products of degradation and

decomposition have been used to measure oxidative stress. Some examples include: hydroperoxides commonly expressed as conjugated dienes, and end products such as malondialdehyde, 4-hydroxy-2,3-*trans*-nonenal (4-HNE) and F2-isoprostanes [86,87].

DNA damage as a result of oxidative stress has disastrous consequences. It is estimated that 10^5 oxidative DNA lesions are formed per day leading researchers to believe that it is the most common insult affecting the genome [89]. The cumulative mutations caused by ROS have the potential to disrupt cellular homeostasis; altering signaling cascades, gene expression, inducing or arresting transcription, and causing replication errors [89]. Chemical and structural modifications to purine and pyrimidine bases as well as 2'-deoxyribose are the result of oxidative DNA damage. ROS can also cause single- and double-stranded breaks. The modified guanine base, 8-oxo-7,8-dihydroguanine (8-OHdG), is the most popular indices of DNA damage caused by oxidative stress [90,91].

6.3 Gene expression profiling

Originally radio-labeled Northern blots and slot blot hybridizations were used to explore differences in gene expression [92,93]. However, these methods were limited in the number of genes that could be investigated in each experiment. It wasn't until cDNA could be spotted onto glass substrates, that muliplex gene expression/microarray studies became a reality [92,93]. Microarray technology has become extremely powerful, allowing researchers to simultaneously monitor the gene expression patterns of tens of thousands of genes. Today oligonucleotide-based microarrays have surpassed cDNA arrays as the most widely used system. This is because oligonucleotides can be stringently designed such that they perform in a much more predictable manner. They can be designed such

that all the oligonucleotides are thermodynamically matched and bind only a specific gene or splice variant. As well, they allow the user the flexibility of specifying precisely which oligos appear on the array [92,93].

There are many applications for microarrays. They can be used for biomarker discovery, measuring genetic markers of disease and/or progression, patient genotyping and drug development [92,93]. In the context of this project, microarrays have been used to detect changes in the expression pattern of multiple genes and/or cellular pathways. These changes may be prerequisites of disease development, which accumulate before any observable symptoms.

6.4 Project Goals

The goals of this project were:

1. To use GSH, 4-HNE and 8-OHdG as measures of the effect of prion infection on the oxidative state of scrapie-infected C57BL/6 mice.
2. The measurement of GSH, 4-HNE and 8-OHdG was also employed to determine whether feeding mice an antioxidant diet was able to modulate the level of oxidative stress occurring as a result of the disease.
3. To apply microarray analysis to identify changes in gene expression patterns and cellular pathways resulting from scrapie infection.
4. To determine the influence of oxidative stress on the life span of scrapie infected C57BL/6 mice.

7-Materials and Methods

All procedures involving infectious materials were carried out in Level 3 containment.

7.1 Animal Care

The Canadian Science Centre for Human and Animal Health Animal Care Committee approved all procedures.

A 1% brain homogenate in PBS (pH 7) was prepared from either control or ME-7 infected mice that had reached the clinical stage of disease. Brains were homogenized with a tissue homogenizer (Omni International, cat. #TH115) using 7mm x 110 mm tips (Omni International, cat. #3050), diluted to 1% w/v and stored at -80°C until use. Prior to injection the homogenate was thawed, sonicated for 3 x 30 seconds at amp40 and centrifuged at 500g for 10 minutes. C57BL/6 mice between 4-6 weeks of age were anaesthetized with isofluorane prior to performing the procedure. 20μL of the brain homogenate containing 10,000,000 particles of infectious agent, was introduced into the left side of the brain by intracerebral injection using a Tri-Dek stepper equipped with a 26G biomedical needle of 4mm in length (Pepper and Sons Inc., cat. #7400). Mice were fed an antioxidant diet or a placebo diet daily (see Table 4). The antioxidant diet consisted of the components listed in Figure 13, dissolved in vegetable oil and spread onto bagel chips. The placebo diet consisted of vegetable oil spread onto bagel chips. Pressed cotton nestlet squares were added to the mouse cages. Healthy mice shred the nestlet and incorporate the material into bedding. A nestlet remaining intact for 48 hours along with noticeably compacted bedding was recorded as the date when nesting ceased. On scheduled collection dates and terminal stage mice were euthanized

Table 4: The four experimental groups, which were used in experiments.

Experimental Group	Treatment
1	Control mice fed a placebo diet (UN)
2	Control mice fed an antioxidant diet (UD)
3	Infected mice fed a placebo diet (IN)
4	Infected mice fed an antioxidant diet (ID)

Vitamin B1	0.72 mg/day
Vitamin B3	0.72 mg/day
Vitamin B	0.72 mg/day
Vitamin B	0.72 mg/day
Vitamin C	3.6 mg/day
Vitamin D	2.5 IU/day
Vitamin E	1.44 IU/day
Acteyl L-Carnitine	14.4 mg/day
Alpha-Lipoic Acid	0.72 mg/day
ASA	2.5 mg/day
Beta Carotene	50.0 IU/day
Bioflavinoids	4.32 mg/day
Chromium Picolinate	1.44 mg/day
Cod Liver Oil	5.04 mg/day
CoEnzyme Q10	0.44 mg/day
DHEA	0.15 mg/day
Flax Seed oil	21.6 mg/day
Folic Acid	0.01 mg/day
Garlic	21.6 mg/day
Ginger	7.2 mg/day
Gingko Biloba	1.44 mg/day
Ginseng (Canadian)	8.64 mg/day
Green Tea Extracts	7.2 mg/day
L-Glutathione	0.36 mg/day
Magnesium	0.72 mg/day
Melatonin	0.01 mg/day
N-Acteyl Cysteine	7.2 mg/day
Potassium	0.36 mg/day
Rutin	0.72 mg/day
Selenium	1.08 mg/day
Zinc (Chelated)	0.14 mg/day

Figure 14: The contents of the antioxidant diet [80].

by cervical dislocation (see Table 5). Brains for gene expression were placed in RNA*later* and stored at -80°C. Brains for GSH/4-HNE were flash frozen and stored at –80°C. Terminal stage was skin ulceration of any size due to overflow incontinence. Additionally urine from mice was collected at 48, 55, 62, 69, 76, 83, 90, 97, 104, 111, 118, and 125 dpi, by placing mice in a metabolic cage (Fisher Scientific, cat. #012882D) overnight.

7.2 Oxidative Stress Assays

7.2.1 Total GSH and 4-HNE Assay

Total GSH (Bio Vision, cat. #K21-100) and 4-HNE (Oxford Biomedical Research, cat. #FR12) levels were measured in whole mouse brains. Briefly, flash frozen brains were thawed in 1ml GSH buffer. Brains were homogenized for 3 x 30 seconds, 5% SSA was added and the mixture was vortexed. The homogenate was centrifuged at 4°C at 5400 g for 5 minutes. The supernatant was transferred into an Amicon Ultra 5000 MWCO filter (Millipore cat #UFC800524) and centrifuged at 4°C at 3500 rpm for 52 minutes. The flow through was transferred to a 1.5mL microfuge tube and stored on ice.

The MDA standard tube was diluted 1/500 v/v in water and 4-HNE standards were prepared. 200 µL of samples (extracted from brains) and standards were aliquoted into a 1.5mL microfuge tube. 650µL of diluted Reagent 1 was added, except to the sample control and mixed by gentle vortexing. 150µL of Reagent 2 was added to samples,standards and the sample control and mixed by gentle vortexing. All tubes were

Table 5: Experimental design of the *in vivo* model system: collection time points, number of mice collected and intended use of the sample.

	Time of Sacrifice (Days Post Infection)				
	70 dpi	**90 dpi**	**110 dpi**	**130 dpi**	**Terminal**
Group 1: UN	4 mice- (GSH and 4-HNE) 8 mice- (Gene Expression)	4 mice- (GSH and 4-HNE) 8 mice- (Gene Expression)	4 mice- (GSH and 4-HNE) 8 mice- (Gene Expression)	4 mice- (GSH and 4-HNE) 8 mice- (Gene Expression)	
Group 2: UD	4 mice- (GSH and 4-HNE) 8 mice- (Gene Expression)	4 mice- (GSH and 4-HNE) 8 mice- (Gene Expression)	4 mice- (GSH and 4-HNE) 8 mice- (Gene Expression)	4 mice- (GSH and 4-HNE) 8 mice- (Gene Expression)	
Group 3: IN	4 mice- (GSH and 4-HNE) 8 mice- (Gene Expression)	4 mice- (GSH and 4-HNE) 8 mice- (Gene Expression)	4 mice- (GSH and 4-HNE) 8 mice- (Gene Expression)	4 mice- (GSH and 4-HNE) 8 mice- (Gene Expression)	14 mice (Lifespan)
Group 4: ID	4 mice- (GSH and 4-HNE) 8 mice- (Gene Expression)	4 mice- (GSH and 4-HNE) 8 mice- (Gene Expression)	4 mice- (GSH and 4-HNE) 8 mice- (Gene Expression)	4 mice- (GSH and 4-HNE) 8 mice- (Gene Expression)	14 mice (Lifespan)

incubated at 45°C for 1 hour. 200µL of each sample, standard and sample control was added to a 96 well plate. The absorbance was measured at 586nm (Spectra Max Pro Spectrophotometer, Molecular Devices), using Softmax Pro software Substrate, NADPH generating mix, Glutathione reductase, 1% SSA, GSH standards and Reaction mix were prepared according to manufactures instructions. 160µL of the reaction mix was added to a 96 well plate and incubated at room temperature for 10 minutes. 20µL of sample (extracted from brains) and GSH standards were added to the plate and incubated at room temperature for 10 minutes. 20µL of substrate solution was added to the plate and incubated at room temperature for 10 minutes. The absorbance was measured at 412 nm (Spectra Max Pro Spectrophotometer, Molecular Devices), using Softmax Pro software.

7.2.2 8-OHdG Urine Assay

8-OHdG levels were measured in urine using the 8-OHdG urine ELISA (Stressgen, cat. # EKS-350). Briefly, the 8-OHdG Immunoassay plate, 20X wash buffer, sample diluent, antibody diluent, HRP conjugate diluent, TMB substrate and stop solution 2 were brought to room temperature. 8-OHdG samples and standards were prepared. 50µL of the prepared samples and standards were added in duplicate to wells of the 8- OHdG Immunoassay plate. 50µL of diluted anti-8-OHdG was added to each well, except for the blank and incubated at room temperature for 1 hour. The plate was washed. 100µL of diluted anti-mouse IgG:HRP conjugate was added to each well, except for the blank and incubated at room temperature for 1 hour. The plate was washed. 100µL of TMB substrate was added to each well, incubated at room temperature for 15 minutes in the

dark. 100μL of stop solution 2 was added to each well, and the absorbance was measured at 450nm (Spectra Max Pro Spectrophotometer, Molecular Devices) using the Softmax Pro software.

7.3 Differences in Gene Expression

7.3.1 Array Design

4 x 44K multiplex format, whole mouse genome microarrays were purchased from Agilent Technologies (cat. #G4122F).

7.3.2 RNA Extraction

RNA was extracted from whole mouse brain using the RNeasy Lipid Tissue Midi kit (Qiagen, cat. #75842). Briefly, whole mouse brains were thawed on ice. Brains were removed from RNA Later and placed in 5mL of Qiazol. They were then homogenized for 30 seconds and rocked at room temperature for 5 minutes. The homogenate was centrifuged at 4°C at 5000 g for 15 minutes. The supernatant was transferred to a fresh tube, 1mL of chloroform was added, mixed by vortex and rocked at room temperature for 3 minutes. The mixture was centrifuged at 4°C at 5000 g for 15 minutes. The upper aqueous phase was transferred to a new tube, 1 volume of 70% ethanol was added, vortexed and applied to an RNeasy Midi spin column. The column was spun at 23°C at 5000 g for 5 minutes. The flow through was discarded; the column was washed with 4mL of Buffer RW1 and 2x 2.5mL Buffer RPE. The RNeasy Midi spin column was transferred to a new collection tube, and the RNA was eluted in 300μL RNase free water.

The quality and quantity of RNA were then assessed using the Agilent RNA 6000 Nano Kit (Agilent, cat. #5067-1511).

7.3.3 RNA Amplification

RNA was amplified using the Amino Amino Allyl MessageAmp™ II aRNA Amplification kit (Ambion, cat. #AM1753). Briefly, each reaction contained 1μg total RNA, 1μL T7 Oligo(dT) primer, and Nuclease-free water in a total of 12μL. The mixture was heated to 70°C for 10 minutes and then placed on ice. 8μL Transcription master mix was added to each reaction, incubated at 42°C for 2 hours and then placed on ice. 80μL of Second Strand master mix was added to each reaction, incubated for 2 hours at 16°C and the placed on ice. The cDNA was purified and eluted in 18μL of Nuclease-free water. 26μL of IVT master mix was added to each sample and incubated at 37°C for 14 hours. The aRNA was purified and eluted in 100μL of Nuclease-free water. 10μg of aRNA was vacuum dried and resuspended in 9μL coupling buffer and 11μL prepared dye. The reaction was incubated for 1 hour at room temperature in the dark. 4.5 μL 4M hydroxylamine was added and the mixture was incubated for 15 minutes at room temperature in the dark. 5.5μL Nuclease-free water was added to bring each sample to 30μL. The dye labelled aRNA was purified and eluted in 20μL of Nuclease-free water. All incubation steps were performed using a PTC-200 MJ Thermocycler selecting "heated lid".

7.3.4 aRNA Hybridization, Slide Washing, and Scanning

aRNA hybridization, washing and scanning steps were performed according to the Two-Color Microarray-Based Gene Expression Analysis protocol (Agilent Technologies, Version 5.0.1).

Briefly, each hybridization reaction contained 1μg of "treated" labelled aRNA, 1μg of "control" labelled aRNA, 11μL 10X blocking agent, 25X fragmentation buffer, and Nuclease-free water up to 52.8μL. The mixture was heated to 60°C for exactly 30 minutes. 55μL of 2X hybridization buffer was added and the samples were loaded onto the array. Slides were washed at room temperature for 1 minute in GE wash buffer 1 and 1 minute in pre-warmed GE was buffer 2. Slides were scanned using the Agilent DNA microarray scanner (Agilent Technologies, cat. #G2565BA).

7.3.5 Data Analysis

Microarray .tif images were uploaded into Feature Extraction 9.1 (Agilent Technologies). The software program finds the spots and positions the grids. The outlier pixels are removed and statistics are performed on inlier pixels of spots and local backgrounds. Outlier spots and local backgrounds are flagged, the background is subtracted from the spots and error is estimated. Finally dye normalization is performed based upon a Loess/Lowess algorithm and a p-value (0.05) is calculated. The Log_{10} ratios from each grid were moved to a Microsoft excel spreadsheet. The Log_{10} ratios "Treatment-Cy3" / "No Treatment-Cy5" must be inverted as Feature Extraction 9.1 computes Log_{10} ratios based upon Cy5/Cy3.

Statistical analysis of the resulting gene list was performed using the Statistical Analysis of Microarrays software (Standford University Laboratories).

7.3.6 Resources for Interpreting Microarray Results

1. Pathway Ingenuity Analysis (http://www.ingenuity.com/)
2. DAVID Bioinformatics Resources (National Institute of Allergy and Infectious Diseases (NIAID, NIH) (http://david.abcc.ncifcrf.gov/)
3. GeneAssist™ Pathway Atlas (Ambion) (http://www.ambion.com/tools/pathway/)

8-Results

Multiple studies have demonstrated that oxidative stress occurs during prion disease. Should the oxidative stress observed play a role in the pathology of prion diseae, it has been suggested that an anti-oxidant therapeutic strategy has the potential to be an effective treatment. To test this hypothesis a cocktail supplement designed to reduce ROS and inflammation, promote membrane integrity and increase insulin sensitivity was fed to scrapie-infected and control mice.

8.1 Oral administration of an anti-oxidant diet

C57BL/6 mice were divided into four experimental groups. Mice in groups 1 and 2 were i.c. inoculated with uninfected brain homogenate, while mice in groups 3 and 4 were i.c. inoculated with infected brain homogenate prepared from clinical stage Me-7 infected C57BL/6 mice. An antioxidant diet was fed to groups 2 and 4; with groups 1 and 3 receiving the corresponding placebo diet (see Table 4).

Table 5 shows the number of mouse brains collected from each group at the 5 time points and their intended purpose. Additionally, urine from all four groups of mice was collected at 48 dpi, 55 dpi, 62 dpi, 69 dpi, 76 dpi, 83 dpi, 90 dpi, 97 dpi, 104 dpi, 111 dpi, 118 dpi and 125 dpi.

8.2 Measuring the oxidative state

8.2.1 Total Glutathione Levels in whole mouse brain

Total GSH levels in 4 whole mouse brains from each group were measured at 70 dpi, 90 dpi, 110 dpi and 130 dpi (see Figure 14). Scrapie infected mice displayed depleted total GSH levels as compared to control mice at 70dpi, 90dpi, and 130dpi (two-tailed $p=0.001$, $p=0.024$, $p=0.022$ respectively). There was no significant difference between groups at 110 dpi. The antioxidant diet was able to return total GSH levels in scrapie-infected mice to those seen in control mice at 70dpi, and 130dpi.

8.2.2 4-HNE Levels in whole mouse brain

4-HNE levels in 4 whole mouse brains from each group were measured at 70dpi, 90dpi, 110dpi, and 130dpi (see Figure 15). The concentration of 4-HNE was increased at 90dpi ($p = 0.09$) and 130dpi ($p = 0.003$) in scrapie-infected mice as compared to control mice. There was no significant difference between groups at 70dpi and 110dpi. The antioxidant diet was able to significantly reduce 4-HNE levels at 90dpi in infected mice as compared to those just fed the placebo diet ($p = 0.01$). However, it was unable to return levels to those seen in control mice. At 130dpi, the antioxidant diet exacerbated already elevated lipid peroxidation levels in scrapie-infected mice as compared to those fed the placebo diet.

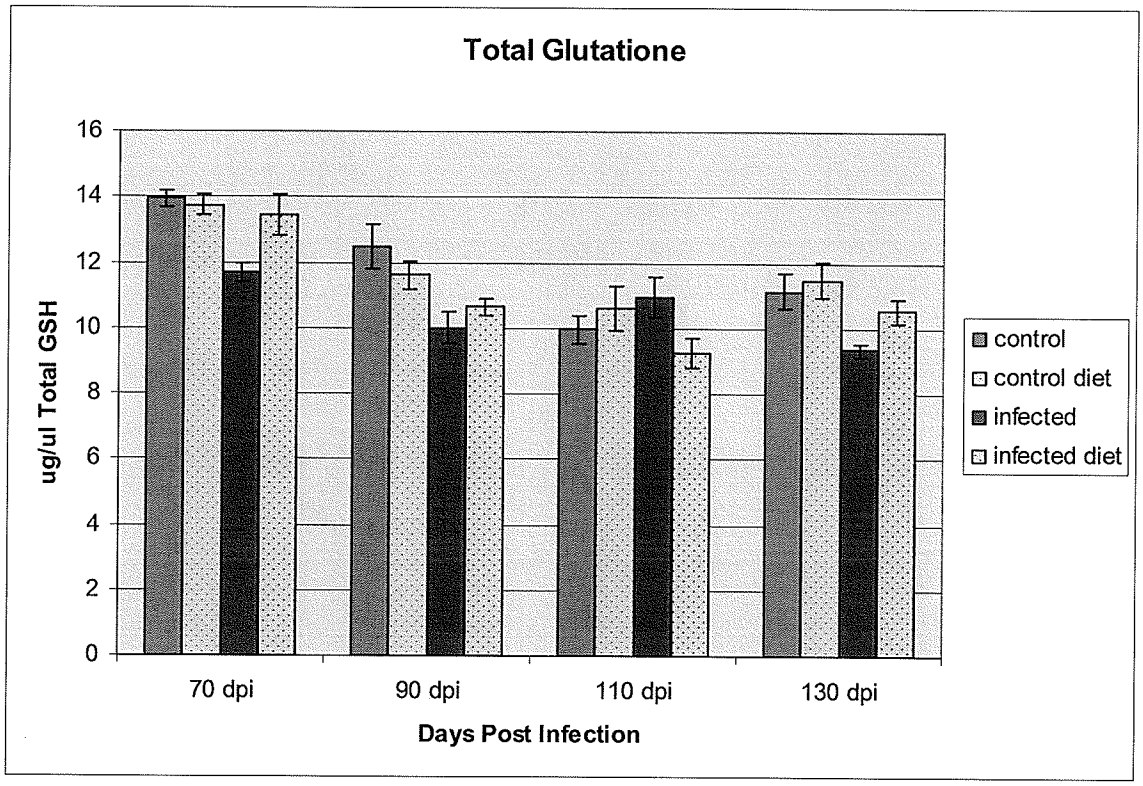

Figure 14: Total GSH levels were measured in whole mouse brain using the Biovision ApoGSH^{TM} Glutathione detection kit. The results represent the average of four biological replicates. At 70, 90, and 130dpi total GSH levels were significantly decreased in infected as compared to control mice ($p=0.001$, $p=0.024$, $p=0.022$ respectively). Total GSH levels in scrapie-infected mice fed the antioxidant diet returned to control levels at 70dpi and 130dpi. At 90dpi the antioxidant diet had no effect on total GSH levels in scrapie-infected mice, as compared to infected mice. There was no significant difference between groups at 110dpi.

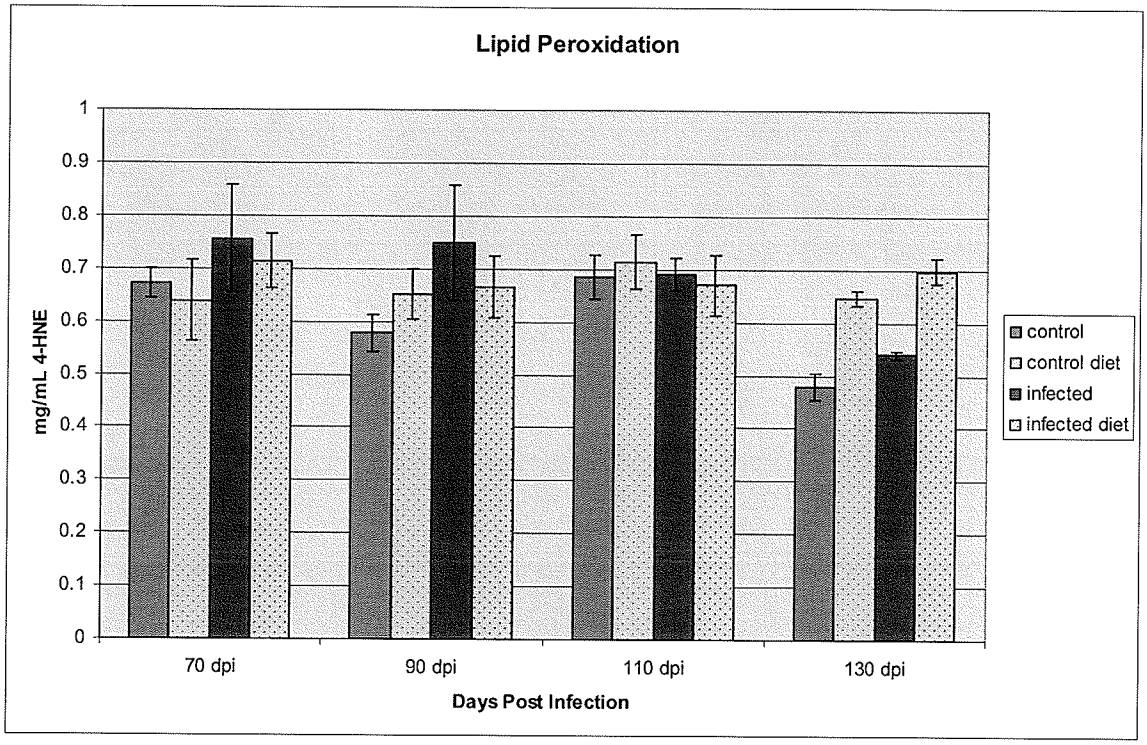

Figure 15: 4-HNE levels were measured in whole mouse brain using the Oxford Biomedical Research colormetric assay for lipid peroxidation. The results represent the average of four biological replicates. There was no significant difference between groups at 70dpi and 110dpi. The concentration of 4-HNE was increased at 90dpi (almost significant $p=0.09$) and 130dpi ($p=0.003$) in scrapie-infected mice as compared to control mice. The antioxidant diet was able to significantly reduce 4-HNE levels at 90dpi in scrapie-infected mice as compared to those just fed the placebo diet ($p=0.01$). However, it remained significantly higher than in control mice. At 130dpi, the antioxidant diet exacerbated already elevated lipid peroxidation levels in scrapie-infected mice as compared those fed the placebo diet.

8.2.3 8-OHdG Levels in urine

Four mice from each group were placed overnight in a metabolic cage for 16 hours and the urine collected at 12 time points, from 48dpi-124dpi, during the course of the disease. The urine from three consecutive time points was averaged, generating four major time points throughout the disease course. In scrapie-infected mice, the level of 8-OHdG was significantly increased from 91dpi-110dpi and 111-125dpi ($p = 0.04$ and $p = 0.01$ respectively) as compared to control mice (see Figure 16). Increased levels of 8-OHdG were not apparent prior to 89dpi. The antioxidant diet was unable to alter the amount of DNA damage which is occurring as a result of prion infection from 91dpi-110dpi ($p = 0.23$) and 111-125dpi ($p = 0.33$).

8.3 Changes in Gene Expression in whole mouse brain

4 x 44K multiplex format, whole mouse genome microarrays (Agilent technologies) were used to determine changes in gene expression in RNA extracted from whole mouse brains at 90 and 130dpi. Eight biological replicates were used to increase the statistical power of the experiment. 41, 000+ mouse genes and transcripts are spotted four times onto one slide, thus each slide contains four identical microarrays. The four-plex format is highly reproducible, as the smaller array size facilitates concentration of the hybridization solution, which results in an increase in the detectable signal. Using 4x44K microarrays researchers are able to detect greater gene expression than ever before.

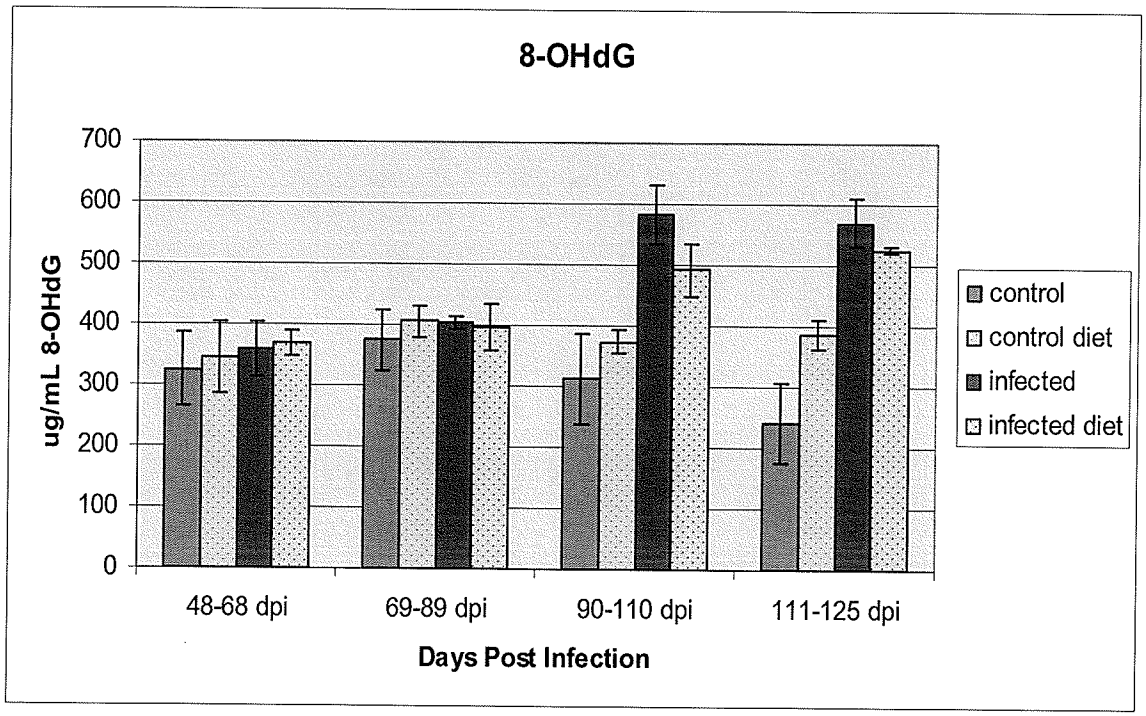

Figure 16: 8-OhdG levels were measured in urine from mice using the Stressgen StressXpress DNA damage ELISA kit. The results represent the average of three consecutive timepoints. There was no significant difference between groups at 48-68dpi and 69-89dpi. In scrapie-infected mice, the level of 8-OHdG was significantly increased at 91-110dpi and 111-125dpi ($p = 0.04$ and $p = 0.01$ respectively) as compared to control mice. The antioxidant diet was unable to alter the amount of DNA damage, which is occurring as a result of prion infection at 91-110dpi and 111-125dpi.

Finally the four-plex format is compatible with Feature Extraction 9.1 (FE 9.1), automating data analysis of the arrays.

Whole mouse brains were collected at 70, 90, 110, and 130dpi and stored at –80°C in RNA*later*. RNA*later* inactivates RNases and stabilizes the RNA within the tissue. RNA was extracted from whole brains collected at 90 and 130dpi, using the RNeasy Lipid Tissue Midi kit (Qiagen). The time point's 90dpi and 130dpi were chosen as they represent pre-clinical and clinical stages of the disease respectively. Total RNA yield and integrity (RIN) was determined using the Agilent 2100 expert bioanalyzer (see Figure 17). Concentrations obtained ranged from 240ug/brain-450ug/brain with an RIN between 7.2-9.0.

At each time point RNA from two different groups; infected no diet (IN) vs. uninfected no diet (UN) and IN vs. infected antioxidant diet (ID) was competitively hybridized. At each time point 16 microarrays were preformed; 8 IN vs. UN arrays and 8 IN vs. ID arrays, for a total of 32 arrays. The array experiments were performed such that individual RNA samples from one group were hybridized against individual RNA samples from the other group. A dye swap method was also employed in order to minimize the labelling bias of the fluorscent dyes (see Figure 18).

Figure 19, shows a brief overview of the extraction process. The normalized data obtained from FE 9.1 was then analyzed using the statistical analysis of microarrays

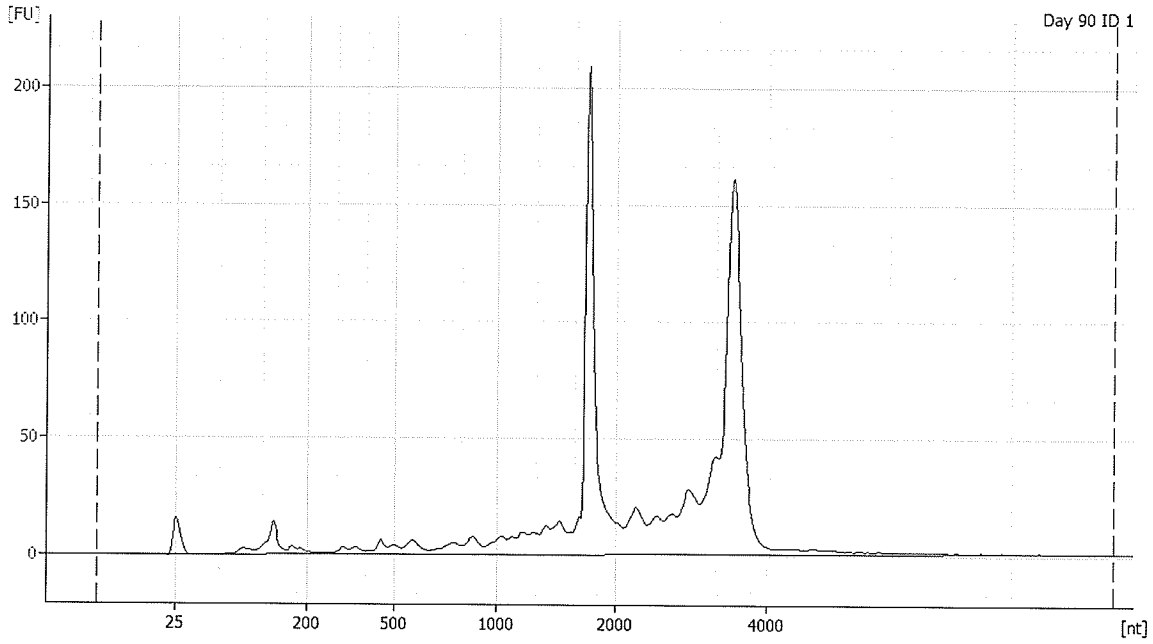

Overall Results for sample 1: **Day 90 ID 1**

RNA Area:	912.0
RNA Concentration:	537ng/ul
rRNA Ratio [28s / 18s] :	1.3
RNA Integrity Number (RIN):	8.6 (B.02.03)

Fragment table for sample 1: **Day 90 ID 1**

Name	Start Size [nt]	End Size [nt]	Area	Area% of total
18s	1,580	2,074	194.1	21.3
28s	2,780	3,951	296.2	32.5

Figure 17: An example of the electropherogram and overall results of obtained using the 2100 bioanalyzer.

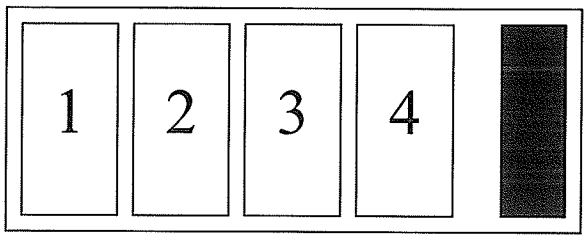

Array 1-4: Control Samples labelled green
Treatment Samples labelled red

Green = Cy3 Labelling
Red = Cy5 Labelling

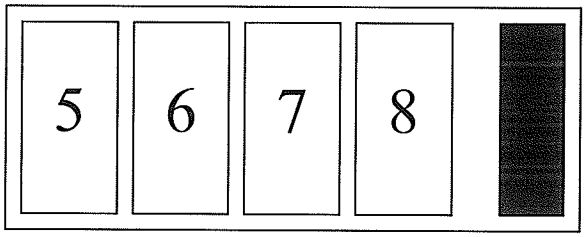

Array 5-8: Control Samples labelled red
Treatment Samples labelled green

Red = Cy5 Labelling
Green = Cy3 Labelling

Figure 18: An example of the Dye Swap method used. Four individual control samples were labeled with Cy3 on arrays 1-4 and four treatment samples were labeled Cy5 on arrays 1-4 (slide 1). Four individual control samples were labeled with Cy5 on arrays 5-8 and four treatment samples were labeled with Cy3 on arrays 5-8 (slide 2).

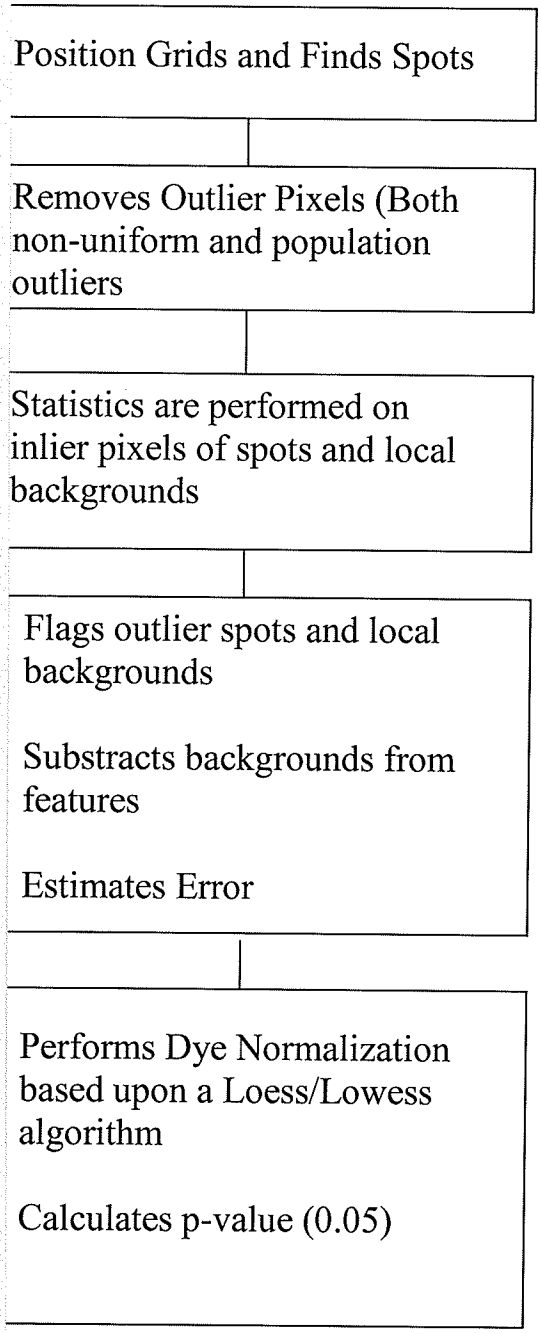

Figure 19: A brief overview of the automated extraction process performed by the FE software program.

(SAM) software. SAM finds significantly changed genes in a set of microarray experiments by standardizing a set of gene specific t-tests. The SAM output provides researchers with two important measurements for each gene, a SAM score and a false discovery rate (FDR). Each genes SAM score (or modified t-statistic) is assigned based upon a change in gene expression relative to that standard deviation of repeated measurements for that gene. For a gene to be considered potentially significant, its SAM score must be greater than the user-determined threshold. The FDR is the percentage that potentially significant genes are identified by chance. It is estimated by simultaneously analyzing permutations of the measurements.

8.3.1 The effect of scrapie-infection on whole brain gene expression

In the following section both groups were fed the placebo diet. Eight microarrays at 90 and 130 dpi respectively were performed on total RNA extracted from whole brain of scrapie-infected and uninfected mice. A one-class SAM was performed on the normalized data. Genes that were considered to be significant had a fold change ≥ 1.5 and FDR $\leq 5\%$. Genes that had no known Human Gene Organization (HUGO) Symbol were excluded.

Figure 20 is the SAM plot generated which represents the gene expression profile of scrapie-infected mice fed the placebo diet at 90dpi. A total of 50 genes influenced by scrapie-infection were identified as being differentially expressed (48 of these genes were up-regulated and 2 were down-regulated (see Tables 6 and 7 respectively).

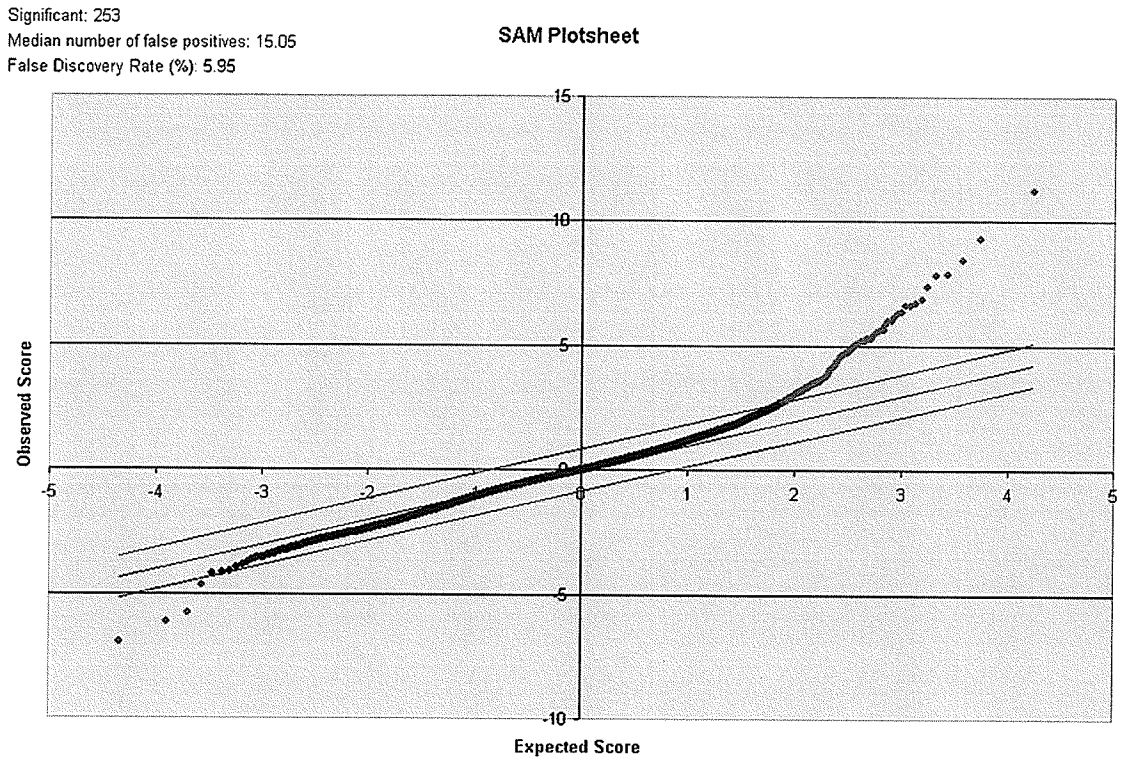

Figure 20: A one-class SAM plot of normalized microarray data obtained from scrapie-infected mice at 90dpi. Red indicates genes that are up-regulated, green indicates genes that are down-regulated and black indicates genes with no change.

Table 6: Genes up-regulated at 90dpi in whole brain of scrapie-infected mice as compared to uninfected mice.

Accession Number	Hugo Gene Symbol	SAM Score	Fold Change
NM_021274	Cxcl10	7.87	6.8
NM_009977	Cst7	11.25	5.0
NM_021334	Itgax	9.30	3.4
NM_011337	Ccl3	5.17	3.2
NM_008599	Cxcl9	4.75	2.8
NM_008798	Pdcd1	6.87	2.8
NM_020008	Clec7a	8.44	2.6
NM_030701	Gpr109a	4.74	2.5
NM_013653	Ccl5	5.10	2.5
NM_011331	Ccl12	5.88	2.4
NM_013652	Ccl4	7.83	2.4
NM_011333	Ccl2	4.22	2.1
NM_133871	Ifi44	5.11	2.1
AK010014	Ifi27	4.90	2.0
NM_010501	Ifit3	6.34	1.9
NM_011909	Usp18	6.00	1.9
NM_011854	Oasl2	4.70	1.8
NM_172603	Phf11	6.02	1.8
NM_145581	Siglecf	3.61	1.8
NM_011338	Ccl9	5.30	1.8
NM_008533	Cd180	7.38	1.8
NM_009099	Trim30	3.65	1.7
NM_013706	Cd52	6.31	1.7
NM_008331	Ifit1	3.36	1.7
NM_029612	Slamf9	6.72	1.7
K01347	Gfap	5.61	1.6
NM_010846	Mx1	5.20	1.6
NM_008479	Lag3	5.03	1.6
NM_009139	Ccl6	6.16	1.6
NM_021792	Iigp1	3.55	1.6
NM_015783	Isg15	4.58	1.5
NM_031168	Il6	3.35	1.5
NM_030682	Tlr1	6.60	1.5
NM_013654	Ccl7	2.94	1.5
NM_025658	Ms4a4d	3.00	1.5
NM_153510	Pilra	4.53	1.5
NM_016850	Irf7	3.54	1.5
NM_023386	Rtp4	3.68	1.5
NM_007423	Afp	4.77	1.5
NM_145211	Oas1a	3.78	1.5
NM_011905	Tlr2	5.63	1.5

NM_194336	Mpa2l	3.98	1.5
NM_007535	Bcl2a1c	4.62	1.5
NM_013489	Cd84	3.06	1.5
NM_011150	Lgals3bp	3.89	1.5
AK156445	Slamf1	3.09	1.5
NM_018734	Gbp4	3.35	1.5
XM_141353	Gm355	3.60	1.5

Table 7: Genes down-regulated at 90dpi in whole brain of scrapie-infected mice as compared to uninfected mice.

Accession Number	Hugo Gene Symbol	SAM Score	Fold Change
NM_010516	Cyr61	-5.79	1.7
NM_007570	Btg2	-6.95	1.7

Figure 21 is the SAM plot generated which represents the gene expression profile of scrapie-infected mice fed the placebo diet at 130dpi. A total 657 genes influenced by scrapie-infection were were identified as being differentially expressed. 622 of these genes were up-regulated and 35 were down-regulated (see Table 8 and 9 respectively).

To assess the functional significance of the differentially expressed genes identified, genes were divided up into three subgroups: genes which were differentially expressed only at 90dpi, genes which were differentially expressed only at 130dpi and genes were differentially expressed at both 90 and 130dpi. There were: 5 genes up-regulated and 2 genes down-regulated only at 90dpi, 579 genes up-regulated and 35 down-regulated only at 130dpi and 43 genes up-regulated at both 90 and 130dpi (see Table 10).

Seven genes were identified as being differentially expressed only at 90dpi, five up-regulated and two down-regulated. Of the five that were up-regulated, Ifit3, Iigp1 and Gbp4 are induced by interferon, Slamf1 is involved in lymphocyte activation and Gm355 has no known function. The two genes that were down-regulated were Cyr61 and Btg2. Cyr61 has growth factor and heparin binding activity and is involved in cell adhesion and chemotaxis, while Btg2 is involved in the response to DNA damage stimulus, neuron differentiation, and the regulation of apoptosis.

Six hundred and fourteen genes were identified as being differentially expressed only at 130dpi, five hundred and seventy-nine up-regulated and thirty-five down-regulated. Using the software program pathway ingenuity analysis, genes were grouped according

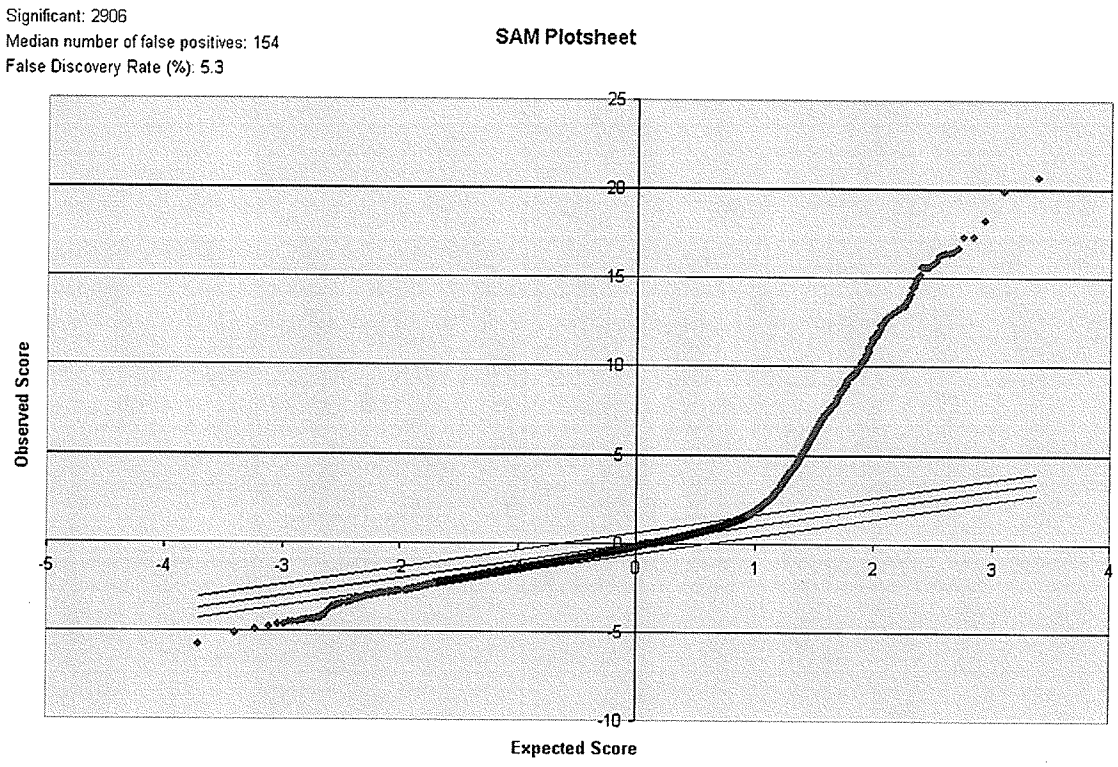

Figure 21: A one-class SAM plot of normalized microarray data obtained from scrapie-infected mice at 130dpi. Red indicates genes that are up-regulated, green indicates genes that are down-regulated and black indicates genes with no change.

Table 8: Genes up-regulated at 130dpi in whole brain of scrapie-infected mice as compared to uninfected mice.

Accession Number	Hugo Gene Symbol	SAM Score	Fold Change
NM_009977	Cst7	19.86	45.1
NM_021274	Cxcl10	18.20	22.0
NM_020008	Clec7a	15.00	21.7
NM_011337	Ccl3	14.89	19.8
NM_008798	Pdcd1	15.57	13.5
NM_013652	Ccl4	13.27	13.0
NM_021334	Itgax	16.44	10.2
NM_030701	Gpr109a	7.76	9.3
NM_031167	Il1rn	6.07	8.1
NM_013706	Cd52	13.30	7.6
NM_011331	Ccl12	11.66	7.5
NM_009139	Ccl6	14.45	7.5
K01347	Gfap	12.76	7.4
NM_145581	Siglecf	10.71	7.0
NM_011338	Ccl9	12.31	6.4
NM_007535	Bcl2a1c	12.33	6.1
NM_013653	Ccl5	9.54	6.0
NM_008599	Cxcl9	6.52	5.9
NM_011905	Tlr2	17.27	5.8
NM_007649	Cd48	20.66	5.6
AK010014	Ifi27	14.12	5.6
NM_013489	Cd84	14.68	5.5
NM_007534	Bcl2a1b	15.57	5.5
NM_008491	Lcn2	4.77	5.5
NM_013532	Lilrb4	8.92	5.2
NM_009890	Ch25h	12.02	5.2
NM_011333	Ccl2	11.33	5.2
NM_133871	Ifi44	9.95	5.2
NM_011854	Oasl2	10.40	5.1
NM_013590	Lzp-s	15.62	5.1
NM_009099	Trim30	8.25	5.1
NM_009252	Serpina3n	13.58	5.0
NM_008479	Lag3	16.24	5.0
NM_010745	Ly86	12.76	4.9
NM_008526	Klrb1b	8.05	4.9
NM_029612	Slamf9	13.46	4.9
NM_007423	Afp	10.26	4.8
NM_008331	Ifit1	9.28	4.8
NM_018866	Cxcl13	4.43	4.7
NM_009779	C3ar1	9.14	4.7
NM_008152	Gpr65	7.92	4.7
NM_172603	Phf11	7.70	4.7
NM_017372	Lyzs	11.16	4.6

NM_007572	C1qa	11.80	4.6
NM_010187	Fcgr2b	12.86	4.5
NM_021281	Ctss	16.37	4.5
NM_009780	C4b	11.43	4.5
NM_009777	C1qb	10.97	4.4
NM_011150	Lgals3bp	13.35	4.3
NM_011909	Usp18	10.14	4.3
NM_011593	Timp1	7.23	4.2
NM_008533	Cd180	6.89	4.2
NM_172796	Slfn9	10.37	4.1
NM_177337	Arl11	8.59	4.1
NM_010737	Klrb1a	7.45	4.1
NM_010846	Mx1	5.34	4.1
NM_030682	Tlr1	11.56	4.1
NM_023386	Rtp4	12.68	4.1
NM_030720	Gpr84	9.28	4.0
NM_007574	C1qc	12.35	4.0
NM_031254	Trem2	11.62	3.9
XM_129176	Mpeg1	10.65	3.9
NM_023158	Cxcl16	11.40	3.8
NM_030707	Msr2	9.96	3.8
NM_010554	Il1a	5.96	3.8
NM_008134	Glycam1	5.82	3.7
NM_021792	Iigp1	7.19	3.7
NM_134158	Cd300d	13.28	3.6
NM_009845	Cd22	6.85	3.6
NM_019388	Cd86	11.29	3.6
NM_053110	Gpnmb	9.28	3.6
NM_011662	Tyrobp	10.15	3.6
NM_013545	Ptpn6	9.59	3.6
NM_007654	Cd72	10.39	3.5
NM_019984	Tgm1	4.82	3.5
NM_145634	Cd300lf	4.33	3.5
NM_178825	Epsti1	5.04	3.5
NM_010728	Lox	9.61	3.5
NM_181542	Slfn10	7.22	3.5
NM_018734	Gbp4	7.39	3.5
NM_016850	Irf7	8.48	3.5
NM_009735	B2m	10.70	3.4
J05020	Fcer1g	9.53	3.4
NM_026835	Ms4a6d	8.41	3.4
NM_015783	Isg15	7.08	3.4
NM_011210	Ptprc	9.85	3.3
NM_021365	Xlr4b	3.49	3.3
NM_010188	Fcgr3	9.52	3.3
NM_008326	Irgm	9.32	3.3
NM_011126	Plunc	2.84	3.2

NM_023044	Slc15a3	8.16	3.2
NM_010186	Fcgr1	10.72	3.2
NM_009853	Cd68	9.92	3.2
NM_145227	Oas2	7.06	3.2
NM_007609	Casp4	8.63	3.2
BC080756	H2-K1	10.21	3.2
NM_008878	Serpinf2	5.40	3.1
NM_144559	Fcgr3a	6.19	3.1
NM_009983	Ctsd	9.74	3.1
NM_010872	Birc1b	8.79	3.1
NM_198095	Bst2	7.98	3.1
NM_010130	Emr1	7.89	3.1
NM_145226	Oas3	4.48	3.1
NM_194336	Mpa2l	12.50	3.1
NM_009982	Ctsc	10.04	3.0
NM_019549	Plek	11.84	3.0
NM_019467	Aif1	7.34	3.0
NM_134250	Havcr2	9.99	3.0
NM_007782	Csf3r	12.48	3.0
NM_011853	Oas1b	9.56	3.0
NM_009141	Cxcl5	7.62	3.0
NM_146023	Evi2b	5.22	3.0
NM_018729	Cd244	4.30	3.0
NM_022431	Ms4a11	9.10	3.0
NM_025658	Ms4a4d	4.73	3.0
NM_145211	Oas1a	7.88	3.0
NM_015811	Rgs1	4.57	2.9
NM_007657	Cd9	10.60	2.9
NM_007807	Cybb	4.30	2.9
NM_023380	Samsn1	9.97	2.9
NM_053214	Myo1f	7.40	2.9
NM_010724	Psmb8	8.27	2.9
NM_181545	Slfn8	5.48	2.9
NM_001039530	Parp14	6.28	2.9
NM_013654	Ccl7	9.61	2.9
NM_007651	Cd53	10.68	2.8
NM_021394	Zbp1	6.37	2.8
NM_028595	Ms4a6c	7.58	2.8
NM_145153	Oas1f	7.04	2.8
NM_023258	Pycard	8.83	2.8
NM_008206	H2-Oa	6.76	2.8
NM_153510	Pilra	7.36	2.8
NM_008534	Ly9	6.01	2.7
NM_011539	Tbxas1	10.53	2.7
NM_011095	Lilrb3	6.03	2.7
NM_172689	Ddx58	4.87	2.7
NM_001038604	Clec5a	8.89	2.7

NM_013606	Mx2	7.74	2.7
NM_175628	A2m	5.59	2.7
NM_173006	Pon3	5.64	2.7
NM_008394	Isgf3g	6.75	2.7
NM_133211	Tlr7	6.40	2.7
NM_010422	Hexb	9.93	2.7
NM_009924	Cnr2	3.45	2.7
NM_028752	Hvcn1	11.07	2.6
NM_013612	Slc11a1	11.24	2.6
NM_138677	Edem1	7.89	2.6
NM_010876	Ncf1	7.05	2.6
NM_010391	H2-Q10	6.09	2.6
NM_027209	Ms4a6b	5.58	2.6
NM_007498	Atf3	7.47	2.6
NM_011815	Fyb	7.91	2.6
NM_030253	Parp9	8.56	2.6
NM_008320	Irf8	9.04	2.6
AK037574	H2-Q1	8.64	2.6
NM_011019	Osmr	5.30	2.6
NM_010407	Hck	7.76	2.6
NM_178611	Lair1	9.98	2.5
NM_021384	Rsad2	3.80	2.5
NM_022325	Ctsz	7.24	2.5
NM_029499	Ms4a4c	5.15	2.5
NM_010877	Ncf2	7.49	2.5
NM_008199	H2-Bl	7.22	2.5
NM_008200	H2-D4	7.52	2.5
NM_030691	Igsf6	7.98	2.5
NM_027836	Ms4a7	5.52	2.5
NM_010686	Laptm5	7.51	2.5
NM_010380	H2-D1	8.38	2.5
NM_007801	Ctsh	8.33	2.5
NM_011725	Xlr	8.07	2.5
NM_022964	Lat2	6.90	2.5
NM_144830	Tmem106a	7.85	2.5
NM_007806	Cyba	6.25	2.5
NM_008879	Lcp1	8.76	2.4
NM_183168	P2ry6	6.09	2.4
NM_145209	Oasl1	6.18	2.4
NM_010260	Gbp2	6.43	2.4
NM_032400	Sucnr1	6.11	2.4
NM_009841	Cd14	7.24	2.4
NM_007679	Cebpd	7.15	2.4
NM_033601	Bcl3	5.86	2.4
NM_011408	Slfn2	6.72	2.4
NM_133859	Olfml3	8.48	2.4
NM_030684	Trim34	7.69	2.4

NM_010493	Icam1	7.30	2.4
AK041599	Stat1	7.72	2.4
NM_010394	H2-Q7	7.67	2.4
NM_020286	Tspan32	4.07	2.3
NM_026405	Rab32	9.57	2.3
NM_010708	Lgals9	6.70	2.3
AK046736	Fbxo39	7.58	2.3
NM_018738	Igtp	7.74	2.3
NM_009303	Syngr1	7.08	2.3
NM_007979	F9	3.56	2.3
XM_910566	Cybrd1	6.72	2.3
NM_019456	Apbb1ip	6.70	2.3
NM_019455	Ptgds2	6.35	2.3
NM_025378	Ifitm3	7.18	2.3
NM_008880	Plscr2	5.36	2.3
NM_011691	Vav1	8.29	2.3
NM_009690	Cd5l	2.52	2.3
NM_008677	Ncf4	6.54	2.3
NM_009263	Spp1	6.50	2.3
NM_183390	Klhl6	6.63	2.3
NM_008175	Grn	9.43	2.3
NM_010398	H2-T23	7.06	2.3
NM_178911	Pld4	6.21	2.3
NM_011355	Sfpi1	6.02	2.2
NM_013482	Btk	6.93	2.2
BC094937	Rhoh	4.94	2.2
NM_007599	Capg	7.13	2.2
NM_027321	Lrrc39	6.75	2.2
NM_010392	H2-Q2	6.95	2.2
NM_031159	Apobec1	5.58	2.2
NM_009008	Rac2	6.92	2.2
NM_011827	Hcst	5.75	2.2
NM_008198	Cfb	5.45	2.2
NM_008404	Itgb2	7.24	2.2
AK170324	Itgam	4.73	2.2
NM_011609	Tnfrsf1a	5.94	2.2
NM_008361	Il1b	3.69	2.2
NM_028608	Glipr1	5.33	2.2
NM_030710	Slamf6	4.44	2.2
NM_207210	Dyrk4	2.92	2.2
NM_033374	Dock2	5.23	2.2
NM_031168	Il6	2.45	2.1
NM_011823	Gpr34	6.81	2.1
NM_013683	Tap1	7.31	2.1
NM_001033416	Gal3st4	8.37	2.1
NM_027835	Ifih1	2.14	2.1
NM_027206	Tnfaip8l2	5.32	2.1

NM_010393	H2-Q5	5.86	2.1
NM_022024	Gmfg	5.87	2.1
NM_023065	Ifi30	5.95	2.1
NM_007645	Cd37	5.05	2.1
NM_023121	Gngt2	6.23	2.1
NM_001033525	Kcnk6	5.78	2.1
NM_028864	Zc3hav1	10.35	2.1
NM_023738	Ube1l	6.69	2.1
NM_011604	Tlr6	3.37	2.1
NM_008330	Ifi47	7.83	2.1
NM_009146	Frrs1	5.04	2.1
NM_010809	Mmp3	4.05	2.1
NM_010747	Lyn	7.34	2.1
NM_001013365	Osm	2.59	2.1
NM_172648	Ifi205	6.39	2.1
NM_019440	Iigp2	6.54	2.1
NM_020258	Slc37a2	8.09	2.0
NM_008630	Mt2	3.81	2.0
NM_008873	Plau	3.22	2.0
NM_007577	C5ar1	4.93	2.0
NM_013585	Psmb9	6.14	2.0
NM_021293	Cd33	5.97	2.0
NM_013470	Anxa3	6.61	2.0
NM_153404	Liph	4.05	2.0
NM_023835	Trim12	8.36	2.0
AJ428208	Ptprz1	4.42	2.0
NM_011206	Ptpn18	5.53	2.0
NM_201410	Ugt1a6b	6.85	2.0
NM_008278	Hpgd	6.04	2.0
NM_008987	Ptx3	4.05	2.0
NM_009851	Cd44	7.44	2.0
NM_007695	Chi3l1	7.80	2.0
NM_010658	Mafb	5.13	2.0
NM_178440	Myo1g	5.30	2.0
AK049998	Apobec3	4.26	2.0
NM_009700	Aqp4	4.48	2.0
NM_028785	Dock8	5.10	2.0
NM_010696	Lcp2	5.12	2.0
NM_009821	Runx1	5.59	2.0
NM_134152	Lpxn	5.16	2.0
NM_011157	Prg1	7.03	2.0
NM_013563	Il2rg	5.30	2.0
AK156040	Clec4a3	4.89	2.0
NM_008528	Blnk	4.39	2.0
BC068159	Iqgap3	4.16	2.0
NM_011701	Vim	4.90	2.0
NM_030712	Cxcr6	3.97	1.9

NM_173014	Aytl1	7.41	1.9
NM_015766	Ebi3	5.83	1.9
NM_028122	Slc14a1	8.52	1.9
NM_007781	Csf2rb2	5.37	1.9
NM_023141	Tor3a	7.64	1.9
NM_010368	Gusb	7.38	1.9
NM_011405	Slc7a7	7.15	1.9
NM_023209	Pbk	3.41	1.9
NM_007453	Prdx6	7.39	1.9
NM_019494	Cxcl11	6.17	1.9
NM_011173	Pros1	9.55	1.9
NM_010705	Lgals3	5.97	1.9
NM_207105	H2-Ab1	2.99	1.9
NM_008189	Guca1a	4.10	1.9
NM_020568	S3-12	3.68	1.9
NM_010512	Igf1	5.30	1.9
NM_170727	Scgb3a1	4.21	1.9
NM_023124	H2-Q8	4.92	1.9
XM_485982	Gm1966	7.61	1.9
NM_009578	Zfpn1a1	3.82	1.9
NM_011163	Eif2ak2	4.22	1.9
NM_023275	Rhoj	6.37	1.9
NM_173027	Ihpk3	4.31	1.9
NM_153505	Nckap1l	4.56	1.9
NM_010389	H2-Ob	3.74	1.9
NM_008108	Gdf3	3.13	1.9
NM_023142	Arpc1b	5.77	1.9
NM_170758	Cd300a	5.62	1.9
NM_009778	C3	5.72	1.9
AK154286	Csf2rb1	3.79	1.9
NM_153408	Lincr	4.12	1.9
NM_012057	Irf5	5.62	1.9
NM_013454	Abca1	6.53	1.9
NM_024217	Cmtm3	5.29	1.9
AK088370	Ssb	2.31	1.8
NM_019955	Ripk3	3.53	1.8
NM_021325	Cd200r1	3.26	1.8
NM_145423	Slc5a8	2.30	1.8
NM_021893	Cd274	4.09	1.8
NM_009465	Axl	5.94	1.8
NM_021297	Tlr4	4.46	1.8
NM_029926	Irak4	3.86	1.8
NM_177544	Ang4	4.62	1.8
NM_011311	S100a4	4.64	1.8
NM_009984	Ctsl	7.35	1.8
NM_029084	Slamf8	3.22	1.8
NM_007449	Ang2	4.71	1.8

NM_010378	H2-Aa	2.91	1.8
NM_001012401	Hspb6	4.16	1.8
NM_177568	Plcb2	3.02	1.8
NM_001012322	Sctr	1.87	1.8
AK122521	Plce1	2.70	1.8
NM_033616	Csprs	2.62	1.8
NM_009372	Tgif	5.38	1.8
NM_133193	Il1rl2	2.17	1.8
NM_008605	Mmp12	2.68	1.8
NM_011579	Tgtp	4.07	1.8
NM_008332	Ifit2	5.28	1.8
XM_001000802	Prdx6-rs2	7.48	1.8
NM_028279	Naalad2	4.72	1.8
NM_009403	Tnfsf8	2.32	1.8
NM_023409	Npc2	6.67	1.8
NM_008013	Fgl2	6.44	1.8
XM_110620	Slc25a18	5.46	1.8
NM_008207	H2-T24	6.09	1.8
NM_011521	Sdc4	5.06	1.8
NM_133670	Sult1a1	3.99	1.8
NM_015786	Hist1h1c	4.33	1.8
U72672	Ang3	5.22	1.8
NM_013602	Mt1	4.13	1.8
NM_009370	Tgfbr1	5.93	1.8
NM_007707	Socs3	5.81	1.8
BC011440	Hist1h2bc	2.24	1.8
NM_011426	Siglec1	2.83	1.8
NM_172267	Phyhd1	6.86	1.8
NM_031384	Tex11	2.95	1.8
NM_177382	Cyp2r1	3.53	1.8
NM_009987	Cx3cr1	5.05	1.8
NM_008352	Il12b	2.21	1.8
NM_007779	Csf1r	7.06	1.8
NM_011623	Top2a	2.23	1.8
NM_028728	Nfam1	5.27	1.8
NM_013820	Hk2	4.78	1.8
AK155186	Wdfy4	5.03	1.8
NM_026819	Dhrs1	4.56	1.8
NM_028808	P2ry13	5.18	1.8
NM_053094	Cd163	2.20	1.8
NM_010387	H2-DMb1	4.60	1.8
NM_031195	Msr1	2.10	1.8
NM_021472	Rnase4	7.20	1.8
NM_028968	Ifitm7	4.51	1.8
NM_145713	Hist1h1d	2.67	1.7
NM_146064	Soat2	2.23	1.7
NM_010388	H2-DMb2	3.81	1.7

NM_009023	Rapsn	4.72	1.7
NM_027320	Ifi35	3.49	1.7
NM_010870	Birc1e	5.58	1.7
CO802710	Bmp2k	2.98	1.7
NM_025659	Abi3	4.11	1.7
BC069183	Sp100	4.74	1.7
NM_009136	Scrg1	5.44	1.7
NM_009917	Ccr5	5.66	1.7
NM_010421	Hexa	5.17	1.7
NM_019449	Unc93b1	3.86	1.7
NM_021351	Cryba4	3.62	1.7
NM_007659	Cdc2a	3.97	1.7
NM_020272	Pik3cg	4.94	1.7
NM_029000	Gvin1	5.21	1.7
NM_177256	Prdx6-rs1	5.39	1.7
AK133661	Lrrfip1	3.41	1.7
NM_013693	Tnf	2.21	1.7
NM_008563	Mcm3	4.26	1.7
NM_021718	Ms4a4b	3.85	1.7
NM_026611	Rnaset2	5.92	1.7
NM_028195	Pscd4	4.66	1.7
NM_010545	Cd74	2.76	1.7
NM_009277	Trim21	4.62	1.7
BC022125	Tnfrsf14	2.63	1.7
NM_021398	Slc43a3	4.62	1.7
NM_008225	Hcls1	4.11	1.7
NM_172301	Ccnb1	3.53	1.7
AK137645	Fmo5	1.99	1.7
XM_139038	Gm288	3.24	1.7
NM_183031	Ebi2	5.64	1.7
NM_025565	Spbc25	2.93	1.7
NM_007678	Cebpa	4.94	1.7
NM_030711	Arts1	2.58	1.7
AK090367	Smug1	4.89	1.7
NM_031247	Gimap3	1.87	1.7
NM_145838	St8sia6	4.53	1.7
NM_027450	Glipr2	5.31	1.7
NM_007653	Cd63	5.80	1.7
NM_153551	Dennd1c	5.64	1.7
NM_008511	Lrmp	4.85	1.7
NM_010427	Hgf	3.50	1.7
NM_009888	Cfh	3.33	1.7
NM_008287	Hrsp12	4.36	1.7
NM_025760	Ptplad2	4.40	1.7
XM_135211	Gadl1	3.66	1.7
NM_010566	Inpp5d	5.14	1.7
BC031891	Serpina4-ps1	3.18	1.7

NM_031376	Pik3ap1	3.90	1.7
AK165240	Slc16a10	4.01	1.7
NM_011671	Ucp2	4.97	1.6
NM_178165	Fcrl1	2.83	1.6
NM_008026	Fli1	2.69	1.6
NM_007987	Fas	3.76	1.6
NM_001005508	Arhgap30	3.77	1.6
AK013534	Adora3	3.42	1.6
NM_013467	Aldh1a1	3.75	1.6
NM_010734	Lst1	3.64	1.6
AK039267	Aldoc	5.36	1.6
NM_008587	Mertk	3.60	1.6
NM_009775	Tspo	4.00	1.6
NM_007798	Ctsb	4.77	1.6
NM_011723	Xdh	3.75	1.6
NM_026473	Tubb6	4.15	1.6
NM_007486	Arhgdib	4.23	1.6
NM_010580	Itgb5	4.84	1.6
BC060276	Flnc	4.11	1.6
NM_009292	Stra8	1.76	1.6
NM_019417	Pdlim4	3.27	1.6
AK048226	Chst2	2.36	1.6
AK004668	Tnfrsf13b	5.19	1.6
NM_008871	Serpine1	2.51	1.6
NM_011727	Xlr3b	2.31	1.6
NM_001037724	Adcy7	4.68	1.6
AK154784	Gpr160	5.06	1.6
NM_010265	Gcnt1	4.56	1.6
BC099491	Ceacam15	2.46	1.6
NM_011610	Tnfrsf1b	4.80	1.6
NM_010902	Nfe2l2	3.03	1.6
NM_001033632	Ifitm6	3.43	1.6
AK159148	Slc35d2	4.10	1.6
NM_178706	Siglech	4.17	1.6
NM_011313	S100a6	3.97	1.6
L38281	Irg1	2.30	1.6
NM_007830	Dbi	4.40	1.6
NM_011315	Saa3	2.19	1.6
NM_172647	F11r	5.09	1.6
BC031151	Samd9l	3.19	1.6
NM_010442	Hmox1	4.45	1.6
NM_172893	Parp12	3.08	1.6
NM_144539	Slamf7	3.05	1.6
NM_011893	Sh3bp2	3.65	1.6
AK088352	Itgb3bp	2.45	1.6
NM_013819	H2-M3	4.03	1.6
NM_008245	Hhex	2.28	1.6

NM_134471	Kif2c	2.10	1.6
NM_009515	Was	4.77	1.6
NM_145619	Parp3	5.30	1.6
NM_010755	Maff	3.48	1.6
NM_153098	Cd109	5.74	1.6
AF245475	Mlxipl	3.07	1.6
NM_026960	Gsdmdc1	3.86	1.6
NM_134116	Gpsm3	4.39	1.6
NM_001029929	Zmynd15	4.36	1.6
NM_011361	Sgk	2.92	1.6
NM_021476	Cysltr1	3.78	1.6
NM_020013	Fgf21	2.04	1.6
NM_033622	Tnfsf13b	3.79	1.6
NM_010833	Msn	3.64	1.6
NM_033612	Ela1	4.14	1.6
NM_001030294	Olfm4	4.17	1.6
NM_008510	Xcl1	2.40	1.6
[NM_015790	Icosl	3.14	1.6
NM_009371	Tgfbr2	5.12	1.6
XM_194370]	Adamtsl3	4.32	1.6
NM_023143	C1r	2.79	1.6
AK129290	Rnf44	2.31	1.6
NM_001017959	Lamp2	5.21	1.6
NM_010397	H2-T22	4.39	1.6
NM_134076	Abhd4	6.58	1.6
NM_139233	Fgd4	1.63	1.6
NM_009121	Sat1	3.48	1.6
NM_007778	Csf1	4.79	1.6
NM_008969	Ptgs1	3.87	1.6
NM_009381	Thrsp	3.04	1.6
AK049580	Sema3e	2.25	1.6
NM_194344	Sh3tc1	4.25	1.6
NM_139303	Kif18a	3.21	1.6
NM_139198	Plac8	2.33	1.6
NM_021487	Kcne1l	3.44	1.6
NM_153523	Tcstv3	2.80	1.6
NM_177260	Tmem154	3.66	1.6
NM_018773	Scap2	5.82	1.6
NM_009812	Casp8	4.61	1.6
NM_146131	Pbxip1	4.53	1.6
NM_133990	Il13ra1	4.43	1.6
NM_133209	Pilrb	1.79	1.5
NM_009695	Apoc2	2.93	1.5
NM_019923	Itpr2	3.81	1.5
NM_026410	Cdca5	2.72	1.5
NM_172607	Naprt1	4.02	1.5
NM_019401	Nmi	5.15	1.5

NM_015787	Hist1h1e	4.17	1.5
NM_009230	Soat1	4.55	1.5
AK159194	Hmha1	3.48	1.5
AK086294	Tcfcp2l1	3.09	1.5
NM_011413	C4a	2.65	1.5
AK021164	Fzd9	4.90	1.5
AK045060	Eya4	2.79	1.5
BC005769	Spint1	3.92	1.5
XM_988789	Cdh19	3.83	1.5
NM_009732	Avp	2.65	1.5
BF467941	Hist1h4i	4.51	1.5
NM_009116	Prrx2	4.21	1.5
NM_001033245	Hk3	3.54	1.5
NM_207231	Arl5c	3.49	1.5
NM_009166	Sorbs1	4.20	1.5
NM_177161	P4ha3	3.43	1.5
NM_009477	Upp1	2.12	1.5
NM_175476	Arhgap25	2.73	1.5
NM_008902	Pp11r	3.23	1.5
NM_010736	Ltbr	3.53	1.5
NM_009696	Apoe	2.42	1.5
NM_009546	Trim25	3.94	1.5
NM_011577	Tgfb1	3.67	1.5
NM_146069	Lrrc33	3.61	1.5
NM_015749	Tcn2	4.45	1.5
NM_023132	Renbp	3.45	1.5
NM_177725	Lrrc8a	4.06	1.5
NM_011027	P2rx7	4.94	1.5
NM_126166	Tlr3	4.15	1.5
NM_172572	Rhbdf2	2.61	1.5
NM_008035	Folr2	2.49	1.5
AK079748	Ift57	2.46	1.5
NM_019564	Htra1	4.57	1.5
NM_007385	Apoc4	2.90	1.5
NM_013710	Fgd2	3.95	1.5
NM_027571	P2ry12	2.55	1.5
NM_025383	Necap2	4.20	1.5
NM_009155	Sepp1	1.89	1.5
NM_027260	Vrk2	2.71	1.5
NM_146011	Arhgap9	3.35	1.5
NM_016767	Batf	3.28	1.5
NM_007601	Capn3	3.21	1.5
NM_008176	Cxcl1	1.74	1.5
NM_144875	Rab7l1	5.00	1.5
BC050049	Zfpn1a2	3.04	1.5
NM_177320	Pik3r5	3.75	1.5
NM_175655	Hist1h4f	3.90	1.5

NM_008521	Ltc4s	2.56	1.5
NM_205536	Elk3	3.92	1.5
NM_010764	Man2b1	5.14	1.5
NM_175088	Mdfic	3.18	1.5
NM_028333	Angptl1	4.27	1.5
NM_019738	Nupr1	3.27	1.5
NM_175316	Slco2b1	3.41	1.5
NM_008728	Npr3	1.68	1.5
NM_177350	Gldn	2.07	1.5
NM_172514	Tmem71	1.82	1.5
NM_008390	Irf1	4.71	1.5
NM_009640	Angpt1	2.98	1.5
NM_026418	Rgs10	4.73	1.5
NM_009805	Cflar	3.27	1.5
NM_008339	Cd79b	2.77	1.5
AK007221	Herc5	2.13	1.5
NM_183201	Slfn5	4.27	1.5
NM_010276	Gem	3.41	1.5
NM_008348	Il10ra	3.60	1.5
NM_145852	Ropn1l	3.40	1.5
NM_010620	Kif15	1.75	1.5
NM_138672	Stab1	3.34	1.5
AK138175	Mipol1	1.70	1.5
NM_172767	Loh11cr2a	2.90	1.5
NM_022305	B4galt1	3.41	1.5
NM_024469	Bhlhb3	1.63	1.5
NM_175654	Hist1h4d	3.35	1.5
AK033361	Gm505	2.50	1.5
NM_009848	Entpd1	4.10	1.5
NM_013777	Akr1c12	2.94	1.5
NM_013689	Tec	4.01	1.5
NM_013901	Slc39a1	2.92	1.5
NM_013492	Clu	3.83	1.5
NM_009663	Alox5ap	3.75	1.5
AK045953	Usp53	3.16	1.5
NM_153801	Srd5a2l2	2.20	1.5
NM_024253	Nkg7	2.68	1.5
XM_110743	Gm8	2.08	1.5
NM_009351	Tep1	3.10	1.5
NM_138310	Apob48r	2.84	1.5
NM_026785	Ube2c	2.18	1.5
NM_053007	Cntf	4.07	1.5
AF384098	Mlph	2.77	1.5
NM_178280	Sall3	2.94	1.5
NM_016753	Lxn	4.48	1.5
NM_008625	Mrc1	2.34	1.5
AK048650	Smc4	1.68	1.5

NM_033596	Hist2h4	3.51	1.5
NM_009807	Casp1	4.42	1.5
NM_009222	Snap23	4.89	1.5
AK046688	Slc1a3	3.30	1.5
NM_027307	Golph2	4.15	1.5
NM_022321	Parvg	3.27	1.5
NM_011309	S100a1	3.16	1.5
NM_001033122	Cd69	2.12	1.5
NM_008377	Lrig1	3.26	1.5
NM_007746	Map3k8	1.69	1.5
NM_009776	Serping1	3.93	1.5
NM_011507	Suclg2	3.34	1.5
NM_028071	Cotl1	3.50	1.5
NM_010171	F3	4.28	1.5
NM_007825	Cyp7b1	3.94	1.5

Table 9: Complete list of genes down-regulated at 130dpi in whole brain of scrapie-infected mice as compared to uninfected mice.

Accession Number	Hugo Gene Symbol	SAM Score	Fold Change
NM_018790	Arc	-5.15	-2.3
NM_010118	Egr2	-4.63	-2.2
NM_153553	Npas4	-4.19	-2.1
NM_010444	Nr4a1	-4.80	-1.9
NM_007504	Atp2a1	-5.78	-1.8
NM_011618	Tnnt1	-3.55	-1.8
NM_020509	Retnla	-2.58	-1.8
NM_029987	Rpe65	-3.32	-1.8
NM_013642	Dusp1	-4.50	-1.7
NM_013912	Apln	-4.91	-1.7
XM_901510	Synpo2	-3.12	-1.6
NM_013665	Shox2	-3.31	-1.6
NM_009393	Tnnc1	-3.14	-1.6
AK041673	Slc2a13	-2.60	-1.6
NM_010678	Aff3	-2.46	-1.6
NM_025980	Nrarp	-4.30	-1.6
NM_010234	Fos	-3.00	-1.6
NM_024204	Ankrd22	-2.65	-1.6
NM_145935	Glyat	-2.71	-1.6
AK081588	Ntrk1	-3.91	-1.6
NM_007913	Egr1	-2.92	-1.6
NM_153107	Cpz	-2.96	-1.6
NM_019690	Gnas	-2.56	-1.6
NM_010262	Gbx2	-3.37	-1.5
NM_010499	Ier2	-3.47	-1.5
NM_008295	Hsd3b5	-2.95	-1.5
NM_011540	Tcap	-2.81	-1.5
NM_010419	Hes5	-3.54	-1.5
NM_011607	Tnc	-2.76	-1.5
XM_979146	Klhl14	-3.10	-1.5
NM_009496	Vamp1	-3.28	-1.5
NM_013639	Prph1	-2.48	-1.5
NM_011103	Prkcd	-4.49	-1.5
NM_030699	Ntng1	-2.64	-1.5
NM_020596	Egr4	-2.52	-1.5

Table 10: Genes up-regulated at 90dpi and 130dpi in whole brain of scrapie-infected mice as compared to uninfected mice.

Accession Number	Hugo Gene Symbol	SAM Score @ 90dpi	Fold Change @ 90 dpi	SAM Score @ 130dpi	Fold Change @ 130dpi
NM_021274	Cxcl10	7.87	**6.8**	18.20	**22.0**
NM_009977	Cst7	11.25	**5.0**	19.86	**45.1**
NM_021334	Itgax	9.30	**3.4**	16.44	**10.2**
NM_011337	Ccl3	5.17	**3.2**	14.89	**19.8**
NM_008599	Cxcl9	4.75	**2.8**	6.52	**5.9**
NM_008798	Pdcd1	6.87	**2.8**	15.57	**13.5**
NM_020008	Clec7a	8.44	**2.6**	15.00	**21.7**
NM_030701	Gpr109a	4.74	**2.5**	7.76	**9.3**
NM_013653	Ccl5	5.10	**2.5**	9.54	**6.0**
NM_011331	Ccl12	5.88	**2.4**	11.66	**7.5**
NM_013652	Ccl4	7.83	**2.4**	13.27	**13.0**
NM_011333	Ccl2	4.22	**2.1**	11.33	**5.2**
NM_133871	Ifi44	5.11	**2.1**	9.95	**5.2**
AK010014	Ifi27	4.90	**2.0**	14.12	**5.6**
NM_011909	Usp18	6.00	**1.9**	10.14	**4.3**
NM_011854	Oasl2	4.70	**1.8**	10.40	**5.1**
NM_172603	Phf11	6.02	**1.8**	7.70	**4.7**
NM_145581	Siglecf	3.61	**1.8**	10.71	**7.0**
NM_011338	Ccl9	5.30	**1.8**	12.31	**6.4**
NM_008533	Cd180	7.38	**1.8**	6.89	**4.2**
NM_009099	Trim30	3.65	**1.7**	8.25	**5.1**
NM_013706	Cd52	6.31	**1.7**	13.30	**7.6**
NM_008331	Ifit1	3.36	**1.7**	9.28	**4.8**
NM_029612	Slamf9	6.72	**1.7**	13.46	**4.9**
K01347	Gfap	5.61	**1.6**	12.76	**7.4**
NM_010846	Mx1	5.20	**1.6**	5.34	**4.1**
NM_008479	Lag3	5.03	**1.6**	16.24	**5.0**
NM_009139	Ccl6	6.16	**1.6**	14.45	**7.5**
NM_015783	Isg15	4.58	**1.5**	7.08	**3.4**
NM_031168	Il6	3.35	**1.5**	2.45	**2.1**
NM_030682	Tlr1	6.60	**1.5**	11.56	**4.1**
NM_013654	Ccl7	2.94	**1.5**	9.61	**2.9**
NM_025658	Ms4a4d	3.00	**1.5**	4.73	**3.0**
NM_153510	Pilra	4.53	**1.5**	7.36	**2.8**
NM_016850	Irf7	3.54	**1.5**	8.48	**3.5**
NM_023386	Rtp4	3.68	**1.5**	12.68	**4.1**
NM_007423	Afp	4.77	**1.5**	10.26	**4.8**
NM_145211	Oas1a	3.78	**1.5**	7.88	**3.0**
NM_011905	Tlr2	5.63	**1.5**	17.27	**5.8**
NM_194336	Mpa2l	3.98	**1.5**	12.50	**3.1**
NM_007535	Bcl2a1c	4.62	**1.5**	12.33	**6.1**
NM_013489	Cd84	3.06	**1.5**	14.68	**5.5**

NM_011150	Lgals3bp	3.89	**1.5**	13.35	**4.3**

to their biological function (see Figure 22). A few of the main functions identified include: immune response, tissue morphology, haematological system development and function, cell signalling, cell death, lipid metabolism and vitamin and mineral transport. It is difficult to determine which of the 614 genes are changed in response to disesase-associated oxidative stress. This is because at 130dpi mice are nearing the end of their lives, thus the changes in gene expression observed may be the result of their deteriorating condition and/or prion infection.

Of particular interest were the forty-three genes, which were found to be up-regulated at both 90 and 130dpi. Using the software program pathway ingenuity analysis, genes were grouped according to their biological function (see Figure 23). A few of the main functions identified include: immune response, cellular movement, haematological system development and function, cell signalling, cellular development and neurological disease.

Twenty three of these genes are involved in oxidative stress and can be broken down into three classes. The first class includes genes which may be induced by oxidative stress: Cxcl10, Ccl7, Ccl2, Ccl3, Tlr2, Il6, Cxcl9, Itgax and Cst7. The second class includes genes which release ROS: Ccl2, Ccl3, Ccl4 and Ccl5. The third class includes interferon stimulated genes: Ifi27, Ifi44, Irf7, Ifit1, Mx1, Oasl2, Oas1a, Rtp4, Isg15, Usp18, and Trim 30. There were no genes down-regulated at both 90 and 130dpi.

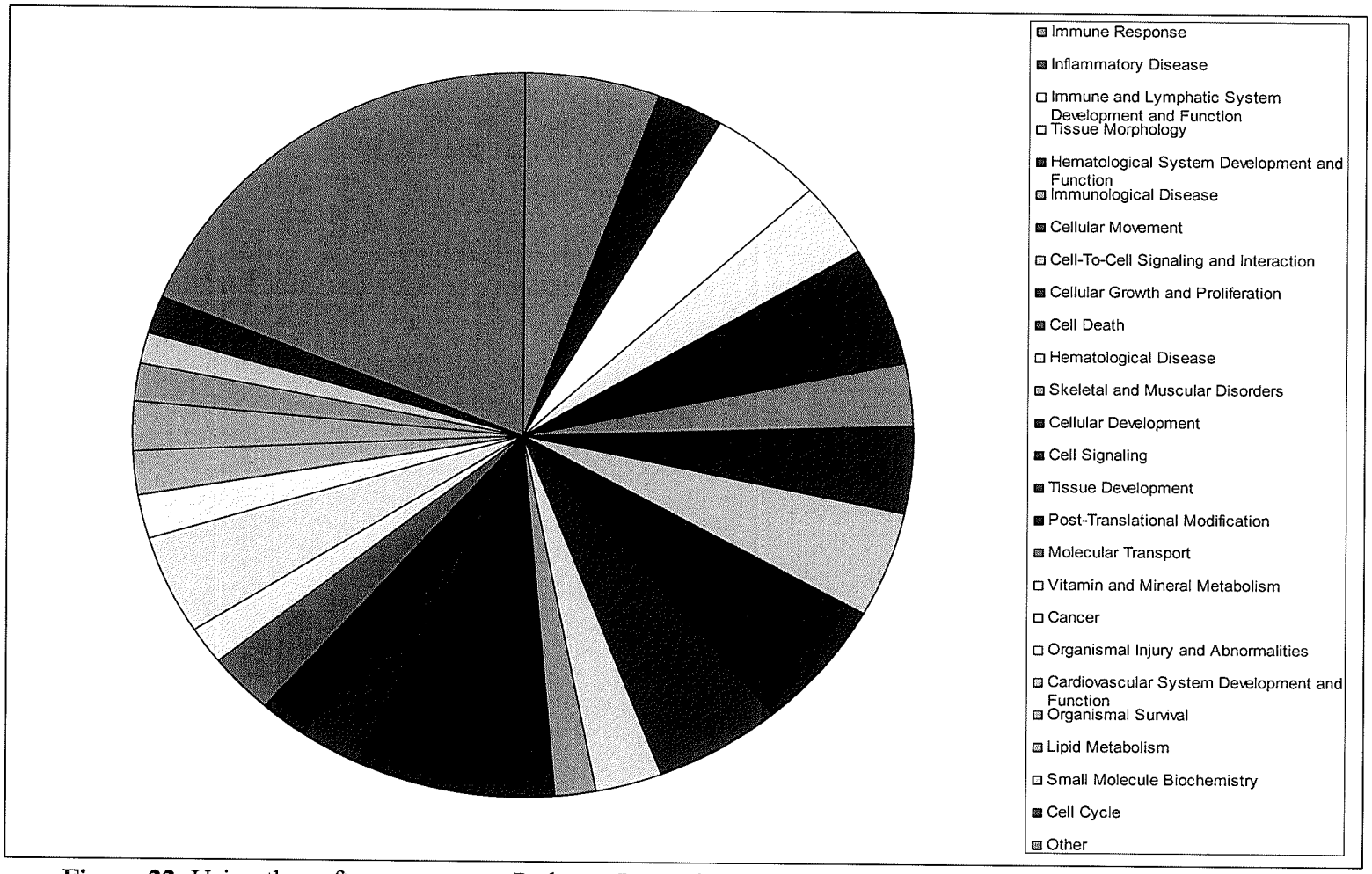

Figure 22: Using the software program Pathway Ingenuity Analysis, differentially expressed genes in scrapie-infected mice at 130dpi were grouped according to their biological function.

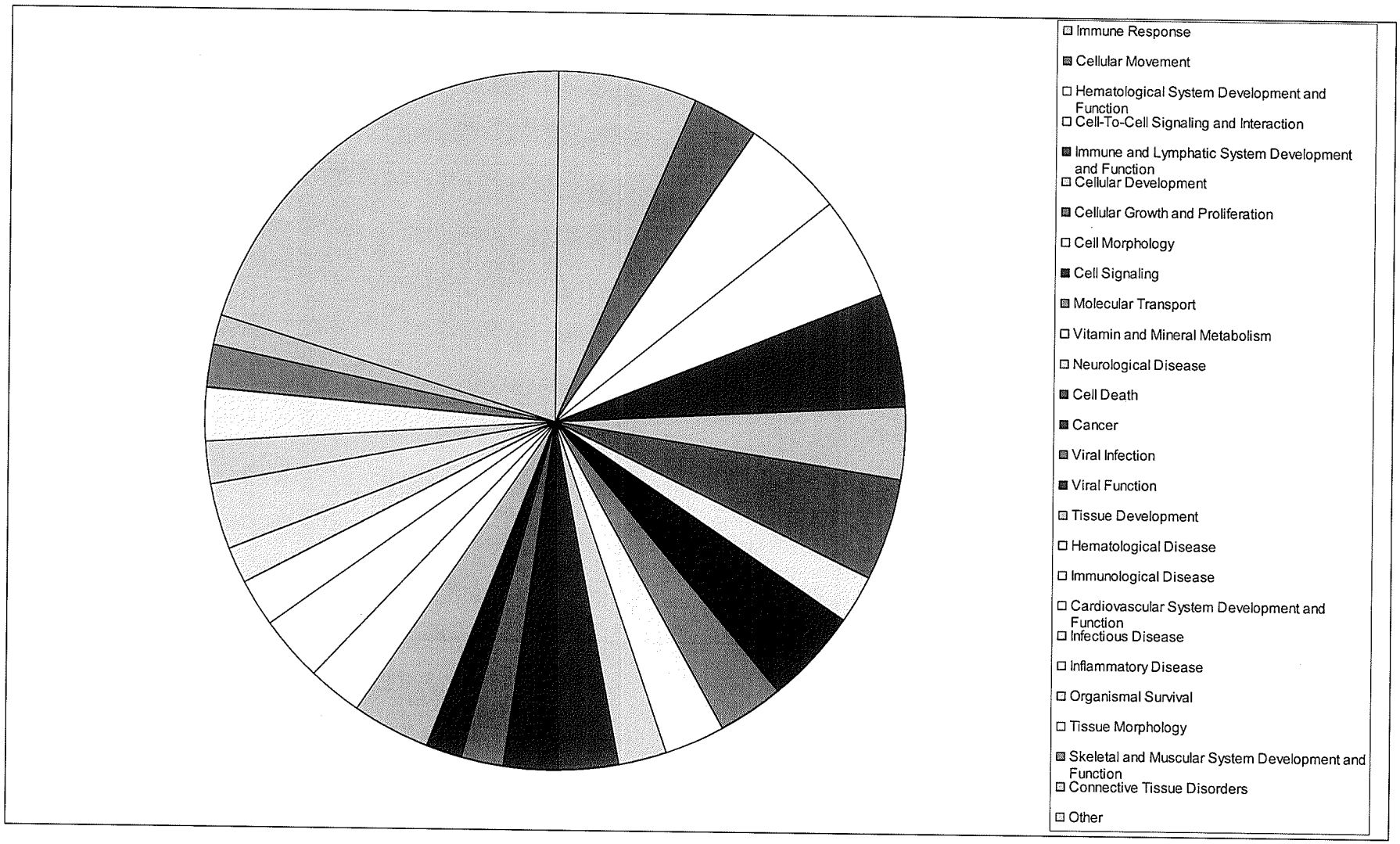

Figure 23: Using the software program Pathway Ingenuity Analysis, differentially expressed genes in scrapie-infected mice at both 90 and 130dpi were grouped according to their biological function

8.3.2 The effect of an antioxidant diet on whole brain gene expression observed in scrapie-infected mice.

Eight microarrays respectively at 90 and 130dpii were performed on total RNA extracted from whole brain of scrapie-infected fed the antioxidant diet and scrapie-infected mice fed the placebo diet. A one-class SAM was performed on the normalized data. Genes that were considered to be significant had a fold change ≥ 1.5 and FDR $\leq 5\%$. Genes that had no known HUGO Symbol were excluded.

Figure 24 is the SAM plot generated which represents the gene expression profile of scrapie-infected mice fed the antioxidant diet at 90dpi. A total of 96 genes influenced by the antioxidant diet were identified as being differentially expressed. All of the 96 genes identified were up-regulated (see Table 10). Using the software program pathway ingenuity analysis, genes were grouped according to their biological function (see Figure 25). A few of the main functions identified include: gene expression, cell cycle, cancer, small molecule biochemistry, cellular development, organism survival, and cellular assembly and organization.

Figure 26 is the SAM plot generated which represents the gene expression profile of scrapie-infected mice fed the antioxidant diet at 130dpi. A total of 5 genes influenced by the antioxidant diet were identified as being differentially expressed. All 5 genes identified were up-regulated (see Table 11). Using the software program pathway

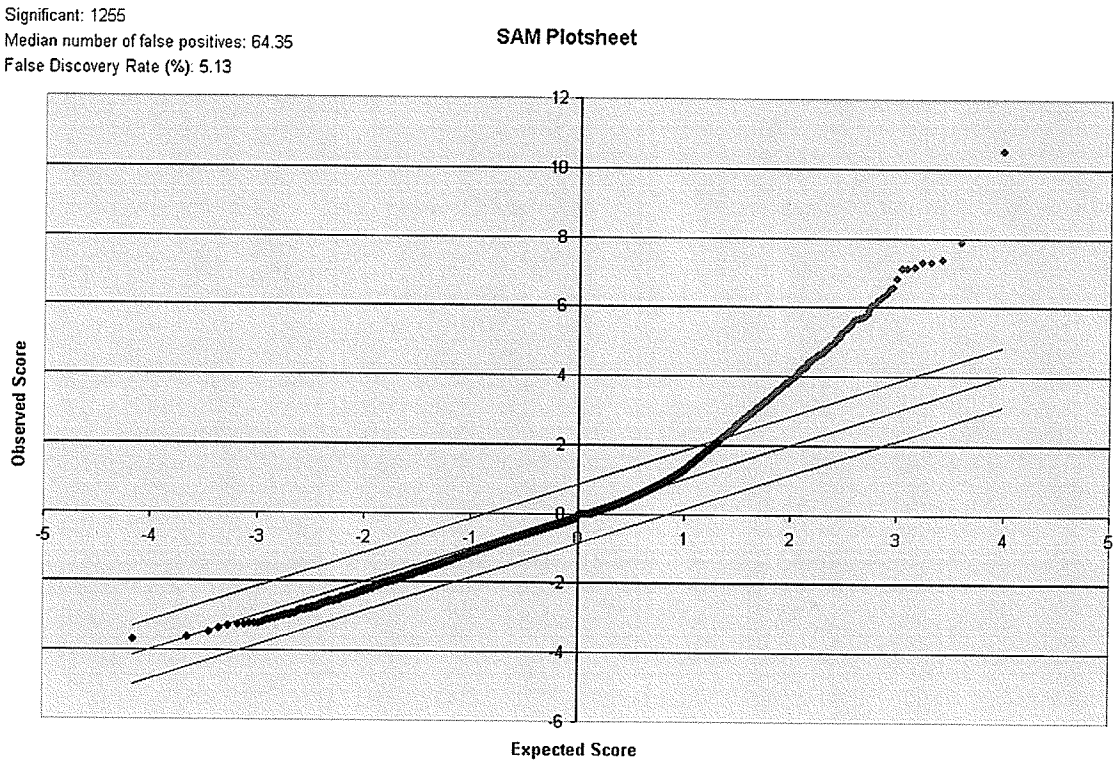

Figure 24: A one-class SAM plot of normalized microarray data obtained from scrapie-infected mice fed the antioxidant diet at 90dpi. Red indicates genes that are up-regulated and black indicates genes with no change.

Table 10: Genes up-regulated at 90dpi in whole brain of scrapie-infected mice fed an antioxidant diet

Accession Number	Hugo Gene Symbol	SAM Score	Fold Change
NM_008224	Hcfc1	0.00	2.6
AK047324	Sh3gl2	0.00	2.5
AK044939	Tmem65	0.00	2.4
AK048499	Mnat1	0.00	2.3
AK035956	Chm	0.58	2.2
NM_008527	Klrb1c	0.00	2.1
NM_177355	Plcxd3	0.00	2.1
AK036570	Ank2	1.06	2.1
BC079861	Mlh3	0.00	2.0
XM_994427	Sh3d19	0.00	2.0
AK143960	Tcfcp2l1	1.06	1.9
AK036310	Syne1	0.00	1.9
AK035860	Pde4d	0.00	1.8
AK053275	Eml5	0.00	1.8
NM_013598	Kitl	0.00	1.8
AK080005	Zfp668	0.86	1.8
XM_897767	Cdh10	0.00	1.8
AK083466	Arih1	3.88	1.8
NM_009877	Cdkn2a	1.75	1.8
NM_144920	Plekha5	0.86	1.7
NM_019825	Ncoa6	0.00	1.7
AK044137	Suhw3	0.00	1.7
AK037826	Ramp1	1.30	1.7
BC004722	Malat1	0.00	1.7
AK085093	Xrcc2	1.67	1.7
AK087183	Csad	3.88	1.7
AK030422	Ppp2r2b	0.00	1.7
NM_029437	Ckap5	1.49	1.7
AK087325	Npal2	1.49	1.7
AK049797	Pcdh9	1.49	1.7
AK036726	Brf1	0.00	1.7
AK044172	Chgb	4.57	1.7
AK042801	Rasa1	2.13	1.7
AK046126	Ing4	0.00	1.7
XM_358382	Dmxl2	1.75	1.7
AK016255	Speer7-ps1	0.00	1.7
AK041435	Utrn	0.00	1.7
BC024722	Ap3b2	0.00	1.7
XM_915709	Tmem132b	0.00	1.7
NM_029842	Jmjd5	0.00	1.6
NM_172861	Slc7a14	0.00	1.6
AK044228	Cecr5	0.58	1.6
AF546078	Setdb1	3.69	1.6

NM_173868	St18	1.30	1.6
AK040384	Ep300	2.13	1.6
AK036972	Dlgh2	0.00	1.6
AK046208	Zfp398	0.58	1.6
NM_023624	Lrat	1.06	1.6
AK044890	Dgcr8	0.58	1.6
NR_001463	Xist	1.89	1.6
AK052347	Lphn3	0.00	1.6
NM_181324	Ddx6	1.30	1.6
NM_001033261	Psrc2	1.06	1.6
XM_902605	Ankrd11	4.57	1.6
NM_020507	Tob2	0.00	1.6
AK088507	Ap3s1	1.67	1.6
NM_138679	Ash1l	0.00	1.6
AK051283	Pftk1	2.78	1.6
NM_023596	Slc29a3	0.86	1.6
NM_011855	Odz1	1.75	1.6
NM_007520	Bach1	1.30	1.6
BC049181	R3hdm1	0.86	1.5
NM_172868	Palm2	0.00	1.5
AK050035	Lpp	1.06	1.5
AK080472	Zfp711	3.69	1.5
NM_010727	Lnx1	0.00	1.5
NM_145525	Osbpl6	0.00	1.5
AK040761	Vgcnl1	0.00	1.5
NM_178912	Fancm	1.67	1.5
AK036131	Mmd	1.67	1.5
NM_008514	Lrp6	1.89	1.5
AK018652	Saps3	0.86	1.5
NM_153553	Npas4	1.89	1.5
NM_009875	Cdkn1b	0.00	1.5
AK052373	Map4k5	4.57	1.5
AK038572	Zfp292	3.04	1.5
XM_917083	Syne2	0.00	1.5
AK031649	Hs6st2	1.89	1.5
AK033959	Lpin2	3.69	1.5
AK029093	Hivep3	0.58	1.5
NM_177224	Chd9	1.30	1.5
NM_009723	Atp2b2	0.86	1.5
BC023187	Cdc27	0.00	1.5
NM_010243	Fut9	0.58	1.5
AK087577	Eif2c3	1.30	1.5
AK036716	Ebf1	1.06	1.5
AK082640	Chl1	2.42	1.5
BC021404	Ttll3	1.89	1.5
AK038364	Ttc17	0.58	1.5
NM_010871	Birc1f	0.00	1.5

AK039072	Raver2	3.88	1.5
NM_080450	Gje1	1.06	1.5
NM_178930	Gbf1	0.86	1.5
NM_199007	Sgol2	1.89	1.5
NM_198094	Brd4	1.30	1.5
NM_010731	Zbtb7a	1.06	1.5

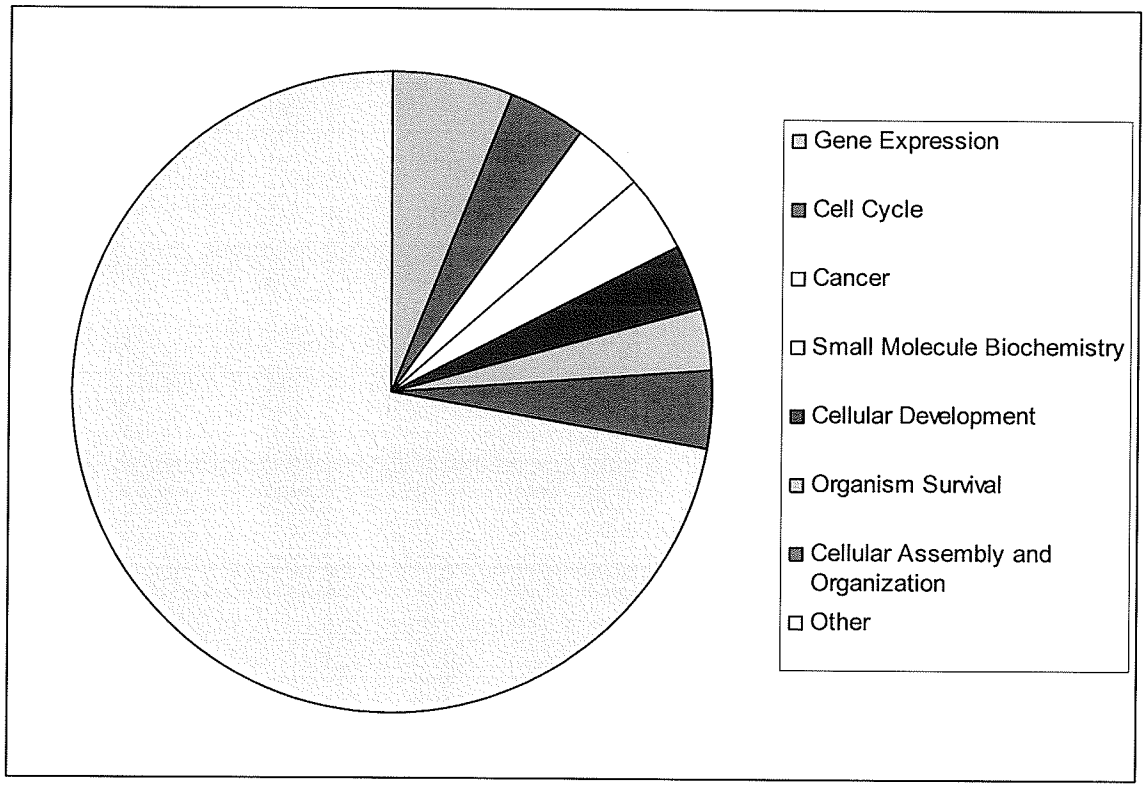

Figure 25: Using the software program Pathway Ingenuity Analysis, differentially expressed genes in scrapie-infected mice at 90 dpi fed an antioxidant diet were grouped according to their biological function.

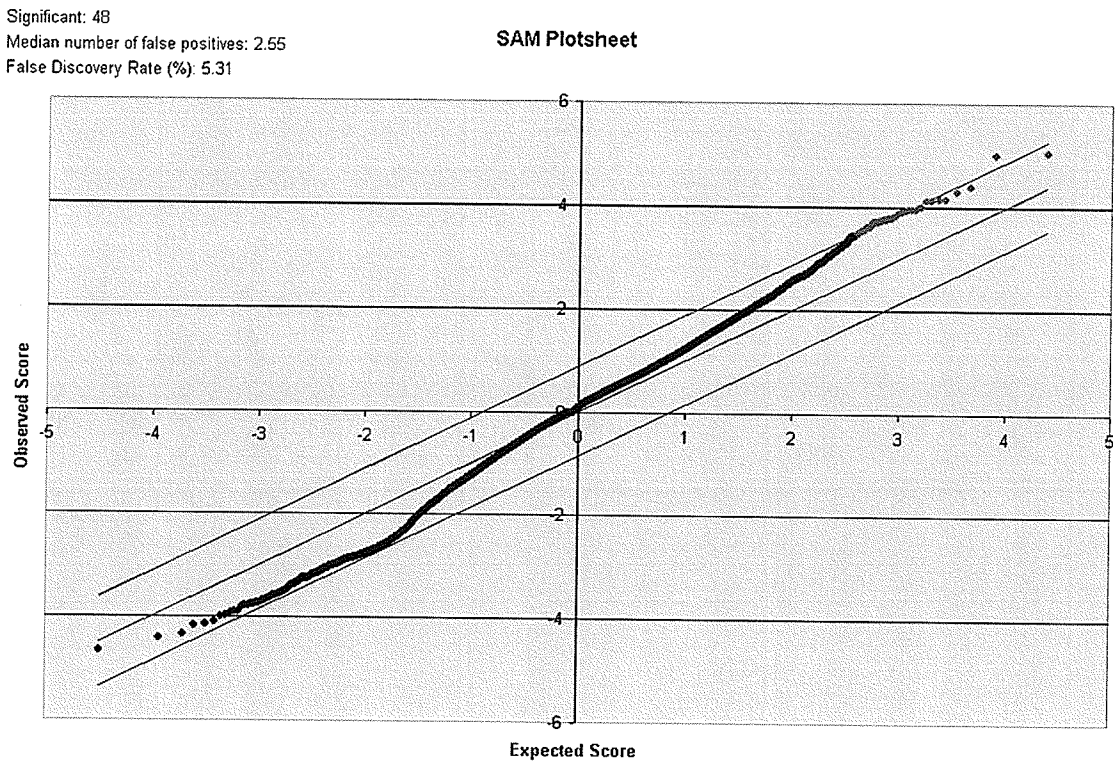

Figure 26: A one-class SAM plot of normalized microarray data obtained from scrapie-infected mice fed the antioxidant diet at 130dpi. Red indicates genes that are up-regulated and black indicates genes with no change.

Table 11: Genes up-regulated at 130dpi in whole brain of scrapie-infected mice fed an antioxidant diet

Accession Number	Hugo Gene Symbol	SAM Score	Fold Change
NM_011111	Serpinb2	4.60	1.9
NM_027552	Kynu	4.60	1.6
AK046903	Wwox	4.60	1.5
NM_008337	Ifng	4.60	1.5
NM_177798	Frs2	0.00	1.5

ingenuity analysis, genes were grouped according to their biological function (See Figure 27). The main functions identified include: cell-to-cell signalling and interaction and haematological system development and function.

Interestingly, all genes that were identified as being differentially expressed at 90 and 130dpi as a result of infection were not directly influenced by the antioxidant diet.

8.4 The Influence of the Antioxidant diet on lifespan of scrapie-infected mice

Twenty-eight mice, fourteen scrapie-infected fed the placebo diet and fourteen scrapie-infected fed the antioxidant diet were used to determine the influence of the antioxidant diet on the lifespan of scrapie-infected mice. The average lifespan of scrapie-infected mice fed the placebo diet was 143.4 days, while the average lifespan of scrapie-infected mice fed the antioxidant diet was 143.6 days. Using a Kaplan-Meier survival analysis (Figure 28) it was determined that there was no significant difference in lifespan between infected mice fed the placebo diet and infected mice fed the antioxidant diet ($p = 0.925$). Thus it was concluded that the antioxidant diet was unable to prolong the lifespan of scrapie-infected mice.

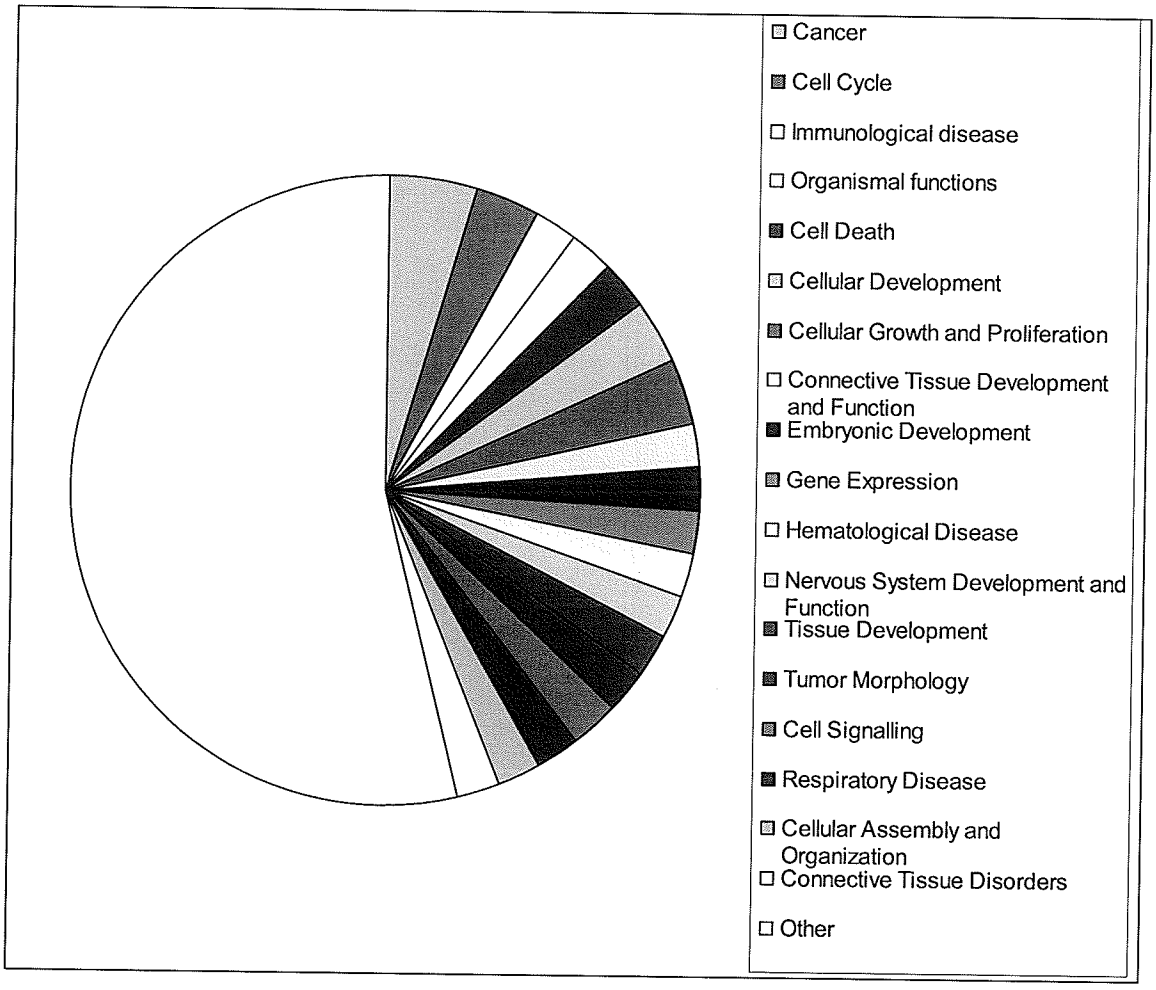

Figure 27: Using the software program Pathway Ingenuity Analysis, differentially expressed genes in scrapie-infected mice at 130dpi fed an antioxidant diet were grouped according to their biological function.

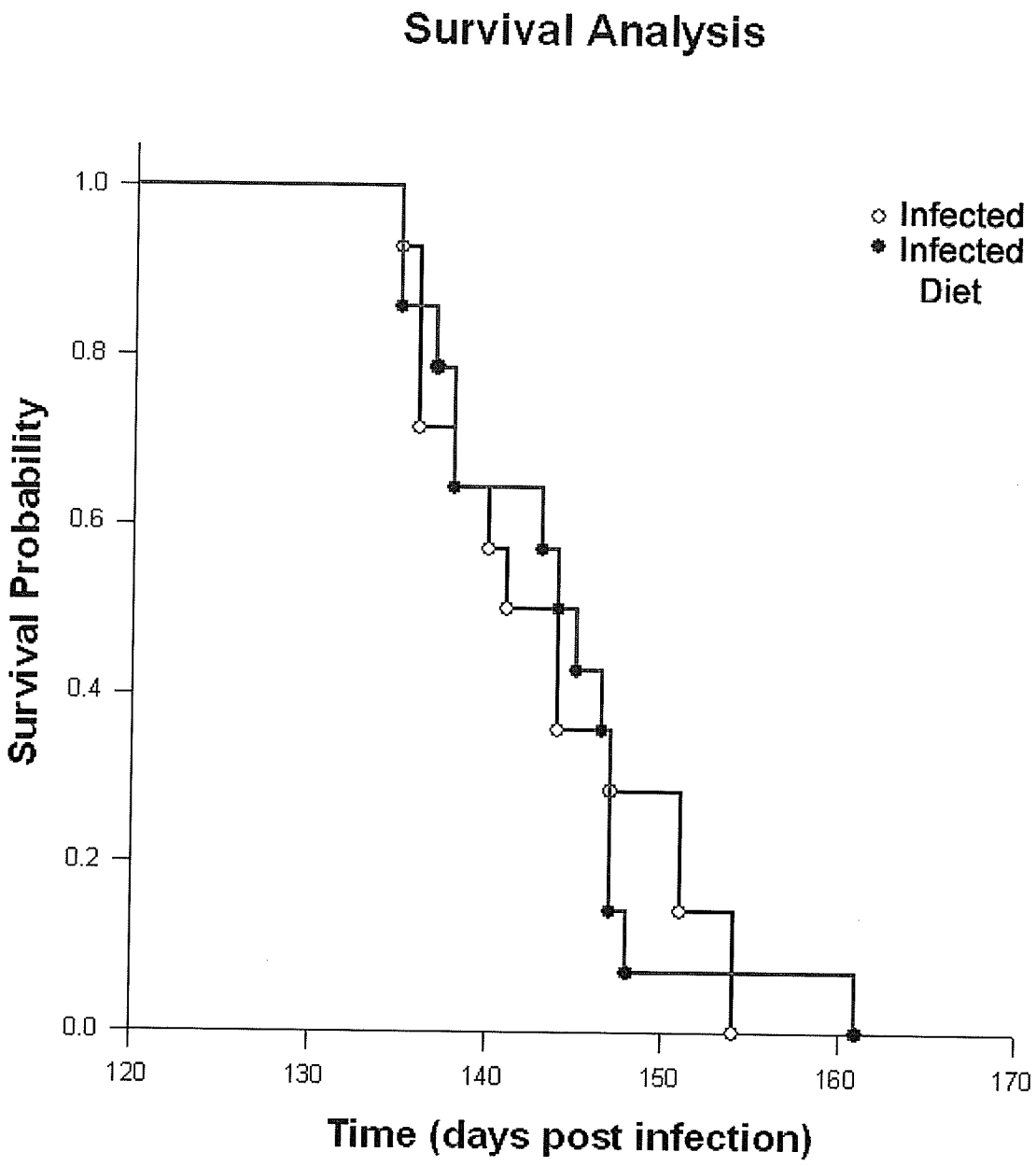

Figure 28: Kaplan-Meier plot depicting the probable amount of time (dpi) that a mouse would survive, from inoculation until death. There was no significant difference in lifespan between infected mice, and infected mice fed the antioxidant diet (p=.925).

9-Discussion

Oxidative stress describes the cellular imbalance between the production of free radicals and the loss of antioxidant protection. To determine whether oxidative stress was in part responsible for neurodegeneration resulting from prion infection, three biochemical tests and an analyses of gene expression were performed at both preclinical ($\leq$110dpi) and clinical ($\geq$130dpi) stages of the disease. Total GSH was employed as a measure of antioxidant capacity, while 4-HNE and 8-OHdG served as indicators of oxidative damage.

GSH is a powerful anti-oxidant, functioning as a redox buffer. With the aid of glutathione peroxidase (GPx), reduced GSH is able to donate it's thiol groups to keep other molecules in a reduced condition [84,85]. In the brain GSH removes excess H_2O_2 by coupling the reduction of H_2O_2 with the oxidation of GSH. H_2O_2 itself is not reactive, however in the presence of reduced metal (i.e. Cu^{2+}), H_2O_2 forms the highly reactive OH* [79].

Significantly depleted levels of total GSH were observed in the brains of scrapie-infected mice relative to controls. This suggests that prion infection makes brain cells more vulnerable to oxidative stress induced damage. In control mice, it is also interesting to note that total GSH levels tend to be reduced as the animals age. This trend is consistent with literature which reports that antioxidant protection is reduced as humans age [79].

Lipid peroxidation is the result of free radical attack, usually on polyunsaturated fatty acids. The corollary is a decrease in membrane fluidity, easier exchange of phospholipids between membrane halves, increased permeability to substances that do not normally cross the membrane other than through a specific channel, and damage to proteins; such as receptors, enzymes or ion channels [86,87,88]. 4-HNE is the most commonly measured marker of lipid peroxidation [79]. In this study, 4-HNE levels were significantly increased in the brains of scrapie-infected mice relative to controls.

Oxidative DNA damage is the most common insult affecting the genome [89]. The interaction of ROS with DNA occurs in a variety of ways resulting in cumulative mutations that cause genomic instability [89.91]. Damage can include; chemical and structural modifications to purine and pyrimidine bases as well as 2'-deoxyribose and single- and double-stranded breaks [89.90]. 8-OHdG is the most commonly used index of DNA damage caused by oxidative stress. 8-OHdG is produced by the addition of a hydroxyl radical to the C8 position of guanine, which in turn preferentially pairs with adenine rather than cytosine, resulting in G:C to T:A transversions following replication [89,90,91].

8-OHdG levels were significantly increased in the urine of scrapie-infected mice relative to controls. 8-OHdG levels were measured in urine as there is a commercial ELISA available. This negated the technical difficulties experienced when trying to determine 8-OHdG levels in gDNA isolated from the brain. The 8-OHdG found in urine most likely

originates in the brain as prion induced pathology has not been noted in any other organs even if high levels of PrP^d accumulate [94].

In vivo, the loss of GSH and increased amounts of 4-HNE and 8-OHdG are interrelated. In the experimental model system increases in 4-HNE and 8-OHdG are only observed after GSH stores, have to a certain extent been depleted. Thus a loss of antioxidant protection must be occurring prior to the build up of damaging ROS. Additionally, it is known that 4-HNE is a potent electrophile, thus it is able to modify the cellular redox status by depleting sulfhydral compounds such as GSH [86]. This may have extremely detrimental effects on cell survival, especially in the experimental model in which total GSH is depleted. The consequence of these three interrelated events is often oxidative stress induced cell death. The loss of antioxidant protection and/or increased ROS production initiates a vicious self-perpetuating cascade.

Depleted GSH levels potentially disrupt the mitochondrial transmembrane potential resulting in a rapid loss of mitochondrial function. This in turn results in decreased ATP production, which leads to a reduction in *de novo* GSH synthesis [95,96].

Increased 4-HNE levels may trigger mitochondrial and proteasomal dysfunction. 4-HNE has been shown to induce the release of Cytox from the mitochondria into the cytoplasm [48,97]. The release of Cytox augments the production of O_2^-, as Cytox is no longer able to prevent its release during oxidative phosphorylation. Additionally the presence of Cytox

in the cytoplasm initiates a cascade of caspase activation resulting in neuronal cell death [98]. 4-HNE is able to alter proteasome activity by directly binding to proteasomal subunits and/or indirectly by association of other HNE-modified proteins with the proteasome [51]. This may result in the failure to degrade oxidized proteins causing more oxidative stress and increasing sensitivity to neurotoxins.

DNA mutations generated by oxidative stress have the potential to alter signaling cascades, gene expression, induce or arrest transcription and cause replication errors disrupting cellular homeostasis [89,90,91]. Incorporation of 8-OHdG into mitochondrial DNA has been described in association with cell death [32,99]. The modified base causes mispairing, random point mutations and deletions. Damage to mitochondrial DNA may be particularly harmful since enzymes required for mitochondrial replication are encoded in genomic DNA. Thus, defective mitochondrial DNA, which encodes respiratory enzymes would continue to be transcribed, leading to impaired electron transport and increased production of ROS, eventually resulting in further oxidative stress, and damage to mitochondria [99].

In the experimental model the source of oxidative stress, which triggers decreased antioxidant protection and increases in lipid peroxidation end products and DNA base oxidation products is unknown. The presence of PrP^d may directly and/or indirectly increase the production of free radicals and at the same time decrease the amount of PrP^c thereby decreasing antioxidant protection.

One known function of PrP^c is neuronal copper binding and modulation of copper neurotoxicity [9,41]. Therefore the loss of PrP^c as it is being continuously converted into PrP^d may result in an increase in free Cu^{2+}. When total GSH and PrP^c are depleted there is an increased potential for interaction between H_2O_2 and Cu^{2+}, which leads to increased generation of OH* [79]. The OH* generated may be binding to the C8 position of guanine, resulting in the increased 8-OHdG levels demonstrated in the experimental model.

Prion disease causes neuronal apoptosis by an unknown mechanism. In response to neuronal damage, microglia and astrocytes become activated and secrete inflammatory mediators such as cytokines and chemokines as well as large amounts of NO and ROS [100]. The proinflammatory cytokines such as IL-6 secreted by activated glial cells are part of a positive feedback loop which amplifies ROS production [79]. Therefore, in the experimental model, activated glial cells may be a major source of free radicals, which trigger decreases in total GSH and increases in 4-HNE and 8-OHdG.

Cell death may be triggered by impaired proteasome function due to aggregated PrP^d, which being degraded more slowly than usual, clogs up and overloads the system [51,52,53]. This would result in oxidized proteins accumulating, causing oxidative stress and increasing sensitivity to toxins such as 4-HNE, H_2O_2 and metal ions [51].

To further elucidate when oxidative stress is occurring during disease progression and what is the source, whole mouse genome microarrays were used to detect global changes

in gene expression and/or cellular pathways in response to prion infection. Significant gene expression changes were found at both the pre-clinical (90dpi) and clinical (130dpi) time points measured in the brains of scrapie-infected mice.

Seven of these genes were identified as being differentially expressed only at the pre-clinical stage of the disease as a result of infection. The most interesting of these genes, Btg2 is involved in the response to DNA damage stimulus, neuron differentiation and the regulation of apoptosis [101]. Previously Btg2 was shown to be induced in response to DNA damage and cellular stress, which eventually resulted in apoptotic cell death [101]. However, in the experimental model Btg2 was found to be down-regulated 1.7 fold in scrapie-infected mice. This suggests that cells are not responding as expected to DNA damage as a result of scrapie-infection. In the experimental model 8-OHdG levels significantly increase at time same point during infection that Btg2 is down-regulated.

Forty three of these genes identified as being differentially expressed at the pre-clinical stage were also identified as being differentially expressed at the clinical stage of the disease as a result of infection. All 43 of the genes were up-regulated at 90dpi and further up-regulated at 130dpi. These genes may reveal the most information about disease pathogenesis, since at 130dpi, it is difficult to determine which genes are changed in response to disease-associated oxidative stress. At 130dpi, mice are nearing the end of their lives (143dpi), thus any changes in gene expression observed may be the result of their deteriorating condition and/or prion infection.

Cst7, was the most highly up-regulated gene that was differentially expressed. The function of Cst7 is currently unknown. Cst7 belongs to family 2 of the cystatin superfamily [102]. The expression of some family 2 members has been shown to prevent oxidative stress induced death in neuronal cells [103]. It is therefore quite possible that Cst7 may be induced in srapie-infected mice to protect against cell death as a result of the enhanced ongoing oxidative stress.

Other genes found to be up-regulated in scrapie-infected mice which are also known to help protect against oxidative stress include: Itgax, Tlr2, and Cxcl9. Cxcl9 and Itgax have previously been shown to decrease the production of O_2^-, while Tlr 2 has been shown to protect against oxidative stress induced apoptotic cell death [104,105,106].

Five genes previously demonstrated to be induced in response to oxidative stress were identified as being differentially expressed in the model system. These genes are Cxcl10, Ccl7, Ccl2, Ccl3, and Il6. Perhaps the most important of these genes, Il6 is a pleiotropic cytokine that plays an important role in the regulation of immune response and inflammation [107].

Four genes identified in the model system are known to produce free radicals. Ccl3 and Ccl4 increase H_2O_2 production [108]. The increase in H_2O_2 production combined with the loss of total GSH seen earlier is extremely likely to be contributing to neuronal cell death. Ccl2 increases the release of O_2^- [108]. PrP^c's SOD activity may be impaired by the coversion to PrP^d, thus as disease progresses the O_2^- released is free to exert its cytotoxic effects. Ccl5 increases ROS production in general [109]. The most likely source of these

cytokines producing free radicals is the glial cells, which are activated in response to the presence of PrP^{d} [46].

Eleven genes identified in the model system are known to be induced in response to interferon. These genes are Ifi27, Ifi44, Irf7, Ifit1, Mx1, Oasl2, Oas1a, Rtp4, Trim30, Isg15 and Usp18. Interferon response is strongly associated with an innate immune response resulting in inflammation [110]. Therefore it is possible that up-regulation of these genes activates glial cells, which in turn results in the generation of more ROS and $NO^{\cdot}$.

Depleted total GSH levels, increased 4-HNE and increased 8-OHdG levels at preclinical and clinical stages in scrapie-infected mice demonstrate that the brain is exposed to oxidative stress during disease pathogenesis. The differentially expressed genes identified at 90 and 130 dpi confirm this finding.

With this in mind, scrapie-infected mice were fed an antioxidant diet used in studies by Lemon *et al.* The antioxidant diet was designed based upon the known efficacy of ingredients to reduce ROS and inflammation, promote membrane and mitochondrial integrity and increase insulin sensitivity [80,81]. To determine if the antioxidant diet was able to ameliorate the adverse effects resulting from disease-associated oxidative stress levels of: total GSH, 4-HNE, 8-OHdG and gene expression were measured at preclinical ($\leq$110dpi) and clinical ($\geq$130dpi) stages of disease in scrapie-infected mice fed the antioxidant diet and scrapie-infected mice fed the placebo diet.

The effect of the antioxidant diet on total GSH levels was quite promising. Total GSH levels were restored in scrapie-infected mice fed the antioxidant diet, to those seen in uninfected mice at 70 and 130pdi. Restoration of small molecule defence (i.e. total GSH levels) in these mice may afford a degree of neuroprotection against the adverse affects of the disease.

The antioxidant diet had mixed effects on the level of 4-HNE occurring in scrapie-infected mice. At 90 dpi, 4-HNE levels were decreased in scrapie-infected mice fed the antioxidant diet as compared to those just fed the placebo diet. However, it was unable to return levels to those seen in control mice. From these findings it appears that the diet is somewhat effective in reducing the amount of ROS and/or repairing the damage caused by the ROS that result in lipid peroxidation at preclinical stage of disease. Conversely, at 130dpi, the antioxidant diet exacerbated already elevated lipid peroxidation levels in scrapie-infected mice as compared to those fed the placebo diet. As well, the antioxidant diet increased 4-HNE levels in control mice. Therefore it seems that administration of the antioxidant diet was beneficial only up until an unknown point in the disease, at which time the diet should no longer have been fed to the scrapie-infected mice.

The antioxidant diet had no effect on 8-OHdG levels in scrapie-infected mice. From $\geq$90dpi the antioxidant diet was unable to reduce the increased levels of 8-OHdG in scrapie-infected mice. Thus the diet was unable to ameliorate the disastrous consequences described previously, which are potentially occurring in scrapie-infected mice as a result of oxidative DNA damage. Additionally, at clinical stage of disease the antioxidant diet increased 8-OHdG levels in uninfected mice.

Significant gene expression changes were found at both the pre-clinical (90dpi) and clinical (130dpi) time points measured in the brains of scrapie-infected mice fed the antioxidant diet. These changes in gene expression in scrapie-infected mice fed the antioxidant diet were not as expected.

In scrapie-infected mice fed the antioxidant diet, 96 genes were identified as being up-regulated at the pre-clinical stage of the disease and 5 distinct genes were identified as being up-regulated at the clinical stage of the disease. Unfortunately none of these genes were the same as the 43 genes identified as being differentially expressed at both 90 and 130dpi in scrapie-infected mice fed the placebo diet. Additionally all genes identified were up-regulated, which means that even if any of these genes are involved in glial cell activation, ROS production or loss of antioxidant protection they would only be functioning to exacerbate the already elevated levels. Finally it is interesting to note that 10 of the 96 genes identified as being differentially expressed at the pre-clinical stage of the disease, are involved in organism viability. These genes are Ank2, Brd4, Cdkn1b, Cdkn2a, Ep300, Lrp6, Ncoa6, Rasa1, Utrn and Xrcc2 [111-120]. The induction of these genes in various situations has been shown to result in death of the organism.

As the antioxidant diet was only moderately effective at ameliorating the adverse effects resulting from disease-associated oxidative stress it is not surprising that scrapie-infected mice fed the diet died at the same time as scrapie-infected mice fed the placebo diet (see Figure 28).

In the experimental model used the antioxidant diet may not have been effective at amerliorating the adverse effects for a variety of reasons. Two possible explanations result from the logistical problem that individual monitoring of dietary uptake was not performed. Group-housed mice were not weighed before and after administration of the antioxidant diet. Furthermore, the antioxidant diet may have tasted different than the placebo diet. Therefore it is impossible to be sure that all mice received the same amount of the diet. Since the results reflect the impact of the diet on the "average mouse", in such a situation the anticipated effects of the diet may be masked. However, it is unlikely that the effects of the diet were masked, as the standard deviation of mouse lifespan is not as large as you would expect it to be if some mice received a higher dose of the antioxidant diet.

Additionally Lemon *et al.* never demonstrated that the diet had a direct effect on moderating the oxidative state of their mice. The level of ROS or antioxidant protection was never measured. Therefore it is possible that the diet abolished age-related cognitive decline and shortened life span otherwise observed in transgenic C57BL/6 mice over expressing growth hormone, by some unknown mechanism, which is independent of the level of oxidative stress.

10-Conclusions

It was hypothesized that oxidative stress is partially responsible for prion provoked neurotoxicity. To test the hypothesis an *in vitro* and *in vivo* model system were used.

The *in vitro* model system generated a mixed culture with mainly post mitotic neuronal cells and a few glial cells, which is suitable for studying the molecular and cellular processes involved in $PrP^{106-126}$ cytotoxicity. The culture proved to be incompatible with planned experiments; however the advantageous characteristics of this model system can be exploited provided that future experiments require minimal manipulation of the cells.

The *in vivo* model system demonstrated that prion infection results in a loss of antioxidant protection, an increase in lipid peroxidation and an increase in DNA oxidation in scrapie-infected C57BL/6 mice. Microarray analysis further confirmed this and suggests that one of the main sources of ROS in the experimental model is activated glial cells. Changes in gene expression also reveal that prion infection results in the failure to recognize oxidative DNA damage. The antioxidant diet was able to restore antioxidant protection at 70 and 130dpi. Thus there may be a certain time-point during the course of the disease when antioxidant protection is critical for survival. Alternatively the loss of total GSH is not playing a major role in the pathogenesis of prion disease. For the most part the antioxidant diet was unable to ameliorate the level of lipid peroxidation and DNA oxidation resulting from disease-associated ROS. Used as the sole intervention strategy, the antioxidant diet was unable to prolong the lifespan of

scrapie-infected mice, or restore redox homeostasis. Thus the role oxidative stress in prion provoked neurotoxicity remains unknown.

11-Future Directions

In the *in vitro* model system, measuring apoptosis using flow cytometry proved to be problematic. One possible explanation for this occurrence was the number of wash steps prior to the addition of the annexin-PI cocktail. In the future, altering the experimental protocol, to include fewer wash steps, will mostly likely improve the recovery of intact undamaged cells. Additionally, it would be informative to compare the physical state of the cells under the microscope to the flow analysis obtained. This could be accomplished by staining a portion of the cells at various stages throughout the preparation process for flow cytometry using trypan blue.

As the enriched neuronal population generated was an adherent cell line, laser scanning cytometry may prove to be an attractive alternative method for measuring apoptosis [121]. Laser scanning cytometry has the advantage of generating quantitative data while cells remain in the environment, which they are grown, such as on a coverslip or in a microtiter well. This would negate the physical manipulation limitations incurred in the experiment. As well it allows researchers to generate hi-resolution digital images of the cells of interest [121].

In the *in vivo* model system, the dietary supplement was only moderately effective at abating the adverse effects of disease-associated oxidative stress. One major source of disease-associated oxidative stress appears to be the activation of microglia and astrocytes. In the future, it may be beneficial to mediate this inflammatory response in conjunction with the dietary supplement. The vasoactive intestinal peptide (VIP) is a

potent anti-inflammatory neuropeptide, which has been shown to prevent activated microglia-induced neurodegeneration under some inflammatory conditions [122]. VIP acts as endogenous macrophage/microglia de-activating factor. It inhibits the expression and release: of IL-12, TNFα, Ccl3, Ccl4, Ccl2, Cxcl2, keratinocyte-derived chemokine, and Ccl5; inhibits the expression of iNOS and subsequent release of NO and enhances the production of IL-10 [123]. The combination of VIP administration and an anti-oxidant dietary supplement may potentially ameliorate the adverse effects of prion disease-associated oxidative stress.

Appendix 1

Almazan Medium

100x neuronal supplement* / 50 ml

5mg	*Human Transferrin* (Sigma cat.# T-1147)
50ul	2mM Hydrocortisone-21-phosphate (1mg/ml water) (Sigma cat. # H-2270)
25ul	2mM *L-Cartinine* (2mg/5ml water) (Sigma cat.# C-0283)
80.5mg	Putrescine (Sigma cat.# P-5780)
5ul	15mM *Selenious acid* (9.5mg/5ml water) (Sigma cat.# Sigma cat.#21,117-6)
5ul	50mM *Cadmium Sulfate* (0.1925g/5ml water) (Sigma cat.# C-3266)

to 50 ml with water. Filter sterilize, using a 0.2μm filter (Corning, cat. #431219) and store at -20^0C in 10 ml aliquots.

Almazan Media / 500ml

5ml	100x L-Glutamine (0.584g/20ml DMEM) (Sigma cat.# G-3126) Warm to dissolve, then filter sterilize (0.2μm filter) **Make Fresh Everytime!**
5ml	100x Antibiotics/fungicides (Invitrogen cat.# 15240-062)
5ml	100x Vitamin Solution (MEMbase) (Invitrogen cat.# 21040-050)
5ml	100x Neuronal supplement*
5ml	100x Trace Element Mix (VWR Scientific cat.# 4500-714)
500ul	1000x DL-alpha-tocopherol (50mg/5ml 95% EtOH) *light sensitive* (Invitrogen cat.# 13580-014)
100ul	5000x DL-6,8-thioctic acid (1mg/ml 100% EtOH) *light sensitive* (Sigma cat.# T-1395)
5ul	Linoleic acid (10mg(11.11ul) in 1ml 100% EtOH) *light sensitive* (Sigma cat.# L-1012)
500ul	1000x bovine Insulin (1mg/ml water – 1N HCl (VWR, cat. #VW3202-4) added to dissolve) (Sigma cat.# I-6634)
100ml	BSA (0.5g/20ml DMEM) (Sigma cat.# A-9418)
1ml	Normocin (Cedarlane labs cat.# ant-nr-2)

to 500ml with DMEM (Invitrogen cat.# 10313-021). Filter sterilize, wrap in foil and store at 4^0C.

Appendix 2

Cell Type	Specific Transcript
House Keeping Gene	Porphobilinogen deaminase (PBGD) gi: 63586690
Neurons	Microtubule-associated protein 2 (Mtap2) gi : 63474637
Astrocytes	Glial fibrillary acidic protein (Gfap) gi: 26080421
Oligodendrocytes	Galactocerebrosidase (Galacto) gi: 6363009

PBGD

Forward Primer – 5'-TGGGCCAGATTTTGCACCCAGAGGAA-3'

Reverse Primer – 5'-CCCTTTCAGCAATGCAGCGAAGCAGA-3'

Mtap2

Forward Primer – 5'-AAGAGAAGGAAGCCCAATACAAGGAC-3'

Reverse Primer – 5'-GCTGGCGATGGTGGTGGGGAAGGT-3'

Gfap

Forward Primer-5'-TTAAGGAAGATCTATGCGGAGGAAGT-3'

Reverse Primer-5'-AGGGCCGCTGTGACCTCTGG-3'

Galacto

Forward Primer – 5'-TGGGCCATCTAGAGAAAGGAGGAA-3'

Reverse Primer –5'-CTGCCGTCAAGGAGCCATAGAGTA-3'

Appendix 3

PCR reaction:

2µl	50mM dNTPs (mixed from 100mM stocks) (Invitrogen, cat. #10297-018)
2µl	50ng/µl forward primer
2µl	50ng/µl reverse primer
2µl	C57/BL6 mouse cDNA (35ng/µl)
10µl	10x PCR buffer + Mg (Roche, cat. #1647679)
1µl	Taq DNA polymerase (Roche, cat. #1647679)
79µl	18.2MΩ water

	40 Cycles			
Denature	Denature	Anneal	Extension	Final Extension
94°C for 5min.	94°C for 30 sec.	60°C for 30 sec.	72°C for 30 sec	72°C for 10min.

Ligation:

PBGD and Galacto were ligated into pCR2.1 vector

Add:

5ul Sterile Water
1ul 10x Ligation Buffer
2ul pCR2.1 vector (25ng/ul)
1ul fresh PCR product (~10ng)
1ul T4 DNA ligase

Incubate over night at 14°C (PTC-200 MJ Thermocyler).

Mtap2 and Gfap were ligated into pCR4-Topo vector

Add:

4ul fresh PCR product (up to 500ng)
1ul Salt Solution
1ul TOPO vector

Incubate at room temperature for 5 minutes. Place reaction on ice and proceed immediately to transformations.

Appendix 4

Plasmid	**Initial Concentration**	**Dilution Series**
PBGD	2pg/ul	1:10-1:100 000
Mtap2	20pg/ul	1:10-1:100 000
Gfap	200pg/ul	1:10-1:00 000
Galacto	200fg/ul	1:10-1:10 000

For each plasmid:

	Per Capillary
Forward Primer (50ng/ul)	1.25ul
Reverse Primer (50ng/ul)	1.25ul
Sigma Sybr Green Master Mix (Sigma, cat. #S1816)	2.5ul
18.2 MΩ water	15.5ul
Plasmid (25ng/ul)	2.5ul

Gene	Size (bp)	Denature 95°C (sec)	Anneal (°C)	Anneal Time (sec)	Extension 72°C (sec)	Number Cycles
PBGD	150	5	61	5	11	45
Mtap2	97	5	66	5	11	45
Gfap	107	5	65	5	11	45
Galacto	267	5	60	5	11	45

Note: Primer sequences can be found in appendix 1.

Appendix 5

Primary Antibodies used:

Antibody	**Cell Type**
Class III ß-Tubulin (Covance, cat. #MMS-435P)	Neurons
Polyclonal rabbit anti Gfap (Dako, cat. #N1506)	Astrocytes
Polyclonal rabbit anti human Myelin Basic Protein (Dako, cat. #A0623)	Oligodendrocytes

Secondary Antibodies used:

Antibody	**Cell Type**
Alkaline Phosphatase-Conjugated Goat Anti-Mouse Immunoglobulins (Dako, cat. #D 0486)	Neurons
Horse Radish Peroxidase rabbit (DAB+) (Dako, cat. #K4010)	Astrocytes, Oligodendrocytes

References

1. Zhu,B.T. Human and animal spongiform encephalopathies are the result of chronic autoimmune attack in the CNS: a novel medical theory supported by overwhelming experimental evidence. Histol. Histopathol. 20, 575-592 (2005).

2. Takemura,K., Kahdre,M., Joseph,D., Yousef,A. & Sreevatsan,S. An overview of transmissible spongiform encephalopathies. Anim Health Res. Rev. 5, 103-124 (2004).

3. Johnson,R.T. Prion diseases. Lancet Neurol. 4, 635-642 (2005).

4. Chakraborty,C., Nandi,S. & Jana,S. Prion disease: a deadly disease for protein misfolding. Curr. Pharm. Biotechnol. 6, 167-177 (2005).

5. Gajdusek,D.C. & ZIGAS,V. Degenerative disease of the central nervous system in New Guinea; the endemic occurrence of kuru in the native population. N. Engl. J. Med. 257, 974-978 (1957).

6. Gajdusek,D.C., Gibbs,C.J. & Alpers,M. Experimental transmission of a Kuru-like syndrome to chimpanzees. Nature 209, 794-796 (1966).

7. Liberski,P.P. & Brown,P. Kuru: a half-opened window onto the landscape of neurodegenerative diseases. Folia Neuropathol. 42 Suppl A, 3-14 (2004).

8. Ladogana,A. et al. Mortality from Creutzfeldt-Jakob disease and related disorders in Europe, Australia, and Canada. Neurology 64, 1586-1591 (2005).

9. Prusiner,S.B. Prions. Proc. Natl. Acad. Sci. U. S. A 95, 13363-13383 (1998).

10. Caramelli,M., Ru,G., Acutis,P. & Forloni,G. Prion diseases: current understanding of epidemiology and pathogenesis, and therapeutic advances. CNS. Drugs 20, 15-28 (2006).

11. Aguzzi,A. & Glatzel,M. Prion infections, blood and transfusions. Nat. Clin. Pract. Neurol. 2, 321-329 (2006).

12. Wilson,J.F. Why prion diseases are a mystery, and why they matter. Ann. Intern. Med. 143, 773-776 (2005).

13. Prusiner,S.B. Novel proteinaceous infectious particles cause scrapie. Science 216, 136-144 (1982).

14. Bueler,H. et al. Mice devoid of PrP are resistant to scrapie. Cell 73, 1339-1347 (1993).

15. Brown,D.R. Molecular advances in understanding inherited prion diseases. Mol. Neurobiol. 25, 287-302 (2002).

16. Manuelidis,L. A 25 nm virion is the likely cause of transmissible spongiform encephalopathies. J. Cell Biochem. 100, 897-915 (2007).

17. Glatzel,M. & Aguzzi,A. The shifting biology of prions. Brain Res. Brain Res. Rev. 36, 241-248 (2001).

18. Rohwer,R.G. The scrapie agent: "a virus by any other name". Curr. Top. Microbiol. Immunol. 172, 195-232 (1991).

19. Chesebro,B. BSE and prions: uncertainties about the agent. Science 279, 42-43 (1998).

20. Klamt,F. et al. Imbalance of antioxidant defense in mice lacking cellular prion protein. Free Radic. Biol. Med. 30, 1137-1144 (2001).

21. Nunziante,M., Gilch,S. & Schatzl,H.M. Prion diseases: from molecular biology to intervention strategies. Chembiochem. 4, 1268-1284 (2003).

22. Aguzzi,A. & Weissmann,C. Prion research: the next frontiers. Nature 389, 795-798 (1997).

23. Heske,J., Heller,U., Winklhofer,K.F. & Tatzelt,J. The C-terminal globular domain of the prion protein is necessary and sufficient for import into the endoplasmic reticulum. J. Biol. Chem. 279, 5435-5443 (2004).

24. Brown,D.R. et al. The cellular prion protein binds copper in vivo. Nature 390, 684-687 (1997).

25. Leliveld,S.R., Dame,R.T., Wuite,G.J., Stitz,L. & Korth,C. The expanded octarepeat domain selectively binds prions and disrupts homomeric prion protein interactions. J. Biol. Chem. 281, 3268-3275 (2006).

26. Westergared,L., Christensen, H.M., & Harris, D.A. The cellular prion protein (PrP(C)): Its physiological function and role in disease. Biochim. Biophys. Acta. 6, 629-644 (2007).

27. Aguzzi,A. & Polymenidou,M. Mammalian prion biology: one century of evolving concepts. Cell 116, 313-327 (2004).

28. Chen,S.G. & Gambetti,P. A journey through the species barrier. Neuron 34, 854-856 (2002).

29. Vanik,D.L., Surewicz,K.A. & Surewicz,W.K. Molecular basis of barriers for interspecies transmissibility of mammalian prions. Mol. Cell 14, 139-145 (2004).

30. Bruce,M.E. TSE strain variation. Br. Med. Bull. 66,99-108 (2003).

31. Milhavet,O. et al. Prion infection impairs the cellular response to oxidative stress. Proc. Natl. Acad. Sci. U. S. A 97, 13937-13942 (2000).

32. Petersen,R.B. et al. Redox metals and oxidative abnormalities in human prion diseases. Acta Neuropathol. (Berl) 110, 232-238 (2005).

33. White,A.R. et al. Prion protein-deficient neurons reveal lower glutathione reductase activity and increased susceptibility to hydrogen peroxide toxicity. Am. J. Pathol. 155, 1723-1730 (1999).

34. Yun,S.W., Gerlach,M., Riederer,P. & Klein,M.A. Oxidative stress in the brain at early preclinical stages of mouse scrapie. Exp. Neurol. 201, 90-98 (2006).

35. Wong,B.S. et al. Oxidative impairment in scrapie-infected mice is associated with brain metals perturbations and altered antioxidant activities. J. Neurochem. 79, 689-698 (2001).

36. Choi,C.J., Kanthasamy,A., Anantharam,V. & Kanthasamy,A.G. Interaction of metals with prion protein: possible role of divalent cations in the pathogenesis of prion diseases. Neurotoxicology 27, 777-787 (2006).

37. Sakudo,A. et al. Octapeptide repeat region and N-terminal half of hydrophobic region of prion protein (PrP) mediate PrP-dependent activation of superoxide dismutase. Biochem. Biophys. Res. Commun. 326, 600-606 (2005).

38. Brown, D.R. & Besinger, A. Prion protein expression and superoxide dismutase activity. Biochem. J. 334, 423-429 (1998).

39. Brown, D.R., Schulz-Schaeffer, W.J. Schmidt, B., & Kretzschmar, H.A. Prion protein-deficient cells show altered response to oxidative stress due to decreased SOD-1 activity. Exp. Neurol. 146, 104-112 (1997).

40. Hutter,G., Heppner,F.L. & Aguzzi,A. No superoxide dismutase activity of cellular prion protein in vivo. Biol. Chem. 384, 1279-1285 (2003).

41. Brown,D.R., Schmidt,B. & Kretzschmar,H.A. Effects of copper on survival of prion protein knockout neurons and glia. J. Neurochem. 70, 1686-1693 (1998).

42. Llanos, R.M. & Mercer, J.F.B. The molecular basis of copper homeostasis and copper-related disorders. DNA Cell Bio. 4, 259-270 (2002).

43. Rotilio,G., Carri,M.T., Rossi,L. & Ciriolo,M.R. Copper-dependent oxidative stress and neurodegeneration. IUBMB. Life 50, 309-314 (2000).

44. Chiarini, A., Dal Pra, I., Whitfield, J.F. & Armato, U. The killing of neurons by β-amyloid peptides, prions, and pro-inflammatory cytokines. Ital. J. Anat. Embryol. 4, 221-246 (2006).

45. Brown, D.R. & Kretzchmar, H.A. Microglia and prion disease: a review. Histol. Histopathol. 12, 883-892 (1997).

46. Burwinkel, M., Riemer, C., Schwarz, A., Schultz, J., Neidhold, S., Bamme, T. & Baier, M. Role of cytokines and chemokines in prion infections of the central nervous system. Int. J. Devl. Neurosci. 22, 497-505 (2004).

47. Colton, C.A., Chernyshev, O.N., Gilbert, D.L. & Vitek, M.P. Microglial contribution to oxidative stress in alzheimer's disease. Ann N Y Acad Sci. 899, 292-307 (2000).

48. Choi,S.I. et al. Mitochondrial dysfunction induced by oxidative stress in the brains of hamsters infected with the 263 K scrapie agent. Acta Neuropathol. (Berl) 96, 279-286 (1998).

49. Jin,J.K. et al. Increased expression of phospholipase D1 in the brains of scrapie-infected mice. J. Neurochem. 92, 452-461 (2005).

50. Rossi,L., Lombardo,M.F., Ciriolo,M.R. & Rotilio,G. Mitochondrial dysfunction in neurodegenerative diseases associated with copper imbalance. Neurochem. Res. 29, 493-504 (2004).

51. Halliwell,B. Proteasomal dysfunction: a common feature of neurodegenerative diseases? Implications for the environmental origins of neurodegeneration. Antioxid. Redox. Signal. 8, 2007-2019 (2006).

52. Hooper,N.M. Could inhibition of the proteasome cause mad cow disease? Trends Biotechnol. 21, 144-145 (2003).

53. Kang SC, Brown DR, Whiteman M, Li R, Pan T, Perry G, Wisniewski T, Sy MS, Wong BS. Prion protein is ubiquitinated after developing protease resistance in the brains of scrapie-infected mice. J. Pathol. 203, 603-608 (2004).

54. Ma,J. & Lindquist,S. Conversion of PrP to a self-perpetuating PrPSc-like conformation in the cytosol. Science 298, 1785-1788 (2002).

55. Stefani,M. & Dobson,C.M. Protein aggregation and aggregate toxicity: new insights into protein folding, misfolding diseases and biological evolution. J. Mol. Med. 81, 678-699 (2003).

56. Pieri,L. et al. The yeast prion Ure2p native-like assemblies are toxic to mammalian cells regardless of their aggregation state. J. Biol. Chem. 281, 15337-15344 (2006).

57. Mattson,M.P. Impairment of membrane transport and signal transduction systems by amyloidogenic proteins. Methods Enzymol. 309, 733-746 (1999).

58. Solassol,J., Crozet,C. & Lehmann,S. Prion propagation in cultured cells. Br. Med. Bull. 66, 87-97 (2003).

59. Laude,H. et al. New in vivo and ex vivo models for the experimental study of sheep scrapie: development and perspectives. C. R. Biol. 325, 49-57 (2002).

60. Beranger,F., Mange,A., Solassol,J. & Lehmann,S. Cell culture models of transmissible spongiform encephalopathies. Biochem. Biophys. Res. Commun. 289, 311-316 (2001).

61. Clarke, M.C. & Haig, D.A. Evidence for the multiplication of scrapie agent in cell culture. Nature. 225, 100-101 (1970).

62. Race,R.E., Fadness,L.H. & Chesebro,B. Characterization of scrapie infection in mouse neuroblastoma cells. J. Gen. Virol. 68 (Pt 5), 1391-1399 (1987).

63. Bosque,P.J. & Prusiner,S.B. Cultured cell sublines highly susceptible to prion infection. J. Virol. 74, 4377-4386 (2000).

64. Sakudo, A., Nakamura, I., Ikuta, K. & Onodera, T. Recent developments in prion disease research: diagnostic tools and *in vitro* cell culture models. J. Vet. Med. Sci. 69, 329-337 (2007).

65. Schatzl,H.M. et al. A hypothalamic neuronal cell line persistently infected with scrapie prions exhibits apoptosis. J. Virol. 71, 8821-8831 (1997).

66. Mellon, P.L., Windle, J.J., Goldsmith, P.C., Padula, C.A., Roberts, J.L. & Weiner, R.I. Immortalization of hypothalamic GnRH neurons by genetically targeted turmorigenesis. Neuron. 5, 1-10 (1990).

67. Rubenstein,R., Carp,R.I. & Callahan,S.M. In vitro replication of scrapie agent in a neuronal model: infection of PC12 cells. J. Gen. Virol. 65 (Pt 12), 2191-2198 (1984).

68. Rubenstein,R., Scalici,C.L., Papini,M.C., Callahan,S.M. & Carp,R.I. J. Gen. Virol. 70, 825-831 (1990).

69. MacPherson,P.A. & McBurney. P19 embryonal carcinoma cells: a source of cultured neurons amenable to genetic manipulation. A Companion to Methods in Enzymology. 7, 238-252 (1995).
70. Forloni,G., Angeretti,N., Chiesa, R., Monzani,E., Salmona,M., Bugiani,O. & Tagliavini,F. Neurotoxicity of prion protein fragment. Nature. 362, 543-546 (1993).

71. Singh,N. et al. Prion peptide 106-126 as a model for prion replication and neurotoxicity. Front Biosci. 7, a60-a71 (2002).

72. DeArmond,S.J. Discovering the mechanisms of neurodegeneration in prion diseases. Neurochem. Res. 29, 1979-1998 (2004).

73. Vermes,I., Haanen,C. & Reutelingsperger,C. Flow cytometry of apoptotic cell death. J. Immunol. Methods. 243, 167-190 (2000).

74. Engbers-Buijtenhuijs,P., Kamphuis,M., van dre Sluijs Veer,G., Poot,A.A., Feijen,J. & Vermes,I. A novel time resolved fluorometric assay of anoikis using europium-labelled annexin V in cultured adherent cells. Apoptosis. 10, 429-437 (2005).

75. Kimberlin,R.H. Experimental scrapie in the mouse: a review of an important model disease. Sci. Prog. 63, 461-481 (1976).

76. Baron,T. Mouse models of prion disease transmission. Trends Mol Med. 8, 495-500 (2002).

77. ZLOTNIK,I. & RENNIE,J.C. The pathology of the brain of mice inoculated with tissues from scrapie sheep. J. Comp Pathol. 72, 360-365 (1962).

78. Chandler,R.L. Encephalopathy in mice produced by inoculation with scrapie brain material. Lancet 1, 1378-1379 (1961).

79. Halliwell,B. Oxidative stress and neurodegeneration: where are we now? J. NeuroChem. 97, 1634-1658 (2006).

80. Lemon,J.A., Boreham,D.R. & Rollo,C.D. A dietary supplement abolishes age-related cognitive decline in transgenic mice expressing elevated free radical processes. Exp. Biol. Med. (Maywood.) 228, 800-810 (2003).

81. Lemon,J.A., Boreham,D.R. & Rollo,C.D. A complex dietary supplement extends longevity of mice. J. Gerontol. A Biol. Sci. Med. Sci. 60, 275-279 (2005).

82. Milhavet,O. & Lehmann,S. Oxidative stress and the prion protein in transmissible spongiform encephalopathies. Brain. Res. Reviews. 38, 328-339 (2002).

83. Schulz,J.B., Lindenau,J., Saeyfried,J. & Dichgans,J. Glutathione, oxidative stress and neurondegeneration. Eur. J. Biochem. 267, 4904-4911 (2000).

84. Bains,J.S. & Shaw,C.A. Neurodegenerative disorders in humans: the role of glutathione in oxidative stress-mediated neuronal death. Brain Res. Reviews. 25, 335-358 (1997).

85. Pastore,A., Federici,G., Bertini,E. & Piemonte,F. Analysis of glutathione: implication in redox and detoxification. Clinica. Chimica. Acta. 333, 19-39 (2003).

86. Benzie,I.F. Lipid peroxidation: a review of causes, consequences, measurement and dietary influences. Int. J. Food Sci. Nutr. 47, 233-261 (1996).

87. Dotan,Y., Lichtenberg,D. & Pinchuk,I. Lipid peroxidation cannot be used as a universal criterion of oxidative stress. Prog. Lipid Res. 43, 200-227 (2004).

88. Morabito,F. et al. Lipid peroxidation and protein oxidation in patients affected by Hodgkin's lymphoma. Mediators. Inflamm. 13, 381-383 (2004).

89. Powell,C.L., Swenberg,J.A. & Rusyn,I. Expression of base excision DNA repair genes as a biomarker of oxidative DNA damage. Cancer Lett. 229, 1-11 (2005).

90. Measurement of DNA oxidation in human cells by chromatographic and enzymic methods. Free Radic. Biol. Med. 34, 1089-1099 (2003).

91. David,S.S., O'Shea,V.L. & Kundu,S. Base-excision of oxidative DNA damage. Nature. 447, 941-950 (2007).

92. McShea,A., Marlatt,M.W., Lee,H., Tarkowsky,S.M., Smit,M. & Smith,M.A. The application of microarray technology to neuropathology: cutting edge tool with clinical diagnostics potential or too much information? J. Neuropathol. Exp. Neurol. 65, 1031-1039 (2006).

93. Larrson,O., Wennmalm,K. & Sandberg,R. Comparative microarray analysis. OMICS. 10, 381-397 (2006).

94. Stobart,M.J., Parchaliuk,D., Simon,S.L., Lemaistre,J., Lazar,J., Rubenstein,R. & Knox,J.D. Differential expression of interferon responsive genes in rodent models of transmissible spongiform encephalopathy disease. Mol. Neurodegener. 16, 2:5 (2007).

95. Seyfried,J., Soldner, F., Schulz,J.B., Klockgether,T., Kovar,K.A. & Wullner,U. Differential effects of L-buthionine sulfoximine and ethacrynic acid on glutathione levels and mitochondrial function in PC12 cells. Neurosci. Lett. 264, 1-4 (1999).

96. Wullner,U., Seyfried,J., Groscurth,P., Beinroth,S., Winter,S., Gleichmann,M., Heneka,M., Loschmann,P., Schulz,J.B., Weller,M. & Klockgether,T. Glutathione depletion and neuronal cell death: the role of reactive oxygen intermediates and mitochondrial function. Brain Res. 826, 53-62 (1999).

97. Raza,H. & John,A. 4-Hydroxynonenal induces mitochondrial oxidative stress, apoptosis and expression of glutathione S-transferase A4-A and cytochrome P450 2E1 in PC12 cells. Toxicol. Appl. Pharmacol. 216, 309-318 (2006).

98. Anuradha,C.D., Kanno,S. & Hirano,S. Oxidative damage to mitochondria is a preliminary step to caspase-3 activation in fluoride-induced apoptosis in HL-60 cells. Free Radic. Biol. Med. 31, 367-373 (2001).

99. de la Monte,S.M., Luong,T., Neely,T.R., Robinson,D. & Wands,J.R. Mitochondrial DNA damage as a mechanism of cell loss in Alzheimer's disease. Lab. Invest. 80, 1323-1335 (2000)

100. Chiarine,A., Dal Pra,I., Whitfield,J.F. & Armato,U. The killing of neurons by beta-amyloid peptides, prions, and pro-inflammatory cytokines. Ital. J. Anat. Embryol. 111, 221-246 (2006).

101. Tirone,F. The gene PC3(TIS21/BTG2), prototype member of the PC3/BTG/TOB family: regulator in control of cell growth, differentiation, and DNA repair? J. Cell Physiol. 187,155-65 (2001).

102. Schuttelkopf,A.W., Hamilton,G., Watts,C. & van Aalten,D.M.F. Structural basis of reduction-dependent activation of human cystatin F. J. Bio. Chem. 281, 16570-16575 (2006).

103. Nishiyama,K., Konishi,A., Nishio,C., Araki-Yoshida,K., Hatanaka,H., Kojima,M., Ohmiya,Y., Yamada,M. & Koshimizu,H. Expression of cystatin C prevents oxidative stress-induced death of PC12 cells. Brain. Res. 67, 94-99 (2005).

104. Fulkerson,P.C., Zimmermann,N., Brandt,E.B., Muntel,E.E., Doepker,M.P., Kavanaugh,J.L., Mishra,A., Witte,D.P., Zhang,H., Farber,J.M., Yang,M. Foster,P.S. & Rothenberg,M.E. Proc. Natl. Acad. Sci. USA. 101, 1987-1982 (2004).

105. Garnotel,R., Rittie,L., Poitevin,S., Monboisse,J.C., Nguyen,P., Potron,G., Maquart,F.X., Randoux,A. & Gillery,P. Human blood monocytes interact with type I collagen through alpha x beta 2 integrin (CD11c-CD18, gp150-95). J. Immunol. 164, 5828-5934 (2000).

106. Frantz,S., Kelly,R.S. & Bourcier,T. Role of Tlr-2 in the activation of nuclear factor κB by oxidative stress in cardiac myocytes. J. Bio. Chem. 276, 5197-5203 (2001).

107. Nishimoto,N. & Kishimoto,T. Inhibition of Il-6 for the treatment of inflammatory diseases. Curr. Opin. Pharmacol. 4, 386-391 (2004).

108. Oppenheim,J.J., Zachariae,C.O., Mukaida,N. & Matsushima,K. Properties of the novel proinflammatory supergene "intercrine" cytokine family. Annu. Rev. Immunol. 9, 617-648 (1991).

109. Idzko,M., Laut,M., Panther,E., Sorichter,S., Dürk,T., Fluhr,J.W., Herouy,Y., Mockenhaupt,M., Myrtek,D., Elsner,P. & Norgauer,J. Lysophosphatidic acid induces chemotaxis, oxygen radical production, CD11b up-regulation, Ca2+ mobilization, and actin reorganization in human eosinophils via pertussis toxin-sensitive G proteins. J. Immunol. 172,4480-4485 (2004).

110. Baker,C.A., Lu,Z.Y. & Manuelidis,L. Early induction of interferon-responsive mRNAs in Creutzfeldt-Jakob disease. J. NeuroVirol. 10,29-40 (2004).

111. Scotland,P., Zhou,D., Benveniste,H. & Bennett,V. Nervous system defects of AnkyrinB (-/-) mice suggest functional overlap between the cell adhesion molecule L1 and 440-kD AnkyrinB in premyelinated axons. J. Cell Biol. 30,1305-1315 (1998).

112. Houzelstein,D., Bullock,S.L., Lynch,D.E., Grigorieve,E.F., Wilson,V.A. & Beddington,R.S. Growth and early postimplantation defects in mice deficient for the bromodomain-containing protein Brd4. Mol. Cell Biol. 22,3794-3802 (2002).

113. McArthur GA, Foley KP, Fero ML, Walkley CR, Deans AJ, Roberts JM, Eisenman RN. MAD1 and p27(KIP1) cooperate to promote terminal differentiation of granulocytes and to inhibit Myc expression and cyclin E-CDK2 activity. Mol. Cell Biol. 22,3014-3023 (2002).

114. Eischen CM, Weber JD, Roussel MF, Sherr CJ, Cleveland JL. Disruption of the ARF-Mdm2-p53 tumor suppressor pathway in Myc-induced lymphomagenesis. Genes Dev. 20,2658-2669 (1999).

115. Yao TP, Oh SP, Fuchs M, Zhou ND, Ch'ng LE, Newsome D, Bronson RT, Li E, Livingston DM, Eckner R. Gene dosage-dependent embryonic development and proliferation defects in mice lacking the transcriptional integrator p300. Cell. 3,361-372 (1998).

116. Mitchell KJ, Pinson KI, Kelly OG, Brennan J, Zupicich J, Scherz P, Leighton PA, Goodrich LV, Lu X, Avery BJ, Tate P, Dill K, Pangilinan E, Wakenight P, Tessier-Lavigne M, Skarnes WC. Functional analysis of secreted and transmembrane proteins critical to mouse development. Nat. Genet. 28,241-249 (2001).

117. Mahajan MA, Das S, Zhu H, Tomic-Canic M, Samuels HH. The nuclear hormone receptor coactivator NRC is a pleiotropic modulator affecting growth, development, apoptosis, reproduction, and wound repair. Mol. Cell Biol. 24,4994-5004 (2004).

118. Jacks,T. Tumor suppressor gene mutations in mice. Annu. Rev. Genet. 30,603-636 (1996).

119. Burkin DJ, Wallace GQ, Nicol KJ, Kaufman DJ, Kaufman SJ. Enhanced expression of the alpha 7 beta 1 integrin reduces muscular dystrophy and restores viability in dystrophic mice. J. Cell. Biol. 152,1207-1218 (2001).

120. Deans B, Griffin CS, Maconochie M, Thacker J. Xrcc2 is required for genetic stability, embryonic neurogenesis and viability in mice. EMBO J. 24,6675-6685 (2000).

121. Tarnok A. & Gerstner A.O.H. Clinical Applications of Laser Scanning Cytometry. Cytometry. 50, 133-143 (2002).

122. Delgado M. & Ganea D. Vasoactive intestinal peptide prevents activated microglia-induced neurodegeneration under inflammatory conditions: potential therapeutic role in brain trauma. FASEB J. 13, 1922-1924 (2003).

123. Gonzalez-Rey E. & Delgado M. Role of vasoactive intestinal peptide in inflammatory and autoimmunity. Curr. Opin. Investig. Drugs. 11, 1116-1123 (2005).